Digital Comprehensive Summaries of Uppsala Dissertations
from the Faculty of Science and Technology 2509

Dual-Element Onshore Seismic Data Acquisition and Imaging Techniques

Case studies from Seoul metropolitan and Danish CCS sites

SAMUEL ZAPPALÁ

ACTA UNIVERSITATIS
UPSALIENSIS
2025

ISSN 1651-6214
ISBN 978-91-513-2409-8
urn:nbn:se:uu:diva-550140

UPPSALA
UNIVERSITET

Dissertation presented at Uppsala University to be publicly examined in Hambergssalen, Geocentrum, Villavägen 16, Uppsala, Friday, 25 April 2025 at 10:00 for the degree of Doctor of Philosophy. The examination will be conducted in English. Faculty examiner: Research scientist Don White (Geological Survey of Canada).

Abstract
Zappalá, S. 2025. Dual-Element Onshore Seismic Data Acquisition and Imaging Techniques. Case studies from Seoul metropolitan and Danish CCS sites. *Digital Comprehensive Summaries of Uppsala Dissertations from the Faculty of Science and Technology* 2509. 94 pp. Uppsala: Acta Universitatis Upsaliensis. ISBN 978-91-513-2409-8.

This thesis presents the development of an innovative 2D reflection seismic acquisition system and its processing. The dual-element system integrates a nodal geophone array employed for deep imaging, and a MEMS-based landstreamer system employed for near-surface imaging, enabling high-resolution seismic data acquisition across multiple depth ranges. In the Korean Peninsula, where seismic activity has increased following the 2011 Tohoku-Oki earthquake, this system was applied to image crustal-scale fault systems. Three major systems were partially imaged, and the integration of the two datasets helped constrain fault locations in the densely populated, hard-rock environment of metropolitan Seoul, improving the understanding of seismic hazards and earthquake preparedness in the region. In Denmark, the system was employed for large-scale geological surveys to assess potential CO# storage structures, contributing to climate change mitigation efforts. A novel data merging technique was developed to integrate the two datasets, enhancing the imaging of reservoirs, seals, and fault structures. In addition, offshore sensors were considered and analysed to cover an onshore transition to offshore zone. The applied acquisition setup and developed merging technique were crucial to reach the desired resolution at all pertinent depths. A reflection-picked moveout correction processing step was developed for implementing high-resolution near-surface imaging through S-wave reflections as a by-product of large-scale acquisitions. The application of this method increased the reflection continuity in the stacked section that, complemented with velocity analyses, permitted the identification of key geological markers such as the water table depth and the top of the pre-Quaternary layers. Throughout the thesis, application of complementary analyses highlights the importance of leveraging different seismic data characteristics to improve subsurface imaging and geological reconstruction. The adaptability of this system demonstrates its effectiveness in complex environments, supporting both urban seismic risk mitigation and carbon capture and storage (CCS) applications. By addressing seismic hazards and climate challenges, this research underscores the crucial role of reflection seismology in tackling global environmental and societal issues.

Keywords: Onshore seismic reflection, Urban environment, CCS exploration, Fault detection, S-wave imaging

Samuel Zappalá, Department of Earth Sciences, Geophysics, Villav. 16, Uppsala University, SE-75236 Uppsala, Sweden.

ISSN 1651-6214
ISBN 978-91-513-2409-8
URN urn:nbn:se:uu:diva-550140 (http://urn.kb.se/resolve?urn=urn:nbn:se:uu:diva-550140)

List of Papers

During my PhD project I participated to the production of the following papers, which in the text are referred to by their Roman numerals.

I. Malehmir, A., Hong, T. K., Lee, J., **Zappalá, S.,** Brodic, B., Chung, D., Kim, B., Park, S., Lee, J., & Kil, D. (2022). Fault intersections control short period intraplate start-stop seismicity in the Korean Peninsula. *Tectonophysics*, 834. https://doi.org/10.1016/j.tecto.2022.229387

II. **Zappalá, S.,** Malehmir, A., Hong, T. K., Juhlin, C., Lee, J., Papadopoulou, M., Brodic, B., Park, S., Chung, D., Kim, B., & Lee, J. (2022). Crustal-Scale Fault Systems in the Korean Peninsula Unraveled by Reflection Seismic Data. *Earth and Space Science*, 9(9). https://doi.org/10.1029/2022EA002464

III. Papadopoulou, M., **Zappalá, S.,** Malehmir, A., Gregersen, U., Hjelm, L., Nielsen, L., & Haspang, M. P. (2023). Innovating land seismic investigations for CO_2 geologic storage in Denmark. *Geophysics*, 88(5), 1–57. https://doi.org/10.1190/geo2022-0693.1

IV. **Zappalá, S.,** Malehmir, A., Papadopoulou, M., Gregersen, U., Funck, T., Clausen, O. R., & Nørmark, E. (2024). Combined onshore and offshore wide scale seismic data acquisition and imaging for carbon capture and storage exploration in Havnsø, Denmark. *Geophysics*, 89(4), B257–B272. https://doi.org/10.1190/geo2023-0503.1

V. Papadopoulou, M., **Zappalà, S.,** Malehmir, A., Kucinskaite, K., Westgate, M., Gregersen, U., Funck, T., Smit, F., & Vosgerau, H. (2024). Advancements in seismic imaging for geological carbon storage: Study of the Havnsø structure, Denmark. *International Journal of Greenhouse Gas Control*, 137, 104204. https://doi.org/10.1016/j.ijggc.2024.104204Gassum

VI. **Zappalá, S.,** Papadopoulou, M., & Malehmir, A. (in revision). Shear-wave tailored moveout corrections to improve multicomponent reflection seismic imaging. *Near Surface Geophysics*

VII. **Zappalá, S.,** Malehmir, A., Kranis, H., Apostolopoulos, G., Papadopoulou, M. (2025, accepted). Reflection seismic imaging across the Thinia valley (Greece). *Solid Earth*.

This thesis is based on Papers II, III, IV and VI, considered and selected as the most representative of the overall work. Papers I, V and VII are briefly presented as additional work.

Reprints were made with permissions from the respective publishers.

Additionally, during my PhD studies, I have contributed to the following abstracts and papers that are not included in this thesis:

Zappalá, S., Malehmir, A., Hong, T.-K., Lee, J., Brodic, B., Chung, D., Juhlin, C., Kim, B., Papadopoulou, M., Park, S., Lee, J., & Kil, D. (2022). High-resolution reflection seismic imaging of fault systems in Metropolitan Seoul, South Korea. *EGU General Assembly 2022*. https://doi.org/https://doi.org/10.5194/egusphere-egu22-991

Papadopoulou, M., Malehmir, A., **Zappalá, S.,** Gregersen, U., Nielsen, L., & Hjelm, L. (2022). Innovative land seismic data acquisitions for CO_2 and energy storage applications. *28th European Meeting of Environmental and Engineering Geophysics, NSG 2022*, 1-5. https://doi.org/10.3997/2214-4609.202220098

Papadopoulou, M., **Zappalà, S.,** Malehmir, A., Kucinskaite, K., Westgate, M., Gregersen, U., Hjelm, L., Funck, T., & Nielsen, L. (2023). Upscaling Innovative Land Seismic Acquisitions for Geological Storage of CO_2 in Denmark. *84th EAGE Annual Conference & Exhibition*, 1–5. https://doi.org/10.3997/2214-4609.202310385

Zappalá, S., Malehmir, A., Papadopoulou, M., & Apostolopoulos, G. (2023). A High-Resolution Reflection Seismic Survey in the Historical Kefalonia Island, Greece. *29th European Meeting of Environmental and Engineering Geophysics, NSG2023*, 1–5. https://doi.org/10.3997/2214-4609.202320032

Kucinskaite, K., Papadopoulou, M., **Zappalà, S.,** Malehmir, A., Westgate, M., Gregersen, U., & Funck, T. (2023). Near-Surface Effect on Geological CO_2 Storage Site Characterization in Denmark. *The Fourth EAGE Global Energy Transition Conference and Exhibition*, 1–5. https://doi.org/10.3997/2214-4609.202321026

Zappalá, S., Malehmir, A., Papadopoulou, M., Gregersen, U., Hjelm, L., Funck, T., Nørmark, E., Trinhammer, P., & Nielsen, L. (2024). Innovative Reflection Seismic Acquisition for CCS Applications at a Transition Zone in Havnsø Area – Denmark. *85th EAGE Annual Conference & Exhibition*, 1–5. https://doi.org/10.3997/2214-4609.2024101380

Papadopoulou, M., Kucinskaite, K., **Zappalà, S.,** Malehmir, A., Westgate, M., Gregersen, U., & Funck, T. (2024). Seismic characterization of geologic carbon storage sites in Denmark: Near-surface aspects. *SEISMIX 2024*, Abstract Volume, 68.

Zappalà, S., Malehmir, A., Papadopoulou, M., Westgate, M., Putnaite, J., Markovic, M., Gregersen, U., Abramovitz, T., Keiding, M., & Bjerager, M. (2024). Reflection Seismic Acquisition for Onshore CCS Applications in Denmark – an Overview. *Fifth EAGE Global Energy Transition Conference & Exhibition*, 1–5. https://doi.org/10.3997/2214-4609.202421062

Charbaoui, A., Guernouche, M., Kchikach, A., Jaffal, M., Hadri, A., Octavian Cimpoiasu, M., **Zappalá, S.,** Amar, M., & Khadiri Yazami, O. (2024). Understanding the impact of deep structures on the hydrological setting of the Eastern Bahira Basin in Morocco using combined geophysical analysis of gravity, seismic, and electrical resistivity data. *Journal of King Saud University - Science*, 36(11), 103491. https://doi.org/10.1016/j.jksus.2024.103491

Zappalá, S., Papadopoulou, M., & Malehmir, A. (2024). Optimized Workflow to Retrieve and Enhance Shear-Wave Reflections in a Potential CCS Site in Denmark. *AGU annual meeting 2024*. Short abstract.

Contributions

The papers included in this thesis are from collaboration with colleagues from Uppsala University and several international research institutes. The contributions to each paper are summarized below:

Paper I: AM planned the survey and together with the team from Uppsala University and Yonsei University performed the data acquisition, he processed the data for profile 1, prepared the figures and prepared the article. SZ processed the data for profile 2, performed the traveltime tomography and cross-dip analysis. TKH coordinated the project. All authors, particularly, AM, TKH, JL, SZ and BB, were involved in the discussions of the results and their interpretations.

Paper II: SZ was involved in the data acquisition, was responsible for the data preparation, most of the nodal data processing, the traveltime tomography, the cross-dip analysis, the interpretation, and the writing of the article. AM planned and led the data acquisition, processed most of the landstreamer data, helped with the overall processing and especially with the writing of the article and the interpretational aspects and discussion section. CJ worked in the first part of the data processing highlighting the Wangsukcheon fault reflection and modelling its reflection traveltime. JL helped on the acquisition setting and organization and prepared the basis for the maps. MP worked on the surface-waves backscattering analysis. TKH initiated the project, organized the acquisition, and was involved in the discussions of the results and their interpretations. BB contributed to the data acquisition and planning. TKH, BB, CJ, JL, MP, SP, DC, BK and JeL contributed in the final preparation of the paper.

Paper III: MP led the processing, interpretation, discussion of the results and the writing of the article. SZ was involved on the acquisition, processed profile 1 and 1.5 and designed the main data processing for all profiles. AM secured the project, led the data acquisition and processed profile 4. UG initiated the project, helped in the geological interpretation and was involved in the discussions of the results. All authors contributed in the final preparation of the paper.

Paper IV: SZ was involved in the acquisition, was responsible for the data preparation and the data processing of all sensors, the interpretation, and the writing of the article. AM secured the project and led the data acquisition, helped with the overall processing and writing of the article and the interpretational aspects and discussion. MP helped on the processing, interpretation and discussion. UG initiated the project and was involved in the discussions of the results and their interpretations. FT led the OBS acquisition and their data preparation. COR and NE led the marine streamer acquisition and its data preparation. All authors contributed to the final preparation of the paper.

Paper V: MP led the processing, interpretation, discussion of the results and the writing of the article and designed the 3D horizons. SZ was involved in the acquisition, processed profile 1, designed the main data processing for all profiles and helped on the 3D horizons design and interpretation. AM secured the project, led the data acquisition and processed part of the data. KK and MW processed part of the data. UG initiated the project, helped in the geological interpretation and was involved in the discussions of the results. All authors contributed to the final preparation of the paper.

Paper VI: SZ was involved on the acquisition, was responsible for the data preparation, the P- and S-waves data processing, the multicomponent and velocity analyses, the interpretation, and the writing of the article. MP worked on the lateral constrained inversion of the surface-waves and helped on the interpretation and discussion. AM secured the project and planned the data acquisition, helped with the writing of the article, the interpretational aspects and discussion.

Paper VII: SZ was involved in the acquisition, was responsible for the data preparation and the data processing, the interpretations, and the writing of the article. AM led the data acquisition, helped with the overall processing and writing of the article and the interpretational aspects and discussion. HK led the geological interpretation and participated to the results discussion. GA initiated the project and was involved in the discussions of the results and their interpretations. MP helped on the interpretation and results discussion. All authors contributed to the final preparation of the paper.

Contents

1 Introduction 13
1.1 Thesis outline 15

2 Background 17
2.1 Fundamentals of reflection seismology 17
2.1.1 Standard acquisition methods 18
2.1.2 Standard processing workflows 20
2.1.3 Hard-rock environment and fault detection 21
2.1.4 Urban environment and crooked profiles 23
2.1.5 Converted waves 24
2.2 Seismic risk and its mitigation 26
2.3 CCS overview 26
2.4 Geology of the sites 28
2.4.1 South Korea 28
2.4.2 Denmark 29

3 Methodology and data acquisition 33
3.1 Dual-element acquisition system 33
3.2 Combined onshore and offshore acquisition 34
3.3 Processing and merging of the seismic datasets 36
3.4 Complementary analyses 37
3.4.1 Velocity analysis 37
3.4.2 3D cross-dip analysis 38
3.4.3 3D reflection traveltime modelling 39
3.4.4 Surface-wave back-scattering 40

4 Summary of papers 42
4.1 Paper II: Crustal-Scale Fault Systems in the Korean Peninsula Unraveled by Reflection Seismic Data 42
4.1.1 Synopsis 42
4.1.2 Conclusions 50
4.2 Paper III: Innovating land seismic investigations for CO_2 geologic storage in Denmark 51
4.2.1 Synopsis 51
4.2.2 Conclusions 57

4.3 Paper IV: Combined onshore and offshore wide scale seismic data acquisition and imaging for carbon capture and storage exploration in Havnsø, Denmark 58
4.3.1 Synopsis 58
4.3.2 Conclusions 65
4.4 Paper VI: Shear-wave tailored moveout corrections to improve multicomponent reflection seismic imaging 66
4.4.1 Synopsis 66
4.4.2 Conclusions 70

5 Conclusions 72
5.1 Future developments 73

6 Additional studies 75
6.1 Paper I: Fault intersections control short period intraplate start-stop seismicity in the Korean Peninsula 75
6.2 Paper V: Advancements in seismic imaging for geological carbon storage: Study of the Havnsø structure, Denmark. 76
6.3 Paper VII: Reflection seismic imaging across the Thinia valley (Greece) 78

7 Swedish summary 80

Acknowledgments 83

References 85

Abbreviations

1C	One component
2D	Two-dimensional
3C	Three components
3D	Three-dimensional
9C	Nine components
AGC	Automatic gain control
CCS	Carbon capture and storage
CMP	Common midpoint
DAS	Distributed acoustic sensing
DGPS	Differential global positioning system
FDSD	Frequency-domain sweep deconvolution
FWI	Full-waveform inversion
HR	Horizontal radial
HT	Horizontal transverse
LCI	Laterally constrained inversion
MEMs	Micro electro mechanical system
NMO	Normal moveout
Mw	Moment magnitude
OBS	Ocean bottom seismometer
RMS	Root mean square
RTM	Reverse time migration
S/N	Signal-to-noise ratio
V	Vertical
V_P	P-wave velocity
V_S	S-wave velocity

1 Introduction

In 2015, world leaders adopted the 17 Sustainable Development Goals (SDG) to address environmental and societal challenges by 2030. The 9th and 13th goals of the list are respectively "industry, innovation and infrastructure" and "climate action" (United Nations – General assembly, 2015). In this thesis, an innovative 2D reflection seismic acquisition system is upscaled for seismic risk and subsurface characterization for CCS and greenhouse gas mitigation. The system comprises seismic vibrators as sources and two different recording systems. The recording systems consist of a nodal array equipped with 1C vertical geophones, used for long offset coverage with a spacing between 10 and 20 m, and of a 3C MEMs based landstreamer system, used for short offset coverage with a receiver spacing of 2 m. This dual-element acquisition system is optimal for the simultaneous recording of quality data for both shallow and deep subsurface imaging.

Addressing seismic risks in urban areas is a critical aspect for ensuring resilient infrastructures. This is particularly relevant in regions like the Korean peninsula, where increasing seismic activity poses significant challenges for urban safety and preparedness. Therefore, considering the potential high seismic risk in metropolitan Seoul, home to approximately 20 million people, investigations to study the subsurface correlation between crustal-scale fault systems and the recorded seismicity were performed for the first time.

The Korean peninsula, comprised mainly of deformed basement rocks formed between 1.1 and 2.7 Ga (Bae & Lee, 2016; Choi et al., 2012), serves as an important tectonic link between eastern China and Japan. Although traditionally considered to be a stable intraplate region, historical recordings of major earthquakes close to metropolitan Seoul (Lee & Yang, 2006; Park et al., 2020) and a rise of plus M_w 5.0 earthquakes (Hong et al., 2017) after the destructive Tohoku-Oki mega-thrust M_w 9.0 earthquake in 2011 in Japan, have raised the need to investigate subsurface fault systems to better understand seismic hazards and improve the peninsula preparedness (Rosenblueth & Ordaz, 1990; Singh et al., 1980; Wells & Coppersmith, 1994). Nonetheless, urban geophysical investigations, especially in major cities like Seoul metropolitan area, are challenging due to low S/N and logistical constraints (Ishiyama et al., 2016; Malehmir et al., 2011; Sato et al., 2009). Adopting solutions specifically developed to face these challenges can bring important

results and high-quality imaging of the subsurface structures (Brodic et al., 2015; Ishiyama et al., 2016; Malehmir et al., 2022; Sato et al., 2009). **Papers I** and **II** of my thesis describe the dual-element acquisition system for urban environments applied for seismic risk mitigation purposes. **Paper I** focuses on defining relations between tectonic features and recent seismic clusters while **Paper II** focuses on imaging the related crustal-scale fault systems.

Beyond seismic risk, such innovative geophysical methods also have significant potential in tackling pressing global challenges, such as greenhouse gas mitigation. As recommended by the UN's climate panel, CCS is recognized as a solution to reduce the current increase in the atmospheric CO_2 levels (Metz et al., 2005). Denmark, a leader in CCS applications, has prioritized geological CO_2 storage as part of the climate action strategy presented in the Danish 2020 climate law (Danish Ministry of Climate, Energy and Utilities, 2021), serving the ambition to reach carbon neutrality by 2050 (OECD, 2019). To address the knowledge gap regarding geological structures that can host the captured CO_2, a series of seismic investigations were initiated in 2022 (Abramovitz et al., 2024; Gregersen et al., 2023a, 2023b). These surveys aimed to map five onshore geological storage structures across Denmark and estimate their storage capacity, while ensuring that the planned CCS operations will be done safely and in a sustainable way (Zappalà et al., 2024). Thus, a major concern was to identify faults or fractures that can compromise the integrity of the reservoir (Frery et al., 2015; Miocic et al., 2016).

The dual-element acquisition technique proved valuable in characterizing sites at depth while maintaining high resolution at shallow levels. **Papers III-V** describe how the data were acquired and processed across two of the sites, including an area of onshore transition to offshore acquisition. The resulting high-resolution images both at shallow and deep levels allowed to map the reservoir storages, seals and faults affecting the structures.

The dual-element acquisition system offers a unique opportunity to advance shear- (S-) wavefield imaging, which is typically higher resolution, conditioned that similar frequencies are attained, due to the lower velocities of S-waves compared to pressure- (P-) waves (Carr et al., 1998; Krawczyk et al., 2013). **Paper VI** capitalizes on this potential, utilizing part of data from CCS reservoir investigations to perform high-resolution near-surface imaging. The SS-wavefield data processing required a different processing flow and in particular the application of a specially designed moveout correction to enhance reflections masked by the surface-waves. The presented multicomponent data processing workflow offers the possibility to obtain near-surface information at low acquisition costs, as a by-product of large-scale site investigations. This method can be widely applied in different near-surface case studies such as in engineering and hydrological investigations, supporting the Sustainable Development Goals further.

The aims of this thesis are therefore:

1. To determine the feasibility, advantages, and disadvantages of the dual-element acquisition system for hard-rock environments (**Paper II**) and CCS reservoir investigations (**Paper III**) in urban areas.
2. To develop a processing workflow to image, for the first time, three major fault systems in the metropolitan Seoul area and to analyse spatial relationships among these faults and the recorded seismicity in the region (**Paper II**).
3. To develop a processing flow for the dual-element acquisition system that can produce a single wide-scale high-resolution seismic image (**Paper III**).
4. To develop a multi-sensor acquisition and processing workflow for onshore-to-offshore transition zones (**Paper IV**).
5. To interpret geological structures of interest for CCS in Denmark (**Papers III** and **IV**).
6. To establish a seismic processing technique for SS-wavefield imaging from the dual-element acquisition system, overcoming surface-wave contamination, and to exploit multicomponent analyses for detailed near-surface interpretations (**Paper VI**).

1.1 Thesis outline

This thesis is structured in seven chapters. After the Introduction in *Chapter 1*, a review of the theoretical background and of previous studies is presented in *Chapter 2* along with a geological description of the studied sites. The adopted methodologies are described in *Chapter 3*. *Chapter 4* presents a summary of the papers and most relevant results. *Chapter 5* draws out the conclusions of the work and highlights future possibilities. *Chapter 6* describes additional work performed during my PhD that is not included in the main body of this thesis. Finally, *Chapter 7* presents a Swedish summary of the thesis.

This thesis includes four published papers from four different study areas. **Paper II** from metropolitan Seoul, South Korea, focuses on crustal-scale fault systems detection for geo-hazard mitigation purposes. **Papers III, IV** and **VI** are from three different sites in Denmark, **Paper III** from Stenlille, **Paper IV** Havnsø, and **Paper VI** from Gassum. In addition to the main purpose of CCS reservoir investigations, different aspects such as acquisition and specific data processing developments are addressed in these papers. Three more papers (**Papers I**, **V** and **VII**) are summarized as additional work but are not attached to this thesis.

This PhD work navigates through the evolution of the dual-element acquisition system processing work. At its first application in the Korean peninsula,

the two datasets were separately processed, with the landstreamer data considered only for the shallower portion while the nodal array data only for the deeper portion (**Papers I** and **II**). During the first work in Denmark, a pre-stack merging processing flow aiming to produce a single comprehensive stacked section was developed, allowing the contribution of both datasets at different depths (**Paper III**). **Paper IV** further advances the pre-stack merging processing for large-scale applications and extends its application to four different datasets for an onshore to offshore transition zone. The full potential of the acquisition setup is highlighted in **Paper VI** where the 3C nature of the landstreamer system is further exploited for multicomponent analyses of the near-surface as a by-product of large-scale site investigations.

During my thesis work, innovative acquisition and processing solutions for reflection seismology were developed, aiming to increase the scope where this geophysical method can be employed. The developed methodologies were applied on real cases for seismic risk and greenhouse gas mitigation addressing goals 9 (industry, innovation and infrastructure) and 13 (climate action) of the Sustainable Development Goals, underscoring the role that geophysical methods can play in these major contemporary challenges.

2 Background

2.1 Fundamentals of reflection seismology

The reflection seismic method is widely used for various applications. It has been developed for decades mainly for oil and gas industry, however, from the 1970s, it started to spread among different fields such as crustal scale studies, mineral exploration, hydrological and engineering studies, and lately for energy transition applications. The broad coverage of the method over different fields shows its adaptability and flexibility to serve different scopes while boosting the development of new specific techniques to achieve optimal results.

The method relies on reflected seismic waves generated at contrasts in the subsurface such as density, porosity, and seismic velocity (Aki & Richards, 2002; Cox et al., 2020; Sheriff, 1980). Seismic sources, either active or passive, create wavefields that propagate downward through the subsurface. When these wavefields encounter impedance contrasts, a portion of the energy reflects to the surface, following Snell's law. Receivers placed on the surface record these reflected signals (Figure 2.1). The recorded raw data are then processed to isolate the desired reflected signals and image the subsurface.

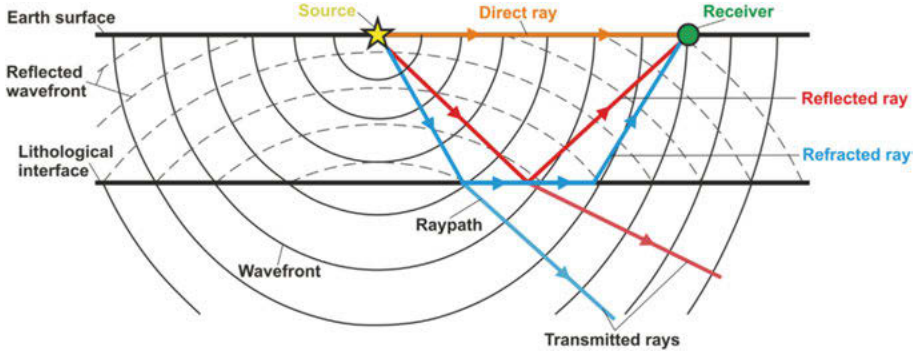

Figure 2.1. Example of wavefield propagation in the half-space of a reflection seismology setup (Cox et al., 2020).

To completely reconstruct the geometry of a medium from waves travelling through it, the wavefield should be fully recorded and analysed. However, in the half-space case (typical for reflection seismology) there are no possibilities to record the transmitted field that travels towards the interior of the model.

The lack of this information can be handled for simple scenarios, introducing assumptions such as homogeneous media, horizontal layers and isotropic propagation, while acquisition and processing techniques can partially compensate for minor deviations from these assumptions. From these principles, standard acquisition and processing techniques have been developed to reconstruct the subsurface geometries from the time that the seismic signal takes to travel from the source to each receiver through the half-space.

2.1.1 Standard acquisition methods

Seismic reflection targets vary in depth and scale, requiring tailored acquisition setups. Stronger sources enable deeper signal penetration but introduce more noise and require more energy. Active sources generate controlled seismic waves and fall into two categories: impulsive (e.g., sledgehammers, explosives) producing sharp, millisecond signals, and vibrational (e.g., vibrator trucks, Figure 2.2a) generating longer, frequency-controlled sweeps. Passive sources, such as vehicles, ocean waves, and earthquakes, are weaker and usually generate ambient noise. Though, this signal can be analysed and processed to partly recover the subsurface structures, offering cost-effective, low-impact subsurface imaging, particularly in urban areas. However, their lower resolution with respect to active seismic methods limits their use in exploration-scale applications (Cheraghi et al., 2017; Colombero et al., 2022; Draganov & Ruigrok, 2015; Draganov et al., 2009; Punzo et al., 2021; Wilczynski et al., 2024).

On the receiver side, geophones (Figure 2.2b) have been the standard onshore sensors, converting ground motion into electrical signals based on the Faraday-Neumann law (Reynolds, 2011). Digital accelerometers, increasingly popular in onshore data acquisitions, work on the same basic principle of the geophones while offering 3C acceleration measurement, a broader frequency range, and immunity to electromagnetic noise (Tellier & Lainé, 2017). Both sensors have evolved from wired to wireless systems for improved deployment and data recovery efficiency. A third type of onshore sensor, DAS systems, use fibre optic cables to measure strain via laser scattering, a rapidly advancing technology in reflection seismology (Hartog, 2017; Rogers, 1999; Song et al., 2023).

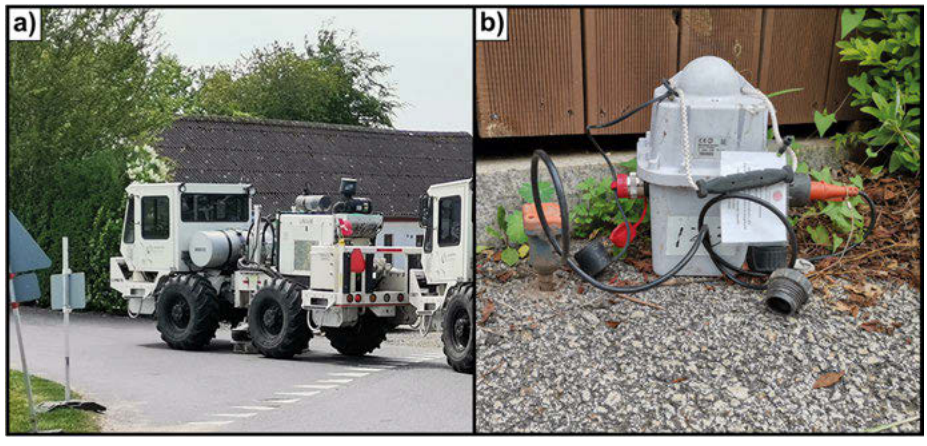

Figure 2.2. Examples of (a) a seismic vibrator truck and (b) a nodal receiver connected to a spike-based geophone, used for active seismic data acquisition in an urban environment setting.

The acquisition setup depends on target depth, size, geometry, physical properties, resolution needs, and background noise. Deeper, larger targets require stronger sources for sufficient energy propagation, while shallow targets need higher frequencies with less noise. Maximum offset is influenced by target depth, size, and dipping geometry since, according to Snell's law, dipping structures reflect energy further downdip with respect to a horizontal target. Signal frequency (typically 10–200 Hz) and receiver spacing must align with expected media velocity and adhere to the Nyquist-Shannon sampling theorem to prevent aliasing, with the receiver spacing less than half of the expected seismic wavelength. The signal frequency impacts also the acquired resolution, and the produced wavelength should be proportional to the target thickness. Higher noise levels require stronger sources and more source positions to improve the S/N (Cox et al., 2020).

In addition to these basic concepts to define an acquisition setup, 3C sensors should be considered to acquire both P- and S-wave data for multicomponent studies, useful to better define elastic properties of the media such as the Poisson's ratio. For horizontally continuous subsurface structures 2D profiles can be acquired where receivers and sources are deployed on a straight line recording the energy that travels along a single plane. However, for more complex geologies 3D data acquisition may be required, in which a grid of receivers and sources is employed over an area of interest, recording the energy travelling in all directions. Finally, cost efficiency is crucial, with longer offsets, denser receiver spacing, and 3D grids significantly increasing the expenses. Stronger sources and additional positions also add costs and time. Ideal setups maximize S/N and spatial resolution but must adapt to onshore terrain challenges (e.g., rivers, forests, roads). This trade-off drives diverse

acquisition strategies, balancing data quality with cost and logistical constraints.

2.1.2 Standard processing workflows

To create a subsurface image, seismic reflection data must be processed to place reflections at their correct depth. Seismic reflection processing can be divided in three main tasks: assigning acquisition geometries, enhancing the desired signal, and reconstructing the subsurface image.

First, coordinates and related offsets of source and receiver positions are added to the data. Next, to enhance the signal, multiple shots per position are stacked to strengthen coherent reflections while reducing random noise. Various processing steps are applied, such as frequency filtering, deconvolution, and static corrections, to remove unwanted noise and correct for topography and near-surface effects. After this, the data are sorted into CMP gathers, grouping traces with the same midpoint between the source and the receiver. Under the assumption of horizontal reflectors, these traces should also share the same information about the subsurface (Figure 2.3a). Stacking these traces enhances the signal and reduces noise. The higher the number of traces in a CMP gather, the more effective this method is. Since reflections arrive at different times due to varying offsets, the NMO correction adjusts for travel time differences before summing the traces into a single seismic trace (Figure 2.3b), which is then displayed to form the subsurface image (Yilmaz, 2001).

For dipping structures, additional migration processing is required to correct for the wrong sub-horizontal assumption and shift the dipping reflections to their real position (Yilmaz, 2001). Different migration processes have been developed depending on the complexity of the subsurface structures and on the available computational power. Simple cases use post-stack time migration, while complex geometries demand pre-stack and depth migrations to correct for higher dips and velocity variations. The most advanced methods, RTM and FWI, can accurately image almost vertical structures and complex velocity fields but require accurate starting models and high computational power (Cox et al., 2020; Yilmaz, 2001).

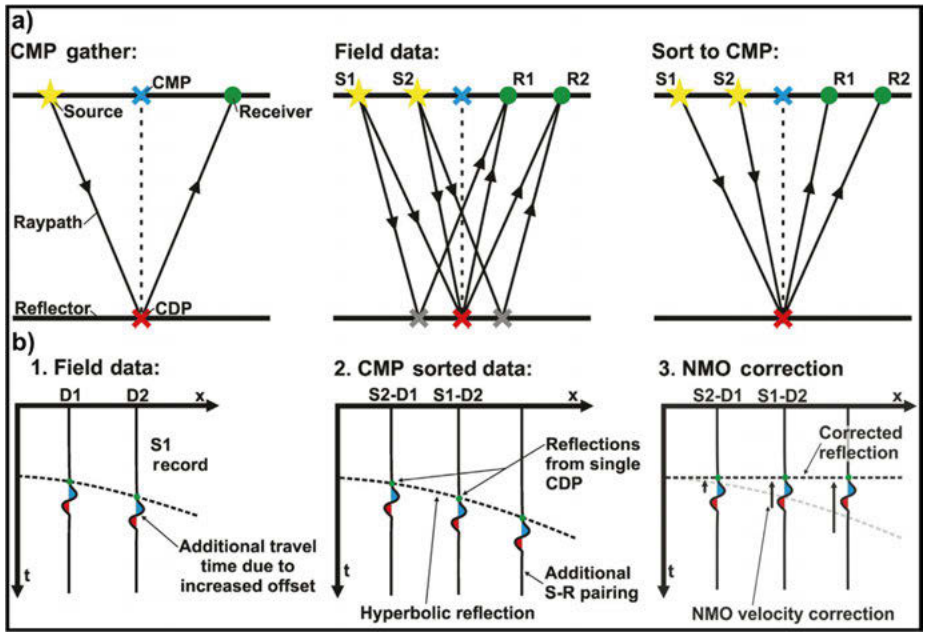

Figure 2.3. Example of CMP gather. (a) Diagram on the use of source-receiver pairings to retrieve CMP gathers during acquisition. (b) Data in a CMP gather before and after correction for the different offsets. S=source; R=receiver; D=data. Modified from Cox et al. (2020).

2.1.3 Hard-rock environment and fault detection

Hard-rock environments, characterized by the dominance of igneous and metamorphic rocks, are widely spread around the globe. Seismic reflection surveys applied to such environments primarily target subsurface reconstruction of hard-rock bodies, as in crustal-scale studies and mineral exploration. For many years, these applications were overlooked due to significant differences from sedimentary basins, where the seismic reflection method was traditionally applied. But pioneering works (Green & Mair, 1983; Pretorius et al., 1987) and large-scale crustal seismic-profiling campaigns in the 1970s (Brown et al., 1986), laid the foundation for hard-rock seismic reflection development in the 1990s, especially for deep mineral exploration (e.g., Koivisto et al., 2012), radioactive waste disposal (Juhlin & Stephens, 2006) and geotechnical investigations. These works established the potential of seismic methods in hard-rock environments (Eaton et al., 2003).

Hard-rock environments can present different characteristics with respect to the sedimentary environment. The general lower porosity and the presence of minerals with higher density in the rock lead to higher density values, and consequently higher seismic wave velocities, than the ones characteristic of sedimentary environments. The lack of stratification reduces the amount of sharp and continuous discontinuities in the subsurface, resulting in lower

impedance contrasts and smaller anomalies. Rock fractures can cause strong energy scattering, hence reducing the signal penetration. Seismic sources and sensors do not require any specific adaptation to the change of environment, but different challenges, including low S/N, discontinuous reflections and energy scattering must be addressed. Key considerations for hard-rock seismic data include: (1) a high CMP-fold is required to compensate the low S/N; (2) frequencies higher than 100 Hz are needed to maintain a high resolution due to the high velocities; (3) robust processing sequences, including statics, surface-consistent deconvolution and dip moveout, should be applied to enhance the low reflectivity; (4) different physical rock property ranges with respect to the sedimentary environment should be considered (Eaton et al., 2003).

Despite these challenges, the reflection seismic method can yield great results in hard-rock environments. For example, faults in hard-rock environments can be detected by seismic methods due to their alteration of the physical properties of the rocks. However, in contrast to the sedimentary environments, it can be challenging to infer their presence from the displacement of subsurface layers (Moon et al., 2021) and the fault plane itself often must be imaged (Beckel & Juhlin, 2019; Juhlin et al., 2016; Juhlin & Lund, 2011; Koivisto et al., 2012; Lucas et al., 1994; White et al., 1994). The presence of faults or other local features (e.g., ore bodies) often generate diffraction patterns in the seismic data, which can be used for their identification (Malehmir & Bellefleur, 2009; Milkereit et al., 2000; Markovic et al., 2020). Challenges to image the faults are caused by the inherent low reflectivity deriving from the absence of strong impedance contrast, and on the potentially high dipping fault planes, that violate the basic assumption of sub-horizontal structures of the seismic reflection method (Yilmaz, 2001). A steeply dipping structure reflects the seismic wavefield farther on the downdip direction respect to the updip direction (Figure 2.4). Therefore, when a priori information is available and acquisition in the downdip direction is needed, a longer offset is required to record this kind of structures. Migration methods should be applied during the processing to correct the position of the reflectors, but they will not compensate for structures that are not recorded at all (e.g., wrong acquisition setups or sub-vertical structures).

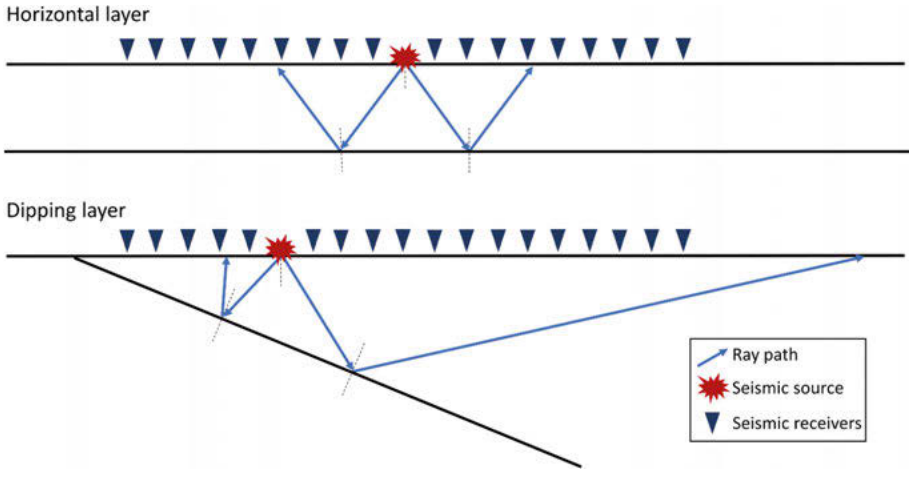

Figure 2.4. Simplified seismic reflection ray path geometries for a horizontal and a dipping layer. Note the symmetrical ray paths spreading in both directions for horizontal layers. In contrast, ray paths for dipping layers spread with larger offset on the downdip direction compared to the updip direction.

2.1.4 Urban environment and crooked profiles

The studies of this thesis are at least partially acquired in urban environments, which often pose challenges such as high electromagnetic and seismic noise, as well as limited access due to infrastructure (e.g., roads, bridges, buildings). Despite these obstacles, adapted geophysical methods like borehole drilling and 2D/3D seismic reflection surveys can be effective. (Adly et al., 2017; Ishiyama et al., 2016; Ma & Qian, 2020; Maggio et al., 2022; Malehmir et al., 2011; Sato et al., 2009; Zoback et al., 2010).

Three main challenges in urban active seismic acquisition are: (1) selecting a suitable source, (2) optimizing receivers, and (3) deploying equipment within human structures. Advances in seismic technology help address these issues.

The active source must be powerful enough to overcome the high background noise, but at the same time the integrity of surrounding infrastructures should be ensured. This removes the choice of explosive (too strong) or weight drop (too light) sources and promotes the use of seismic vibrator trucks (10-20 t in weight) for large-scale acquisitions (Figure 2.2a). Receivers should be compact, well-coupled (e.g., long and thin spikes), and wireless to avoid obstructing roads and pedestrian areas (Figure 2.2b). Digital sensors (e.g., MEMs) help suppress electromagnetic noise (Tellier & Lainé, 2017).

Urban survey profiles must be flexible, adapting to permissions and obstacles like roads and rivers. This often results in crooked profiles, where midpoints often lay on large distributions outside the profile line. If subsurface structures vary perpendicularly to the profile (e.g., dipping horizons),

reflections from different depths mix (Figure 2.5), causing artefacts from out-of-plane structures and reducing reflection continuity if not accounted for during the processing of the data (Nedimović & West, 2003). However, with proper processing, crooked profiles can provide valuable cross-dip information (Wu, 1996).

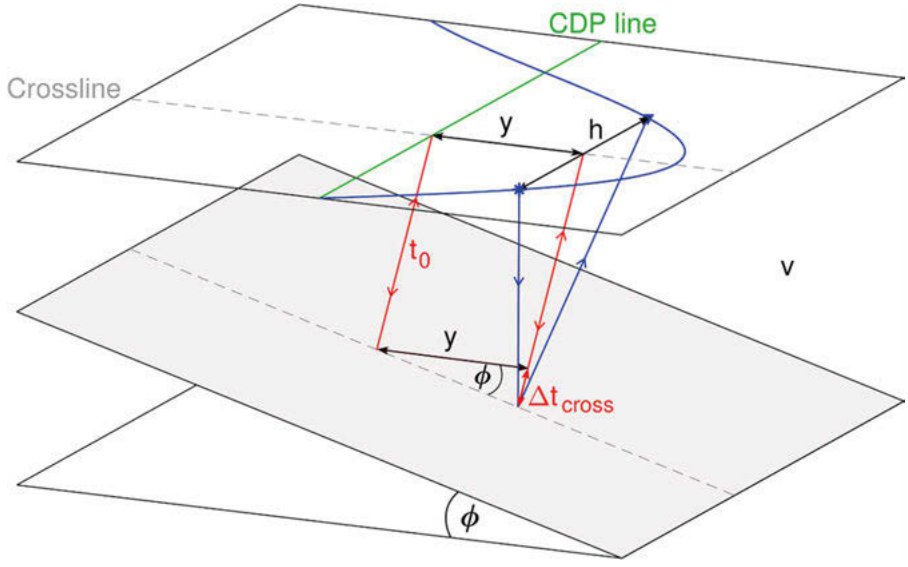

Figure 2.5. Ray geometry for a crooked-line data acquisition above a cross-dipping reflector. y denotes the cross-offset, h the offset between shot and receiver, ϕ the cross-dip angle, v the medium velocity and t_0 the zero-offset traveltime for a ray without cross-offset (Beckel & Juhlin, 2019).

2.1.5 Converted waves

Continuous innovation in prototyping enables cost-effective, simultaneous acquisition of diverse seismic data, enhancing reflection seismology through integrated analysis. Multicomponent (3C or 9C) seismic data acquisition has grown significantly in the past decade (Brodic et al., 2018; Pertuz & Malehmir, 2023b) enabling improved understanding of wave propagation phenomena, wave conversion and inferred properties of the media such as V_P, V_S and anisotropy (Carr et al., 1998; Hardage & Wagner, 2014a, 2014b; Krawczyk et al., 2013a; Yilmaz, 2021). Traditional seismic surveys record only the vertical (V) component, primarily capturing P-waves, while multicomponent acquisition also records the radial (HR) and transverse (HT) components, providing S-wave information for a more complete seismic wavefield. The S-waves recorded can be the result of two different wavefields (Kearey et al., 2002). The P-wavefield interaction with each subsurface interface generates both transmitted and reflected P- and S-waves, with the S- converted wavefield referred to as the PS-wavefield. The S-waves generated

directly at the source position also interact with each subsurface interface, producing both transmitted and reflected P- and S-waves, with this S-wavefield referred to as the SS-wavefield (Figure 2.6).

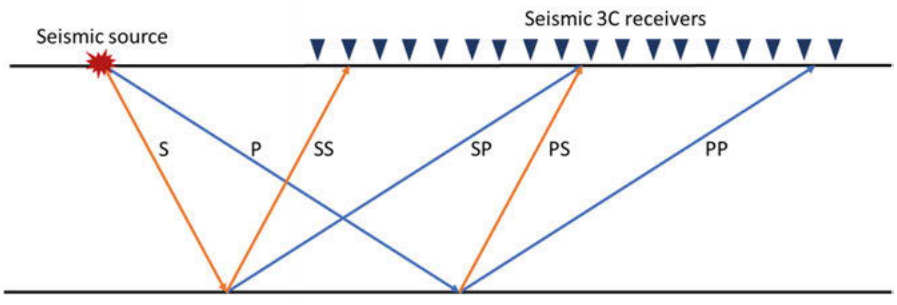

Figure 2.6. Simplified seismic reflection ray path geometries for a source exciting P- and S-waves in a solid media. The seismic source simultaneously generates a P- and an S-wave, when these two waves encounter a discontinuity, they will both generate a P- and an S-wave, resulting on a total of four reflected waves.

For 3C acquisitions usually the receivers are 3C and the source is 1C in the vertical direction because of the difficulty of generating horizontal solicitations, while in the case of 9C acquisition both the receivers and the source are 3C. Research shows that vertical sources generate S-waves based on source-ground coupling and shallow subsurface elastic properties such as V_P and V_S (Brodic et al., 2018; Hardage & Wagner, 2014a, 2014b; Miller & Pursey, 1954; Pertuz & Malehmir, 2023a; Pugin & Yilmaz, 2017). In particular, V_P/V_S controls how much of the energy that is transmitted into S-wave from a vertical source (Pugin & Yilmaz, 2017). This unintended energy dispersion enables SS-wave acquisition without dedicated S-wave sources, reducing related costs of acquisition. S-wave imaging, with lower velocities than P-waves, offers higher-resolution subsurface images if similar frequencies are acquired (Carr et al., 1998; Krawczyk et al., 2013a), benefiting near-surface studies like engineering and hydrological investigations (Bharadwaj et al., 2017; Brodic et al., 2018; Krawczyk et al., 2013b; Malehmir et al., 2016). Nevertheless, S-wave data processing has different challenges compared to the known and well-established P-wave data processing workflows and requires more studies and development. Converted PS- and SP-waves follow asymmetric ray paths due to the different downgoing and upgoing velocities that do not reflect at the midway source-receiver point for horizontal reflectors. These wave modes can also be processed for seismic imaging (Sun et al., 2022), but they are beyond the scope of this thesis. Hodograms are a 3D plot of the 3C signal recorded at a single location. This plot is used to show the particle motion in a 3D space and thus helps to determine the type of signal (e.g., P- or S-waves).

2.2 Seismic risk and its mitigation

Earthquakes occur because of ruptures and movements in the crust (hypocentre) that generate energy which can propagate to the surface (epicentre) and cause its displacement. The ground displacement, the size of the affected area and the repeated occurrence over time contribute to the definition of seismic hazard. Seismic hazard is part of the earth history, and it is independent from the presence of humans. In contrast, seismic risk is the relation between seismic hazard and human vulnerability and is therefore strongly related to the presence of humans and human structures (Wang, 2009). Nothing can be done to decrease seismic hazard, but work must be done to decrease seismic risk. The first step to decrease seismic risk is to evaluate seismic hazard in the area of interest, as for example areas where high seismic risk can be expected. This will help preparedness and city-planning in accordance with the seismic hazard of the area, decreasing the seismic risk.

In order to estimate seismic hazard, it is important to know the seismicity history of a region and in particular to know the largest seismic events that occurred in that area. These large seismic events rarely happened in historical time and thus there is often no record of them. To compensate for this lack of information it is possible to study the effects left on the ground from past seismic events. When earthquakes propagate in the ground, rupture zones denominated as faults appear to accommodate the ground displacement. Therefore, faults are strongly related to earthquakes and to their intensity and studying them helps gather information on the past seismicity of a region (Rosenblueth & Ordaz, 1990; Singh et al., 1980; Wells & Coppersmith, 1994). Rupture parameters such as length and displacement are related to the earthquake's size and can be estimated through different relationships and equations that evolved during the years (Leonard, 2010; Rosenblueth & Ordaz, 1990; Singh et al., 1980; Wells & Coppersmith, 1994). Geophysical methods, in particular reflection seismology, can provide information unavailable at the surface, such as the in-depth geometry of fault structures, and therefore contributing to seismic hazard estimation (ANCORP Working group, 1999; Chen et al., 2018; Feng & McEvilly, 1983; Ito, 1999; McBride et al., 2002; Stefatos et al., 2002).

2.3 CCS overview

CCS methods consist in sequestrating part of the CO_2 from the atmosphere to store it in the subsurface in a safe and stable location. Typically, the geological formations examined for CO_2 storage require a geological trap such as exploited reservoirs of oil and gas (White et al., 2004), deep coal deposits or deep saline aquifers (Ringrose et al., 2021). In addition to these, another type of storage exploits the reaction of CO_2 with raw minerals known as carbon capture and mineral carbonation (CCMC). This process commonly uses basalt

rocks as deposits. Globally a total of 13,000 Gt of CO_2 storage resources is estimated to be available (Dziejarski et al., 2023), with the migration of CO_2 to the surface as the most important safety concern (Mabon et al., 2014).

In this thesis, only deep saline aquifers are investigated as deposits for CO_2. The expected trap structures in the studied deposits are four-way-closure domal structures. For favourable CO_2 storage conditions, CO_2 should be kept in its supercritical state, and thus, deep saline aquifer reservoirs must be at least 800 m deep and under a formation pressure of 7.39 MPa or more (Forbes et al., 2008; Musarra et al., 2022; Smith et al., 2012). Furthermore, the reservoir needs to be sealed to prevent any migration to the surface. Miocic et al. (2016) show that faults and associated fracture networks are the only migration path observed in natural CO_2 reservoirs with upward migration occurring mainly along fractures and faults that are conductive to fluid flow (Frery et al., 2015). Therefore, CO_2 migration is spatially restricted to fault zones, making CO_2 retention completely secure when the reservoir is spatially trapped without intersecting faults. For this reason, the main concern during site investigations and mapping of CO_2 reservoirs is to identify faults and fractures (e.g., Iding & Ringrose, 2009). To effectively identify these features, a high-resolution image on a wide scale is required. Obtaining subsurface images on a wide scale may be challenging since the acquisition setup is often designed to optimize the image at a specific target depth, limiting CCS onshore exploration works and seismic surveys in the past years (Mabon et al., 2014). Time-lapse reflection seismic acquisition can be used for monitoring CO_2 migration during the injection phase (Pawar et al., 2015; White, 2013), ensuring a safe exploitation of the reservoir.

2.4 Geology of the sites

2.4.1 South Korea

Papers I and **II** are from South Korea, north of Seoul city (Figure 2.7)

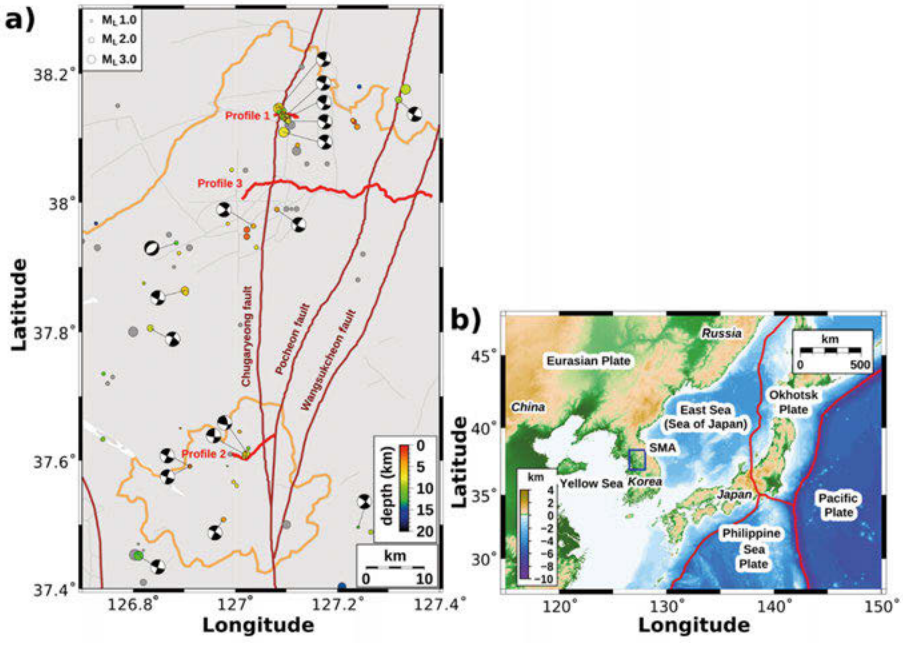

Figure 2.7. (a) Recent seismicity recorded in South Korea and the location of the seismic profiles acquired for **Papers I** and **II**. Profile 3 crosses the three major fault systems with the aim to reconstruct their geometries at depth. The orange contours highlight Seoul city and the national border. (b) Major plate boundaries surrounding the study region.

The Korean peninsula is characterized by three major Paleoproterozoic massifs (lithotectonic domains), Nangrim, Gyeonggi, and Yongnam, separated by the Imjingang and Ogcheon belts (Chough et al., 2000). The northwestern margin of the Gyeonggi massif corresponds to the location of **Papers I** and **II**. The Gyeonggi massif crosses the central part of the Korean peninsula from west to east. Granitic, gneissic, and basaltic rocks from Paleoproterozoic to Cretaceous are the main lithologies constituting the massif. In addition, basalts and fluvial deposits of Quaternary age are also present. Major crustal-scale fault systems from Palaeozoic to Quaternary crosscut the Gyeonggi massif showing evidence of four main deformation phases (Bae & Lee, 2016; Choi et al., 2012). The first deformation phase occurred in the Late Permian-Early Triassic with a main N-S compressional stress. In Middle-Late Triassic an extensional phase still in the N-S direction resulted in ductile shear and normal faulting of the crust. In Middle-Late Jurassic a NNW-SSE compression caused

NW-dipping thrust systems. Finally, the last phase shows evidence of tectonic activity during the Quaternary and is characterized by N-S to NNE-SSW right strike-slip faults associated with NNW-SSE folds and by different Cretaceous basins. The three fault systems that are the focus of these seismic surveys (Chugaryeong fault, Pocheon fault and Wangsukcheon fault in Figure 2.7) are related to the last deformation phase, that is suspected to be still active (KIGAM, 2008). In particular, the Chugaryeong fault seems to be related to recent seismic clusters suggesting a dependence on the current stress field (Hong et al., 2021). During the last decades, several projects have studied these faults, working on their kinematics, geometries and evolution over time. Results from these studies showed that the Chugaryeong fault is likely sub-vertical, the Pocheon fault WNW dipping and the Wangsukcheon fault ESE dipping (Han & Lee, 2019). However, most of the faults in this region show a poor exposure on the surface, limiting geological and geomorphological studies. The studied area is also rich in natural hot springs, suggesting important geothermal activity of the region (Lee et al., 2010).

2.4.2 Denmark

Papers III-VI are from onshore Denmark. Stenlille and Havnsø sites are located in Zealand island while Gassum is located in Jutland (Figure 2.8).

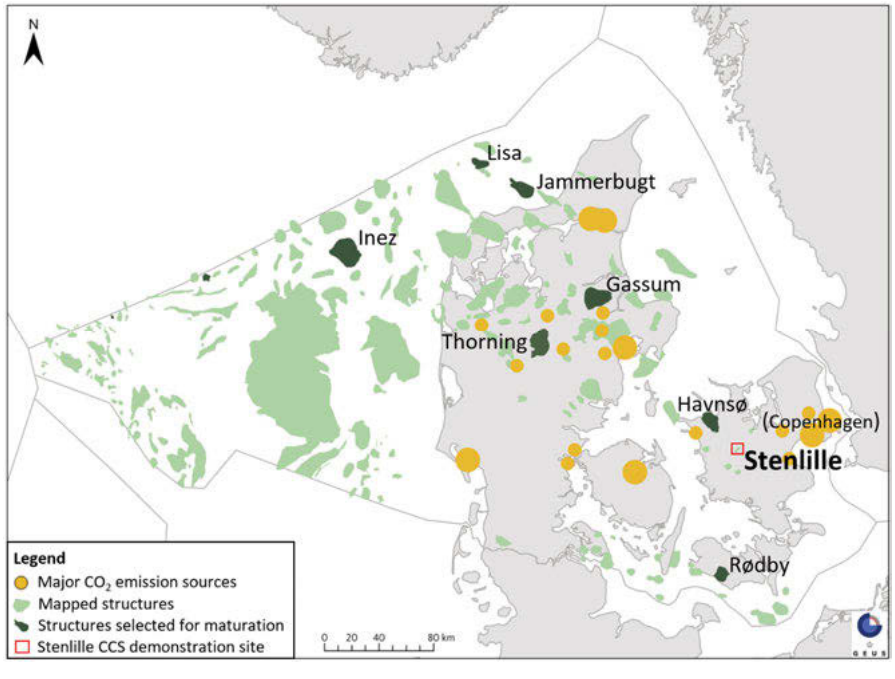

Figure 2.8. Map of Danish structures with potential for geological storage of CO_2. The dark green structures are target of the GEUS' CCS project during 2022-2024 (Gregersen et al., 2023a).

The Danish mainland is located in the Danish Basin corresponding to the eastern part of the Norwegian-Danish Basin. The deep structure of the basin is well known (Gregersen et al., 2023a) and presented in Figure 2.9. A deep crystalline basement and the sedimentary successions from the Cambrian to Lower Permian age underlie the Danish Basin. During the late Permian time mainly evaporites were developed, forming the Zechstein Group while in the Triassic a thick clay and mud-dominated succession deposited with minor sandstones layers, such as the Bunter Sandstone. The widely distributed Gassum Formation formed during the Late Triassic- Early Jurassic time and it consists of alternating sand-rich and clay-rich layers. The latest Triassic to earliest Jurassic time witnessed the deposition of clay-dominated successions with presence of silty and sandy layers. Mainly mudstones successions were deposited during the Early Cretaceous in the Rødby Formation, followed by the chalk of the Chalk Group during the Late Cretaceous. The basin was subjected to normal faulting caused by the Carboniferous-Permian rifting and to structure associated faults caused by the salt mobilization resulting from the Middle-Late Jurassic regional uplift (Gregersen et al., 2023a).

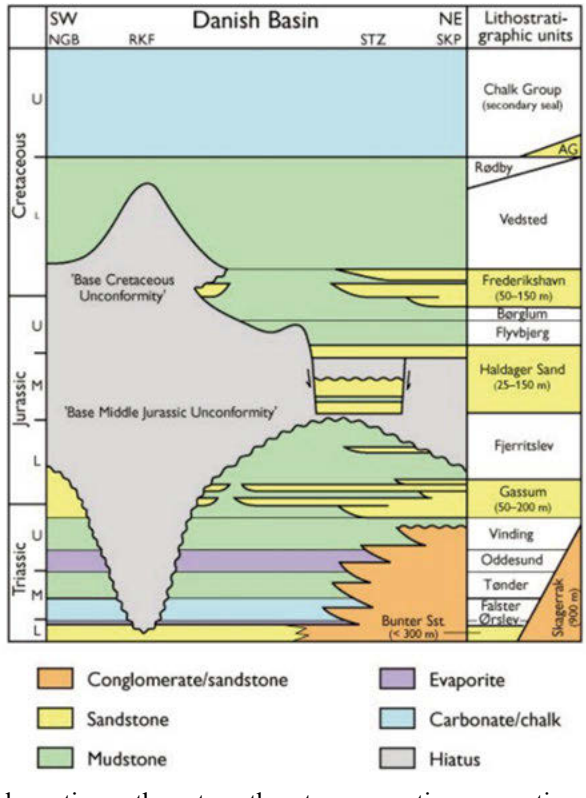

Figure 2.9. Schematic southwest-northeast cross section presenting the stratigraphy of the Danish Basin. AG, Stratigraphic position of the Arnager Grønsand Formation; NGB, North German Basin; RKF, Ringkøbing–Fyn High; SKP, Skagerrak Platform; STZ, Sorgenfrei–Tornquist Zone (Nielsen et al., 2004).

The salt mobilization underlying the largely extended deep saline aquifers of the Danish Basin generated several four-way-closure domal structures in the Danish territory. Many of these structures were identified and selected from legacy seismic data, both offshore and onshore, as possible CO_2 reservoirs in the CCS2022-2024 project (Hjelm et al., 2020) and as target for new subsurface investigations (Figure 2.8).

Previous acquisitions in Denmark consist mainly of 2D seismic reflection profiles from the 1970s and 1980s with usually poor quality and low resolution (Larsen et al., 2003, 2006; Gregersen et al. 2020). For the new onshore exploration in 2022 and 2023, 45 2D reflection seismic profiles over five different sites were acquired and processed for a total length of approximately 650 km (Abramovitz et al., 2024; Malehmir et al., 2024; Westgate et al., 2025; **Papers III-V**). The five sites are, in order of acquisition, Stenlille, Havnsø, Gassum, Rødby and Thorning (Figure 2.8). The expected subsurface stratigraphy and structures are similar, and the target reservoir is the Gassum Formation in all sites except Rødby. In the Rødby area, the Gassum Formation is shallower than the minimum 800 m of depth required for CO_2 to be in a supercritical phase (Forbes et al., 2008), and thus the deeper Bunter Sandstone Formation is the target reservoir. Primary seals are the Ørslev Formation for the Rødby site and the Fjerritslev Formation for the other sites.

The first site (**Paper III**) is close to the town of Stenlille (Figure 2.8). In this area, a small domal structure has been used for decades as a natural gas storage and has been extensively studied with several geophysical surveys including boreholes (Stenlille-19 borehole in Figure 2.10) and a 3D seismic dataset (Gregersen et al., 2023a). This site is the smallest and has been the pilot site to test the acquisition setup and define the most appropriate parameters for the desired target. The Gassum Formation is located at a depth of around 1500 m below sea level and has an estimated storage capacity in the order of 6-10 million tons of CO_2 (Gregersen et al., 2023a). The study area of **Papers IV** and **V** is close to the town of Havnsø in the northwestern part of Zealand (Figure 2.8). The Havnsø domal structure is the main target of the seismic survey. The Gassum Formation is located at a depth of around 1600 m below sea level and has an estimated storage capacity in the order of 35-65 million tons of CO_2 (Gregersen et al., 2023b). The dataset used in **Paper VI** was acquired nearby the town of Randers in the Gassum area (Figure 2.8), with focus of the processing on near-surface structures at less than 50 m of depth.

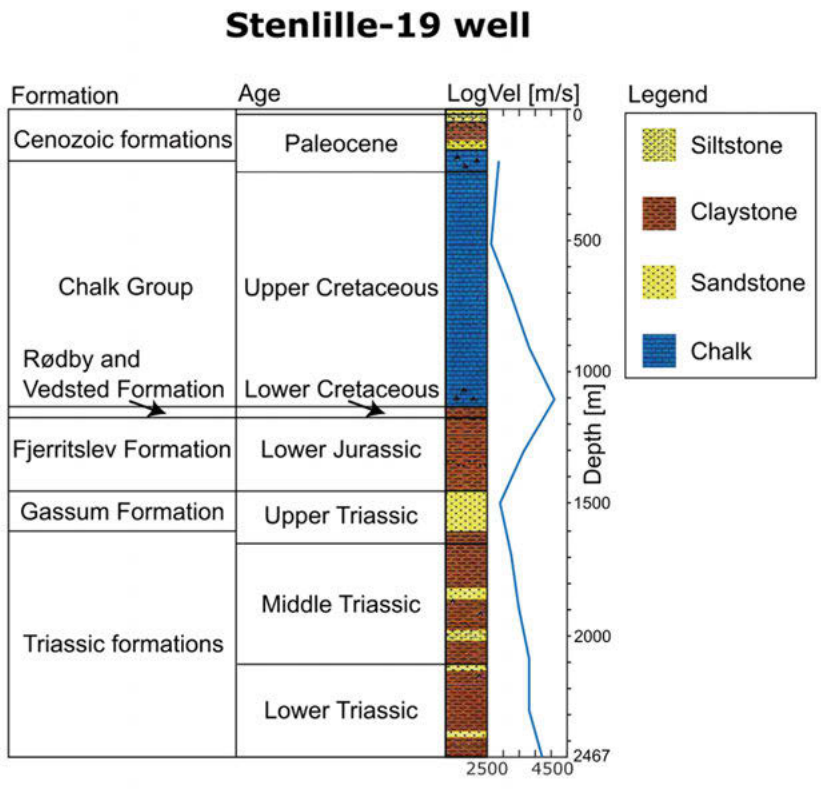

Figure 2.10. The Stenlille-19 well stratigraphic reconstruction and average velocities from the sonic log, simplified from Schokker (2001), showing the target reservoir (Gassum formation) and the primary seal (Fjerritslev Formation) at Stenlille site.

3 Methodology and data acquisition

3.1 Dual-element acquisition system

The application of a dual-element acquisition system, combining a landstreamer and a nodal array (Figure 3.1), ensures flexibility for urban environments while enabling simultaneous high-density and long-offset data acquisition useful for high-resolution imaging and deep reflection retrieval.

The landstreamer, equipped with MEMS sensors mounted on sledges, ensures stable coupling on roads and records 3C acceleration from 0 to 800 Hz, allowing high-resolution data acquisition, multicomponent seismic analyses and electromagnetic noise insensitivity (Tellier & Lainé, 2017). The modular design, with 40 m segments of 20 sensors, allows rapid adaptation to field conditions (Brodic et al., 2015), with spread lengths ranging from 40 to 240 m and a sampling rate of 1 ms for this thesis. The source drags the landstreamer parallel to the nodal array during the shooting sequence in an end-on spread geometry (Figure 3.1).

The nodal array consists of wireless receiver sensors connected to 10 Hz vertical geophones. The use of nodal sensors removes the need of cables, allowing long-profile deployment with minimal obstruction. The profiles presented in this thesis employed 20 m nodal spacing and 1 ms sampling rate for **Papers I** and **II** and 10 m nodal spacing and 2 ms sampling rate for **Papers III-VI**, depending on the target depth and on the expected wave propagation velocities. The maximum recorded offset varies with the different profiles reaching up to 8 km in **Paper IV**. The nodal array is deployed using an asymmetric split-spread fixed geometry or a roll-along geometry for longer profiles.

In this thesis, seismic sources included two 9 t vibrator trucks with an additional 3 t mass each (Figure 3.1), producing 95 kN per vibrator and reaching up to 10 km depth. The two sources were operated in a phase-synchronized mode, to avoid distortion and asynchronous vibration, at most of the nodes' positions with the shot position assigned in between the two seismic vibrators. A linearly increasing sweep with frequencies of 10-140 Hz and a length of 16 s in **Paper III** and 18 s in the other studies was repeated three to four times per shot position.

The coordinates of the receivers' positions for the nodal array were acquired with a decimetre accuracy DGPS system. The landstreamer receiver positions were interpolated from the nodal coordinates, assuming overlap of

the two profiles, to overcome the challenges resulting from its continuous movement during the acquisition. While not rigorously accurate, this approximation proved robust across the different study areas. However, starting from an incorrect assumption this method inherits inaccuracy in the location of the receivers proportionally to the distance between the two recording profiles. In **Paper VI** an alternative method is tested where, for every shot, the DGPS position is sampled at four evenly spaced locations while the remaining sensors' locations are interpolated from them. The resulting coordinates appear more accurate with respect to the previous method, but their manual acquisition is time and cost inefficient and more studies are still in progress.

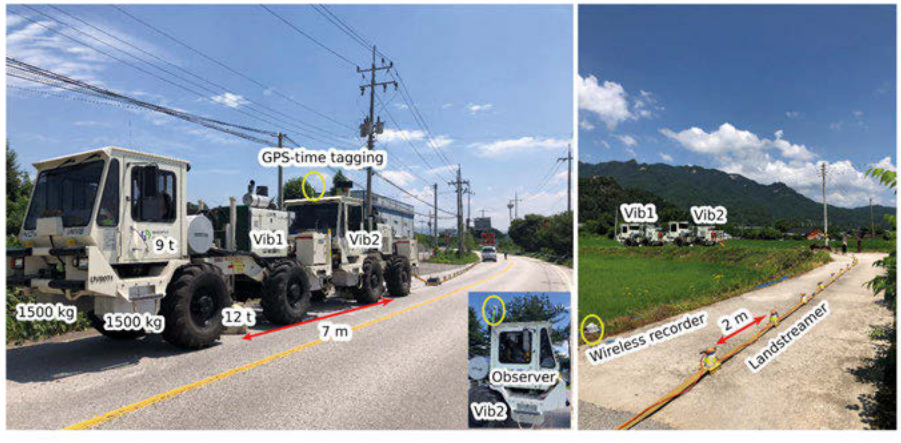

Figure 3.1. Field photos, from South Korea campaign, exemplifying the seismic source and receivers of the dual-element acquisition system.

3.2 Combined onshore and offshore acquisition

During data acquisition over the Havnsø structure (**Paper IV**), there was an interest in revealing the subsurface structures underlaying a marine channel, where the northern closure of the domal structure is expected just offshore of Havnsø coast (Figure 2.8). The marine channel along the profile is approximately 3 km long and has a maximum depth of around 8 m. The shallow sea and the presence of a small island (Nekselø island) in this area renders offshore acquisition challenging, while environmental and marine life restrictions (Natura2000 zone from Council Directive 92/43/CEE) forbid the use of a marine source. To overcome these limitations a combined onshore and offshore acquisition was applied where two marine recording systems were added to the onshore dual-element acquisition (Figure 3.2). Exploiting the strategic presence of Nekselø island, the onshore profile was deployed on both sides of the marine channel with the nodal array covering 4 km on Zealand

island and 2 km on Nekselø island. The landstreamer was deployed with three segments (120 m) on Zealand island and removed due to prohibiting road conditions on Nekselø island, after some of the southernmost shot points acquired with two segments (80 m). This onshore setup recorded the domal structure beneath both islands and, via cross-shooting, its deep portion below the marine channel. It is important to note that the absence of a marine source does not allow recording inside the channel for events located at less than approximately 1000 ms.

Along the marine channel a marine streamer and 18 OBSs were deployed to link the onshore profile. The marine streamer was deployed on the seafloor from Havnsø town towards the centre of the channel for 600 m (Figure 3.2), equipped with 96 receiver groups formed by seven hydrophones. The OBSs, equipped with hydrophones and 3C geophones, were deployed along the whole marine channel with an uneven spacing (Figure 3.2). During the deployment, OBS coordinates were acquired via DGPS, while marine streamer coordinates were interpolated between DGPS-measured start and end points, assuming a straight path. Both marine systems recorded at 1 ms sampling rate, improving signal recovery from shallow events and reducing data gaps where onshore CMP fold coverage was zero.

The shooting was carried out in two days, the first day for 2 km on Zealand island and the following day for 2 more km on Nekselø island, with source positions corresponding to the node positions. While shooting on Nekselø island part of the nodal sensors from the following profile (P2 in Figure 3.2) were already recording, increasing the fold coverage in the marine channel. Note that during these shots different OBSs encountered technical problems.

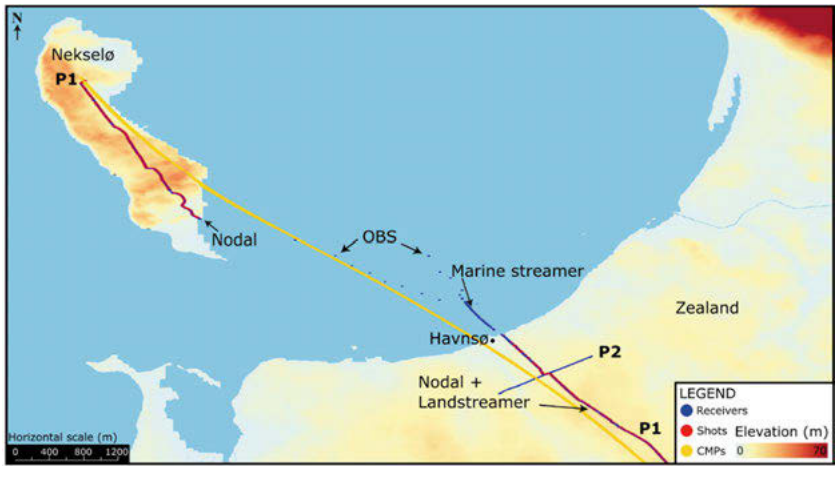

Figure 3.2. The marine channel acquisition setup on the northern part of profile 1 (P1) between the Havnsø town and Nekselø island. In red are the shot positions; in blue are the receiver positions with labels indicating the type of sensors; and in yellow are the adopted CMP positions for the final stack. The offshore areas are shown in light blue.

3.3 Processing and merging of the seismic datasets

After acquiring the datasets, optimizing their processing based on the desired output is crucial. While each dataset required a customized workflow, the overall processing flow remained consistent, with refinements for similar cases. The crookedness of the profiles was compensated during geometry definition using smooth CMP stacking profiles and large perpendicular bin sizes. This reduced strong curvature effects but increased out-of-plane reflections, which were negligible for sub-horizontal structures but required compensation for dipping structures.

Data from **Paper II** show low reflectivity and complex structures because of the hard-rock environment, the complex tectonic history, and the highly-populated area. On the nodal array dataset most of the processing was focused on increasing the reflection coherency and the S/N, with different steps of the processing flow applied on receiver gathers which showed higher reflection continuity compared to shot gathers. The landstreamer dataset was used to image the bedrock reflection that, due to its strong reflectivity, required the application of a basic processing flow. The two resulting migrated sections were merged in the post-stack domain, with the landstreamer section considered down to the bedrock depth and the nodal array section considered for the deeper portion.

The datasets from **Papers III** and **IV** showed strong reflectivity, typical of sedimentary basins, and high levels of urban noise. The processing for these studies is mainly aimed at removing ringing effects and coherent noise (e.g., vehicle noise). These datasets required detailed velocity analysis due to the layered structure, with the nodal array more sensitive to velocity variations than the short-offset landstreamer. To gain the benefits from all datasets, a pre-stack merging is applied in these studies, requiring analysis of the different acquisition domains (pressure, velocity and acceleration) and extra processing for balance. After separately processing the datasets, geometries and headers were set to be coherent, and the processed shot gathers merged. An AGC function was applied for amplitude coherency and spectral balancing to homogenize the frequencies. The resulting shot gathers showed traces with comparable signal features and continuity of the reflections between the different sensors. Velocity analyses and residual static corrections were iterated on the merged shot gathers resulting in a single, comprehensive section after stack.

Paper VI focuses on the landstreamer data for multicomponent near-surface studies. After evaluation of the three-component data, P-wave processing was applied to the V component data and S-wave processing to the HT component data. The identified shallow S-wave reflection is similar in velocity and arrival times to the recorded surface-waves, making the discrimination between the two waves challenging during velocity analysis and the successive stack. To bypass this problem a reflection-picked moveout correction

comprehensive of refraction and residual static corrections was developed and applied, replacing the traditional NMO correction.

3.4 Complementary analyses

To increase confidence in the results and add helpful information for the interpretation process of seismic data, it is often useful to consider analyses that complement the traditional seismic migrated sections. Such additions have been applied in **Paper II**, where the continuity of the reflections in the migrated section was low and not always clear, and on **Paper VI**, to validate the proposed approach and to complement the geological interpretation.

3.4.1 Velocity analysis

There are different types of seismic velocities that can be estimated from seismic data. In the case of obtaining a stacked section, an NMO velocity analysis has to be performed. The NMO velocity depends on the velocity from the reflection layer and from all media above it, but do not correspond to the real medium velocity of the reflected layer.

In **Papers II** and **VI** a first-break traveltime tomography was applied to the data. This method reconstructs the ray paths of the seismic waves measured in the first arrivals to estimate the subsurface velocities (Figure 3.3). Specifically, a diving-wave finite-difference based code (Tryggvason et al., 2002) was used for this thesis. The tomography was run on the nodal array data because of the longer offset and higher fold coverage compared to the land-streamer data, ensuring a stable inversion and a deeper ray penetration (Figure 3.3). The inversion was run on a 3D grid while the results were projected on 2D profiles to match the seismic 2D sections. The cell sizes were chosen between 5 and 20 m according to the desired target resolution and the resulting computational times. This method relies on a reasonable starting model and therefore different starting models were tested during the analyses to evaluate the presence of artefacts. To estimate the accuracy of the inversion, an RMS error was computed, indicating the mismatch between the measured and the estimated arrival times. In this thesis RMS values between 3 and 6 ms are achieved.

The last velocity estimation method used in this thesis (in **Paper VI**) is a surface-wave LCI method. This approach is valid for S-wave velocity estimation from surface-wave analysis. The fundamental modes of surface-wave dispersion curves were picked and inverted using an LCI (Socco et al., 2009). For this method, physical properties of the subsurface have to be inferred from other sources (such as Poisson's ratio) resulting in a lower accuracy of the estimated velocity values compared to the tomography analysis. In-depth information of the surface-waves are dependent on their wavelength and

frequency content, and their results are usually limited to the near-surface. For **Paper VI**, reliable results are achieved down to a depth of 30 m.

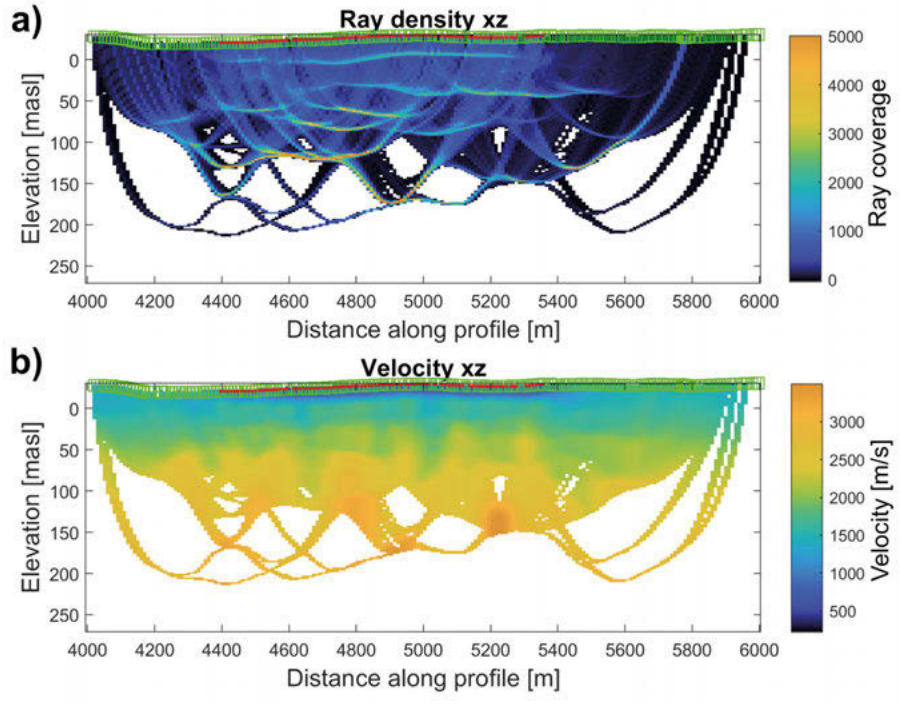

Figure 3.3. Example of first-break traveltime tomography with (a) ray density coverage and (b) resulting estimated velocity model (example computed from **Paper VI** data). Red dots correspond to the source positions and green squares to the receiver positions.

3.4.2 3D cross-dip analysis

To account for the midpoint spread typical of crooked profiles, the selected CMP geometries should consider a large perpendicular bin size. In the case of dipping subsurface geometries, this approach may introduce artefacts in the data from out-of-plane reflections, and this effect needs to be compensated during the seismic processing (e.g., Koivisto et al., 2012). To compensate for reflections resulting from out-of-plane reflectors, a 3D cross-dip analysis was applied on **Paper II** of this thesis. The applied method corrects the reflection arrival times for different dip angles considering a 3D geometry of the horizon. The angle that maximizes the reflection signal coherency will correspond to the dipping angle of the reflector (Beckel & Juhlin, 2019; Bellefleur et al., 1995; Heinonen et al., 2013; Malehmir et al., 2009; Rodriguez-Tablante et al., 2007). In **Paper II** this correction was applied to the recorded central

reflectivity identifying a cross-dip angle of 10° towards the north and delineating a fault-bend fold structure (Figure 3.4).

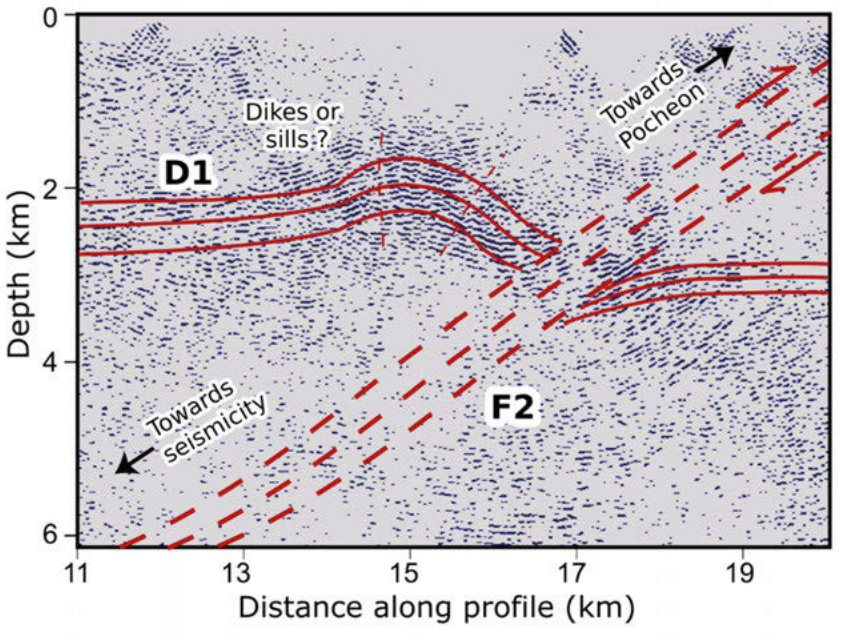

Figure 3.4. Central portion of the migrated stacked section of **Paper II** after 10° cross-dip correction towards the north, illustrating a possible fault-bend-fold structure.

3.4.3 3D reflection traveltime modelling

Traveltime modelling of a reflection can be used to extract information regarding the corresponding reflector such as strike and dip angles. However, to be able to model a reflection, prior information about the reflector geometry and the media are required or should be estimated. When a dipping reflector projects to the surface along the recorded profile it defines an extra geometry constraint, this enables the traveltime to it to be modelled according to Ayarza et al. (2000). This 3D reflection traveltime modelling works in a relatively simple two layer environment with a planar reflector. The modelling requires the definition of the first layer velocity and the distance at the surface between the source and the reflector to estimates its dip and strike.

In this thesis, the described 3D reflection traveltime modelling is applied in **Paper II** on a shallow dipping reflection identified as F1. The first layer velocity was estimated from the first arrival times in the receiver gather (blue line in Figure 3.5). The reflector strike and dip angle were defined in the forward modelling to match the reflection (red line in Figure 3.5) giving us the solution for the in-depth horizon geometry. Incorporate geological knowledge of the area to restrict the possible geometries makes the result quicker and

robust for the geological interpretation. The reflection modelled in this thesis corresponded to an estimated N20E/60E (strike of 20 degrees from the north and dip of 60 degrees towards east) reflector.

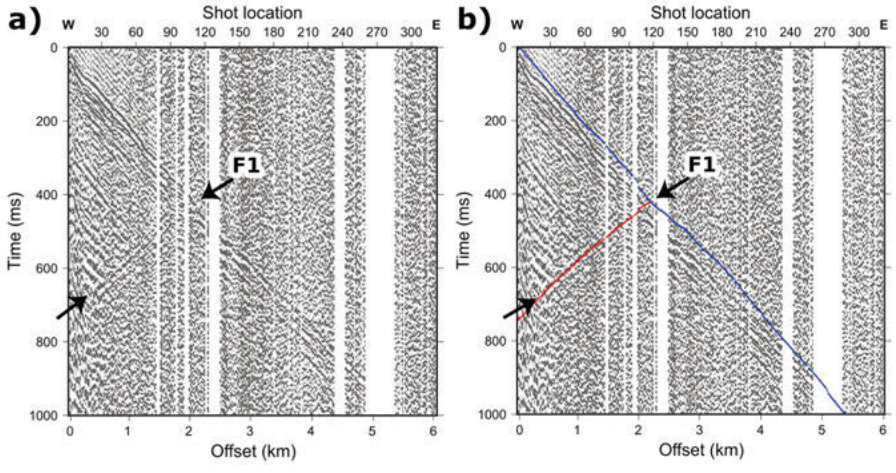

Figure 3.5. 3D reflection traveltime modelling for the F1 reflection observed in **Paper II**. (a) A receiver gather at the easternmost part of the profile where the F1 reflection is observed and the corresponding (b) reflection traveltime (red) for a planar feature of N20E/60E geometry. Blue line shows the direct arrivals calculated and used for the media above the planar feature.

3.4.4 Surface-wave back-scattering

The data acquired in **Paper II** show characteristically back-scattered surface-waves that are an indication of strong lateral variations. Therefore, the method by Zerwer et al. (2005) as implemented by Colombero et al. (2019) was applied to the data to identify sharp lateral variations in the near-surface and estimate their location along the profile and their relative maximum affected wavelength. This method is based on two observations: Rayleigh waves do not propagate behind sharp lateral changes; strong Rayleigh waves are reflected back from sharp lateral changes. This implies a pick of energy on Rayleigh waves at locations with sharp lateral changes and down to the depth of the lateral variation, or down to the deepest propagation of the Rayleigh waves dependent on its wavelength and frequency content. These sharp changes are caused by horizontal discontinuities such as underground artificial constructions, steps in the topography (e.g., cliffs) or geological structures (e.g., dikes or faults). The resulting strong lateral variations detected in this data (Figure 3.6) matched with the back-scattered surface-wave locations identified in the receiver gathers. Two of these locations appear particularly strong, one corresponding to the mapped sub-vertical Chugaryeong fault while the other probably corresponding to a mapped sharp geological boundary. The maximum

affected wavelength of around 100 m (arrows in Figure 3.6) distinguishes these surface-wave back-scattering features from human construction origins such as road or bridge foundations and confirms their geology-related origin.

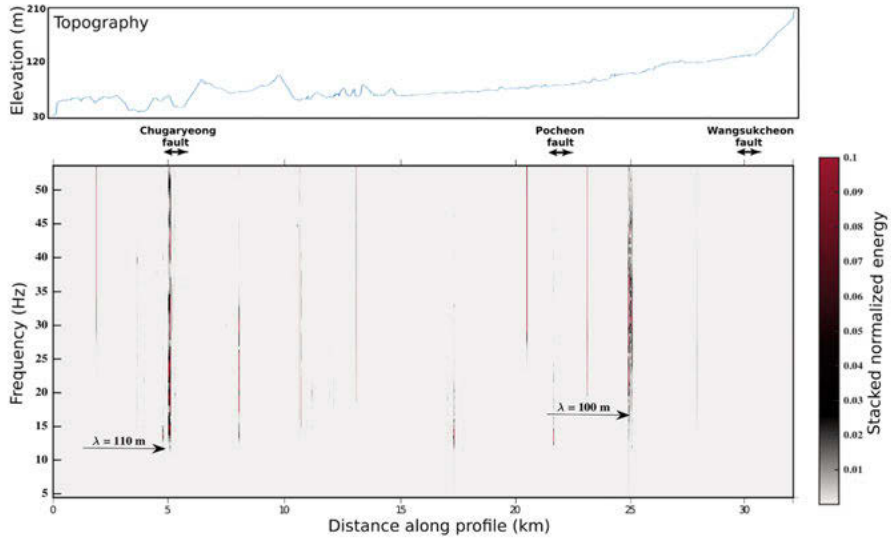

Figure 3.6. Energy from back-scattered surface-waves along the profile of **Paper II** with correspondent profile topography. Most of the points are related to sharp lateral variations and may imply faults or geological contacts, as well as sharp topography. Arrows point the minimum related frequency, hence the maximum related wavelength, of the two strongest events. The high wavelength value allows to exclude human related origins for the surface-waves back-scattering energy.

4 Summary of papers

Among the papers of my PhD work, I chose four papers to summarize in this chapter as best representative of the evolution of the onshore dual-element acquisition system processing and as examples of its wide range of applications in addressing contemporary challenges.

4.1 Paper II: Crustal-Scale Fault Systems in the Korean Peninsula Unraveled by Reflection Seismic Data

Following a previous project targeting seismicity clusters (**Paper I**), the objectives of **Paper II** were to image and interpret crustal-scale fault systems and their possible relation with the local seismicity to improve the seismic risk knowledge of the area (Leonard, 2010; Rosenblueth & Ordaz, 1990; Singh et al., 1980; Wells & Coppersmith, 1994). The hard-rock geological setting and the highly populated area resulted in a challenging environment for the reflection seismic method. However, the adopted dual-element acquisition system and the applied processing and analyses made it possible to obtain a partial reconstruction of the fault systems of interest and the identification of a fault-bend-fold structure.

4.1.1 Synopsis

The study area of **Paper II** is located in South Korea, and in particular in the northern outskirt of Seoul city. This region, historically considered seismically inactive, faced an increase of the recorded seismicity after the occurrence in 2011 of the Tohoku-Oki mega-thrust Mw 9.0 earthquake in Japan (Hong et al., 2017). The concerns raised from this event resulted in a number of studies on the seismicity of the area, especially in highly populated regions as the capital city Seoul, highlighting the reduced knowledge about the local seismicity and the related subsurface structures (Han & Lee, 2019; Hong et al., 2021; Malehmir et al., 2022). The seismic profile studied in **Paper II** (profile 3) was designed perpendicular to three crustal-scale fault systems beneath Seoul city that were suspected to contribute in part to the local seismicity (Figure 4.1). Imaging of these fault systems would enable a correlation with the recorded seismicity and help to prevent potential damage in the case of a high

magnitude earthquake (Leonard, 2010; Rosenblueth & Ordaz, 1990; Singh et al., 1980; Wells & Coppersmith, 1994).

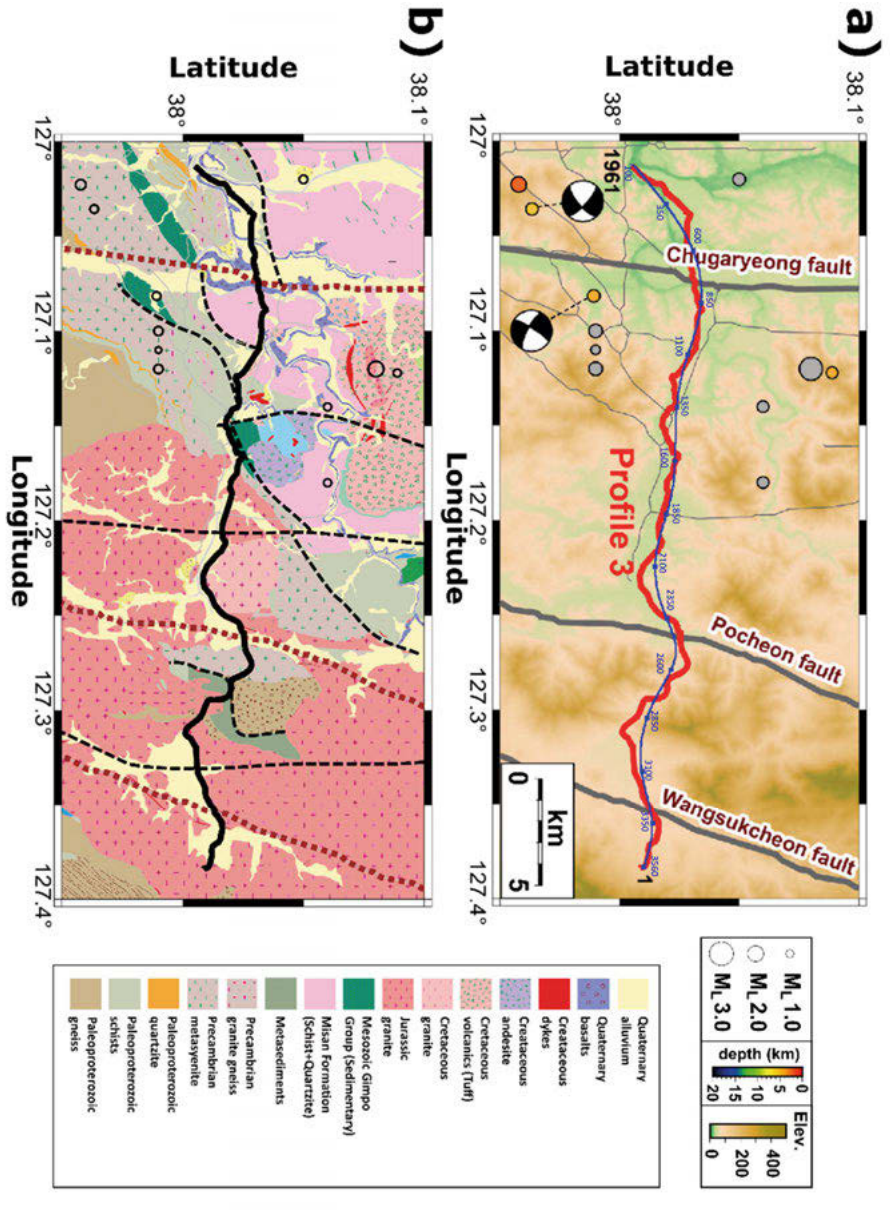

Figure 4.1. (a) Elevation map of the area with in red the location of the seismic profile 3 and in blue the common midpoint line used to process the data. (b) Geological map of the study area; dashed lines show mapped faults close to the profile. Circles correspond to the seismicity of the area.

The need to investigate the subsurface in urban areas is a common challenge (Ishiyama et al., 2016; Malehmir et al., 2011; Zoback et al., 2010). In addition to this, as expected in most hard-rock settings (Figure 4.1b) the area is prone to low reflectivity (Eaton et al., 2003). To obtain an image of the subsurface despite these challenges, a reflection seismology dual-element acquisition system was adopted (Malehmir et al., 2022). The acquisition consisted of a 20-m-spaced nodal array recording the sweep signal generated by two synchronized 12 t vibrator trucks enrolled as sources at most of the receivers' positions. The nodal array data are complemented by a 2-m-spaced MEMs based landstreamer system towed by a vibrator truck and dragged along the profile parallel to the nodal array. The resulting crooked profile, acquired with a split-spread roll-along geometry in the case of the nodal recorders, is approximately 40 km long and with a maximum nodal array offset of approximately 7 km. The landstreamer system was equipped with 20 sensors and a maximum offset of 50 m. Both recording systems were set to a 1 ms sampling rate.

The recorded data from the nodal array show continuous reflectivity in various portions of the profile but also a low S/N in most of the far offset data. The processing of this dataset focuses on increasing the reflections' continuity and the S/N of the data. The data sorted to receiver gathers showed higher coherency respect to the more common shot gathers, and therefore part of the processing flow was applied in this domain. The resulting unmigrated stacked section imaged minor portions of the faults (F1 and F2) and a domed reflective package (D1), still presenting high level of background noise probably due to the environment of the acquisition (Figure 4.2). The landstreamer acquisition was designed to target and image the bedrock reflection at less than 50 m of depth. The landstreamer data show strong and continuous reflections along the whole profile, permitting the application of a straight forward processing flow and resulting in a detailed bedrock reflection in the unmigrated stacked section (Figure 4.3).

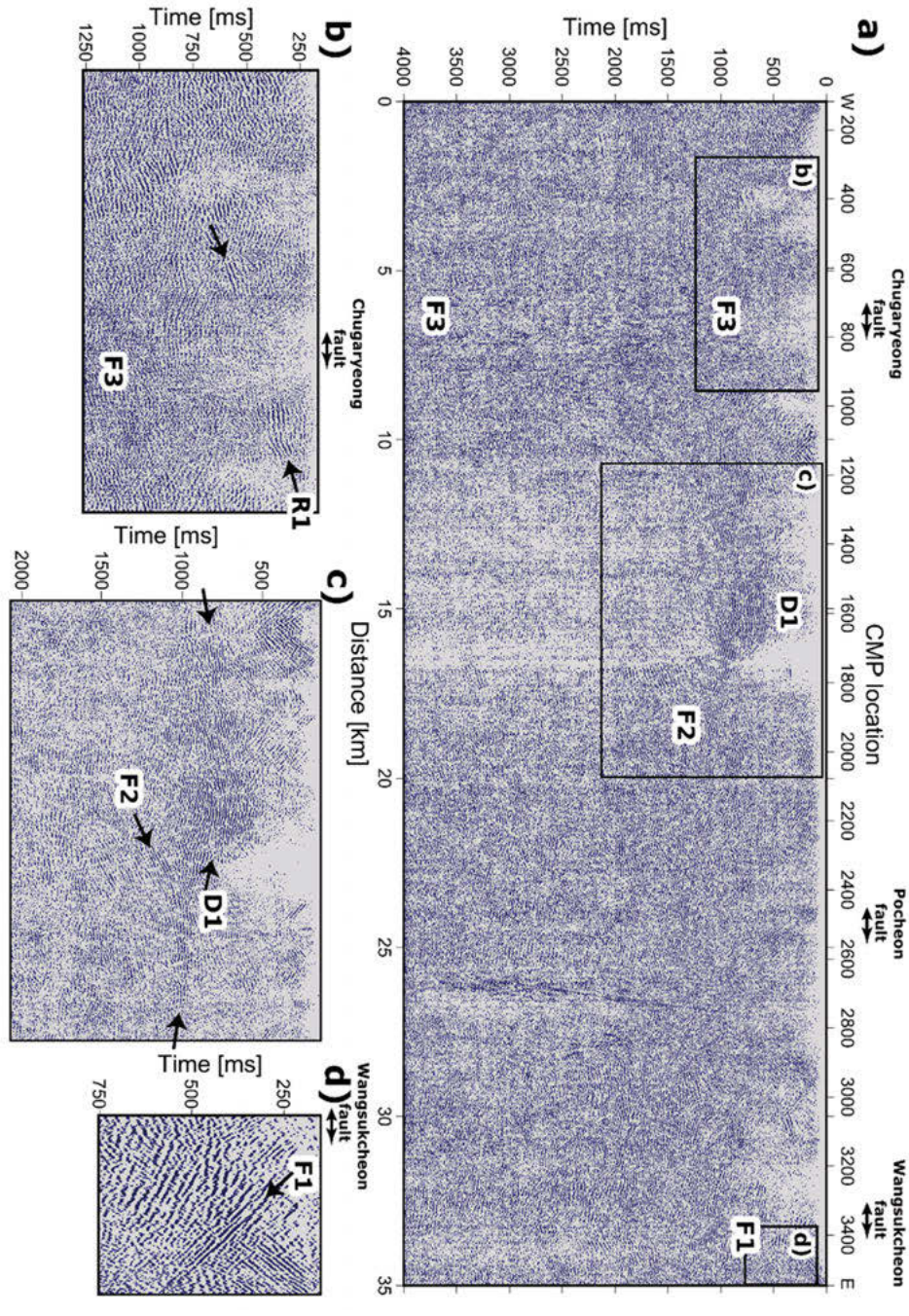

Figure 4.2. (a) Unmigrated stacked section of the nodal array data. Three zoomed windows are shown in panels (b–d). (b) Visible transparent channel of reflectivity indicated as F3. (c) A domed reflective package (D1) and an underlying reflection (F2) are visible in the central part of the profile after applying a cross-dip correction of 10° to the north. (d) An east-dipping reflection indicated as F1.

Complementary analyses were crucial to help understanding and interpretation of these results. Cross-dip analysis was performed on the central area of the profile where a stronger reflectivity was detected. This process takes advantage of the 3D information resulting from a crooked profile to identify out-of-plane reflections, in the presented case a 10° dip towards the north was detected on the central reflectivity and the unmigrated stacked section was corrected for it, increasing the continuity of F2 and D1 reflections (Figure 4.2c).

The nodal array data show surprisingly strong and coherent surface-wave back-scattered signals in the receiver gathers, therefore we decided to further analyse them. The Zerwer et al. (2005) method, as implemented for multifold data by Colombero et al. (2019), was applied to estimate the location of sharp lateral variations in the near-surface and the corresponding maximum affected wavelength. The results highlighted the locations of strong lateral variation along the profile down to a depth of approximately 100 m, suggesting their non-human related origin (Figure 3.6). A first-break traveltime tomography model was obtained (Figure 4.3b) using a diving-wave finite-difference based code (Tryggvason et al., 2002). For the modelling, the picked first-breaks of the nodal array were selected because of their higher maximum offset compared to the landstreamer data, ensuring inversion stability and deeper ray penetration. The resulting velocity model reveals a weathered layer with a thickness ranging from 10 m at its thinner portions and up to 50 m along the river valleys. It is underlain by a high velocity bedrock (> 4000 m/s) and shows a good correspondence with the landstreamer results (Figure 4.3). The complementary analyses were completed by a 3D reflection traveltime modelling. A high-dipping reflection was detected in the shot and receiver gathers, showing the reflection hyperbola intersecting the first-break arrivals. The intersection point between the first-break arrivals and the hyperbolic reflection indicates the position where the respective horizon reaches the surface. This extra information enables the possibility to model the reflection resulting in a N20E strike direction and a dip of 60E for the corresponding modelled horizon.

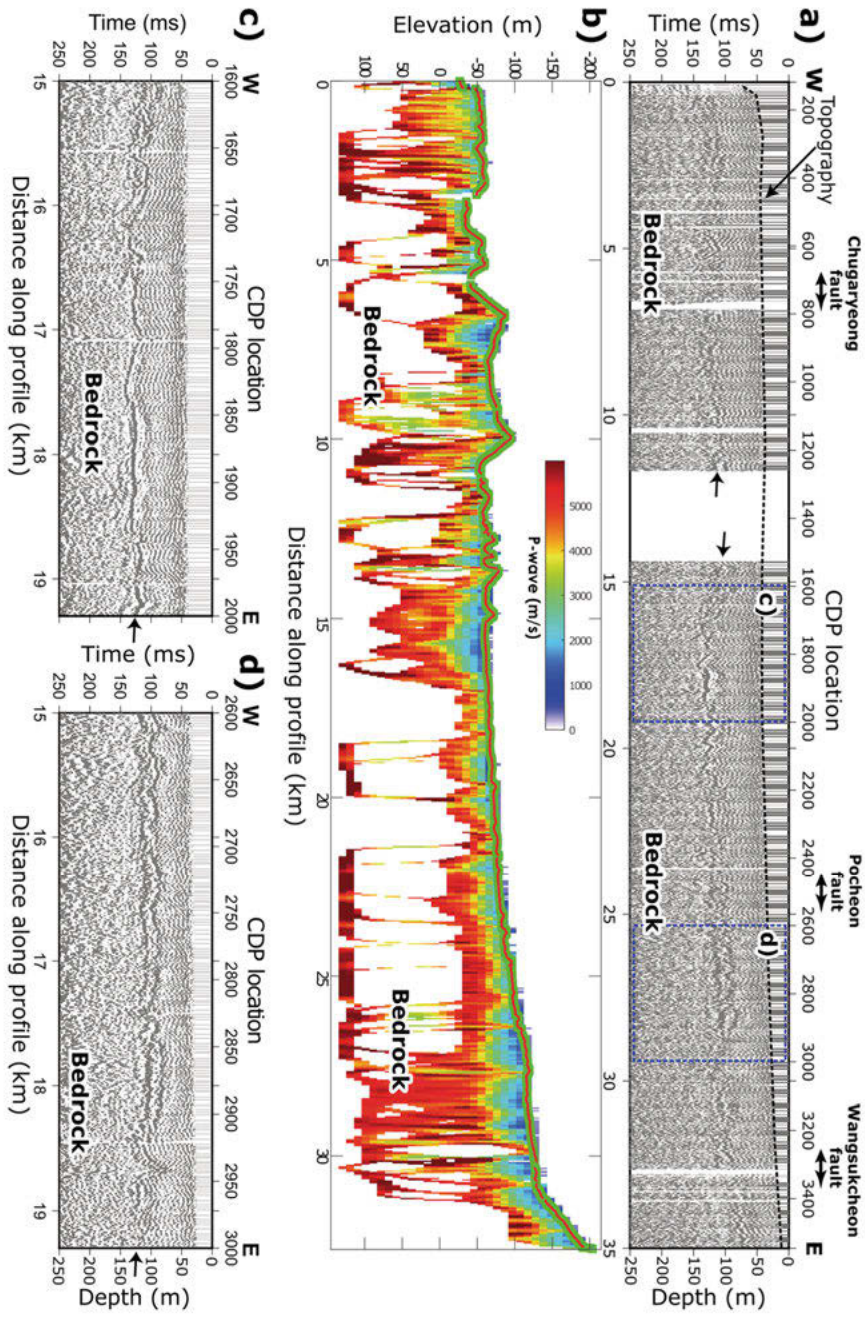

Figure 4.3. (a) Unmigrated stacked section of the landstreamer data. Arrows point at the interpreted bedrock reflection. (b) First-break traveltime tomography results obtained from the nodal array data. Note the correspondence between the low-velocity structures and bedrock reflection geometries. (c and d) Highlighted part of the landstreamer stacked section (blue rectangles in (a)).

Results from the different methods were analysed together for the interpretation, allowing for the identification of the three main fault systems and of a fault-bend-fold structure (Figure 4.4). The Chugaryeong fault is inferred as a sub-vertical structure showing strong surface-wave back-scattering and no coherent reflectivity (F3). In the central part of the migrated stacked section, a 30° NW dipping zone of reflectivity is imaged and interpreted as a fault (F2), propagating into a dyke or sill system (D1) and resulting in the interpreted fault-bend fold structure. This fault, if projected downwards, would intersect the Chugaryeong fault and a series of seismic event hypocentres, suggesting a relation between the two faults intersection and the seismicity, with the implication that both faults may be active and form splays. If this fault is projected to the surface, it will intersect the Pocheon fault surface expression, and the region of related strong surface-wave back-scattering. Unfortunately, there is no imaging of the near-surface geometry of the Pocheon fault to further evaluate this possibility. The Wangsukcheon fault (F1) is interpreted to have a N20E/60E geometry based on the 3D reflection traveltime modelling, implying an opposite dip angle from the other two faults with apparently no associated seismicity.

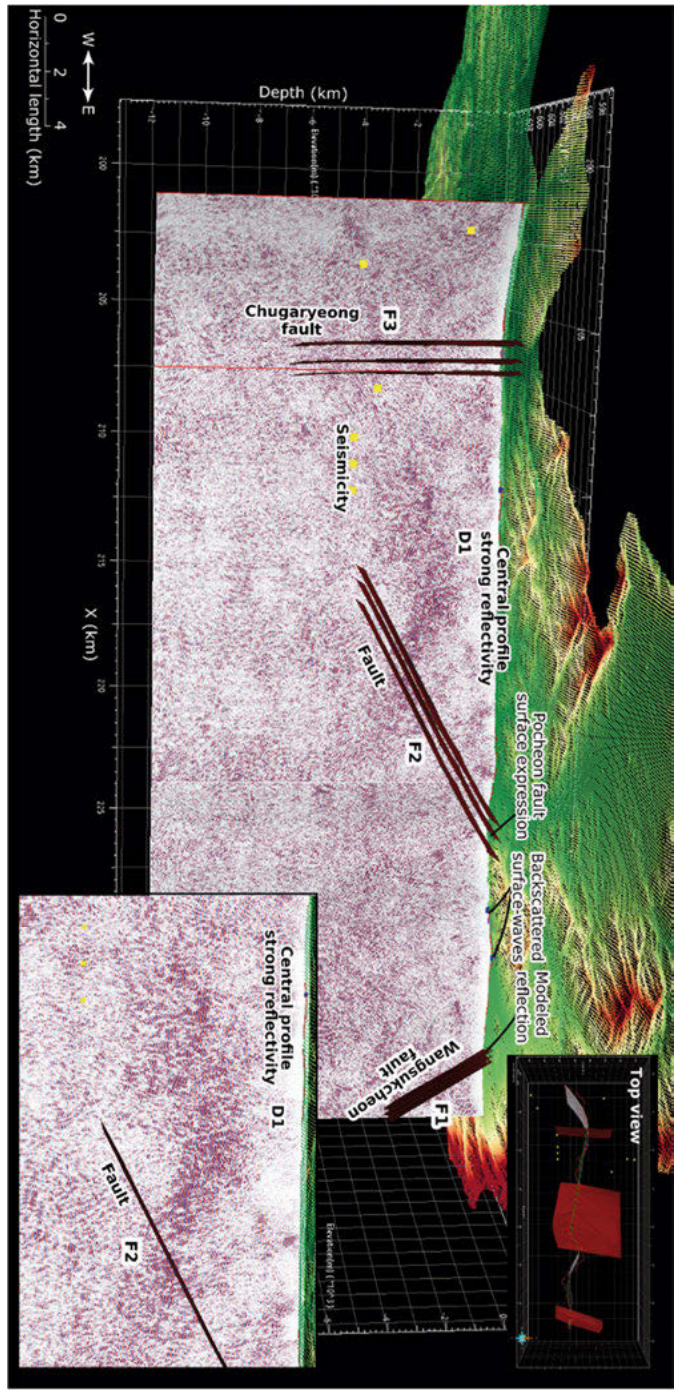

Figure 4.4. 3D view of the interpreted fault systems on the migrated stacked section from the nodal array data. Yellow points represent the recorded seismicity of the area. Inset shows a portion of the central part of the profile where a fault (F2) and an apparent fault-bend fold structure (D1) are interpreted.

4.1.2 Conclusions

Adopting the dual-element acquisition system for this study permitted the acquisition of two separate datasets. The nodal array data aimed to image the deep structures and fault systems down to 4 km of depth. The landstreamer data aimed to image the bedrock reflection down to 50 m depth where an expression of the major faults was expected. The two datasets were separately treated and processed but their results were complementary and fundamental for the overall interpretation. The large-scale data acquisition in a highly populated area required a light and flexible acquisition system and therefore, after evaluation of **Paper I** results, the use of the landstreamer was restricted to a single segment (20 sensors). This setup allowed the recovery of the bedrock reflection uniquely from the landstreamer dataset. The final interpretation partially reconstructed the fault systems and highlighted the connection between the fault intersections and local seismicity. These results contribute to characterizing the earthquakes in the area and therefore to improved preparation and reinforcement strategies for the cities.

4.2 Paper III: Innovating land seismic investigations for CO_2 geologic storage in Denmark

Paper III is the result of a pilot survey conducted in the already largely studied Stenlille domal structure in Denmark. The idea of this study was to test the dual-element acquisition system in a sedimentary basin environment and to evaluate its applicability for CCS site investigations. The need in CCS site investigations to have a high-resolution image in a wide depth range matches the quality of this acquisition system and prompted the goal of a single subsurface image with both nodal array and landstreamer data, where both datasets were merged early in the processing flow. The final unique stacked sections, resulting from a pre-stack merging of the two datasets, showed high-resolution signals from the shallow subsurface to below the reservoir depth. Results were used to successfully identify the reservoir and sealing structures with an overlaying fault, proving the success of the proposed acquisition and processing methods.

4.2.1 Synopsis

In 2021, Denmark included geological storage of CO_2 as a strategy to reach carbon neutrality by 2050 (OECD, 2019). Therefore, investigations for possible CCS structures were initiated across Denmark, both offshore and onshore. The study presented in **Paper III** describes the acquisition and processing of the pilot study for onshore CCS structure investigations. A small structure close to the village of Stenlille, in the northwest of Zealand island, was chosen for the pilot study (Figure 4.5). The Stenlille structure has been in use as storage for natural gas for more than 30 years, resulting in a wealth of information including downhole wireline logs and 2D and 3D seismic data (Bredesen et al., 2022; Gregersen et al., 2020; Nielsen, 2003; Vosgerau et al., 2020). Five 2D seismic profiles were acquired with the dual-element acquisition system for a total length of approximately 12 km (Figure 4.5). Two 12 t vibrator trucks were used as the seismic source, with sweep positions every 10 m. At each profile the nodal array was deployed in a fixed geometry with 10 m spacing, while the MEMs-based landstreamer was towed by the second seismic vibrator parallel to the nodal array, with 2 m spacing and a maximum offset ranging from 90 to 210 m depending on the logistics of the profile. The data were recorded with 1 and 2 ms sampling rate respectively for the landstreamer system and for the nodal array.

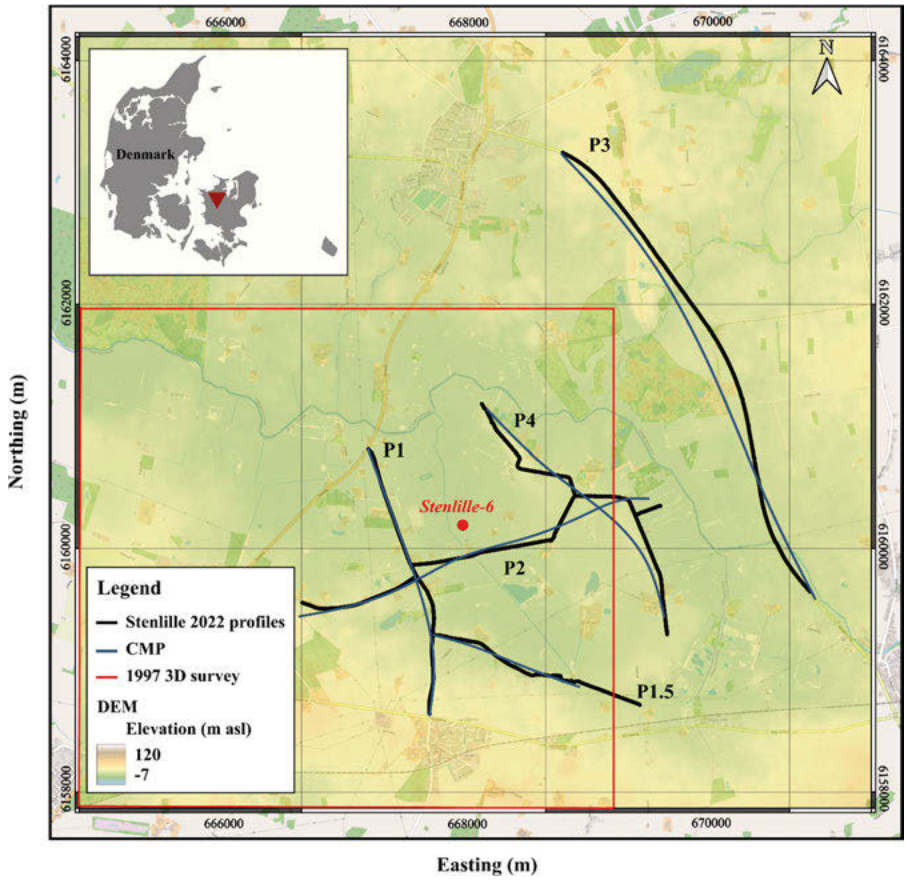

Figure 4.5. Elevation map of the Stenlille area showing the location of the pilot survey seismic profiles. The acquisition lines (in black) partly overlap the area covered by a 1997 3D survey (the red box) and cover a previously unmapped zone toward the north-east. CMP profiles (in blue) selected for data processing are smoother than the acquisition profiles due to the profiling line crookedness.

Recorded shot gathers show different characteristics for the two recording systems. The nodal array shot gathers show continuous reflections down to 1.5 s (R1-R4) due to the acquired offset, the landstreamer data instead show only shallower reflections (R1-R3), but with higher spatial and time resolution. The two datasets were separately processed up to the surface-consistent residual static corrections. Lower frequencies (10–25–130–150 Hz) were maintained in the nodal array data to target deeper reflections, while higher frequencies (30–35–130–170 Hz) are favoured in the landstreamer data to retain the higher resolution. The CMP geometries were set equal in both datasets to enable their later merging using a CMP spacing of 5 m. While the CMP geometry location favoured the nodal data to consider the lateral displacement result of the large offset in crooked profiles, the CMP spacing is set to guarantee a high fold for both datasets while maintaining a horizontal resolution adapt to the target.

After the separate processing, the seismic traces from the two datasets were merged into a single dataset, the different responses measured in the amplitude spectra of the acceleration and velocity sensors are corrected by applying deconvolution (Malehmir et al., 2017), whereas the remaining 90° phase difference is corrected during surface-consistent residual-static corrections (Tellier and Lainé, 2017). Figure 4.6 shows an example of a shot gather after the merging of the two datasets. Focusing on the near offset, where the landstreamer data are present (Figure 4.6b), there is a significant amount of extra information and higher resolution introduced by the landstreamer data to the nodal array data (Figure 4.6b and c) for the near-surface structures. In particular, the number of seismic traces in the data increases from 20 (only nodal array, Figure 4.6c) to 120 (merged data, Figure 4.6b) along the first 200 m of offset where the landstreamer is deployed. Additional pre-stack processing steps were applied to compensate for the differences in the acquired datasets and to obtain a single stacked section. Specifically, a trace energy equalization function followed by two extra iterations of surface-consistent residual static corrections and velocity analysis were applied to compensate for energetic differences between the two datasets and for static corrections due to minor differences in the shallow subsurface.

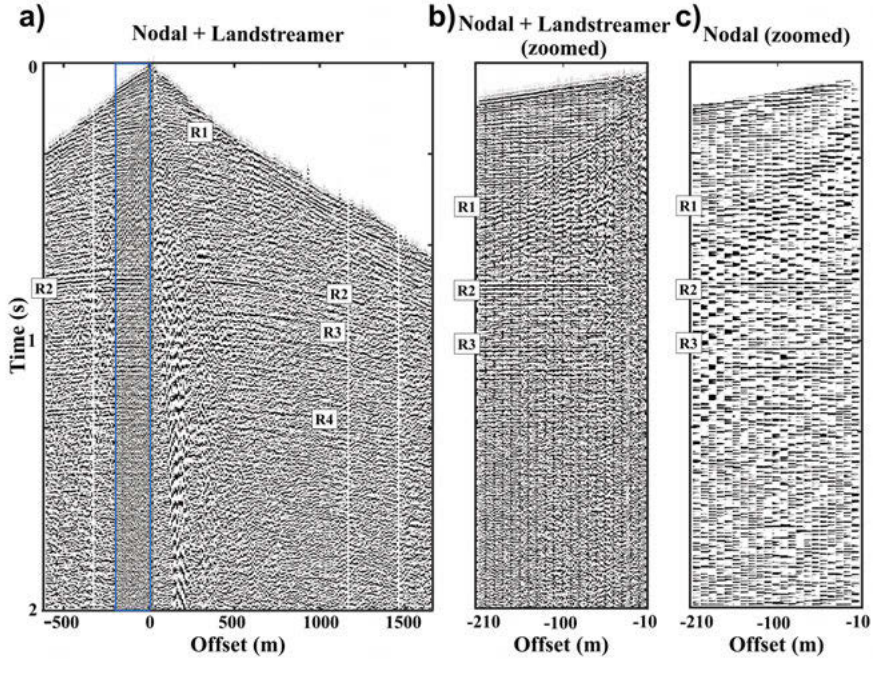

Figure 4.6. Example of a merged shot gather of profile 1 resulting from the combination of the processed shot gathers of the nodal array data and of the landstreamer data. (b and c) A close-up within the blue area in (a) after (b) and before (c) the merging process. Note the increased spatial and time resolution of the record in (b) with an increased continuity of the shallower events respect to (c).

The last processing steps compensated for differences in signal amplitude and coherency changes across datasets, and thus it was possible to proceed to stack the merged data. To evaluate the improvements obtained with a pre-stack merging of the datasets, a total of three migrated stacked sections were generated and compared, one from the nodal array data only, one from the landstreamer data only and one from the merged data (Figure 4.7). The comparison of these results confirms what was previously observed in the shot gathers. The landstreamer migrated section (Figure 4.7a) is able to discern more layers down to 0.5-1 s of data caused by the higher retained frequencies and the higher near offset coverage compared to the nodal array migrated section. On the other hand, the nodal array migrated section (Figure 4.7b) shows deeper reflectivity with high continuity down to more than 2 s of data due to the higher recorded offset. When the two datasets are merged together, the resulting migrated section (Figure 4.7c) maintains the good qualities of both datasets with a stronger contribution from the landstreamer to the first 0.5 s of the section, a stronger contribution of the nodal array on the deeper portion of the section, between 1 and 2 s, and a mix of both between 0.5 and 1 s. A total of six primary reflections were identified and labelled in the final migrated sections (R1-R6 in Figure 4.7).

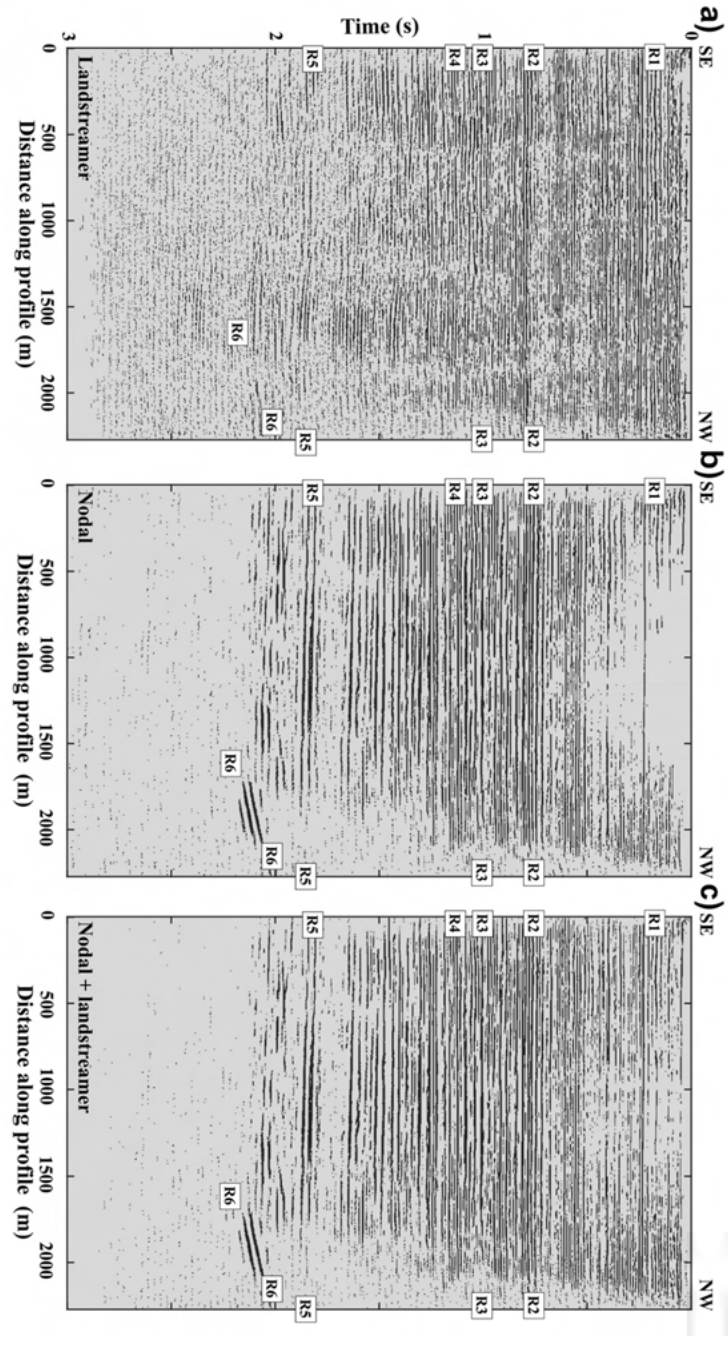

Figure 4.7. Migrated seismic sections resulting from the (a) landstreamer data, (b) the nodal array data and (c) the nodal array and landstreamer merged data. The different characteristics of landstreamer data in (a) and nodal array data in (b) are fused in (c) in a single section with high-resolution and a wide-depth range coverage.

The processing, first developed and tested on profile 1, was similarly applied with minor adaptation to the other profiles. The two datasets of profile 1.5 and 4 were not merged and only the nodal array migrated section is considered. Due to the road conditions along these two profiles, the landstreamer acquisition was restricted to the deployment of a limited number of landstreamer segments. The resulting low quality of the landstreamer data in these profiles made the merging of the two datasets unsuitable.

The migrated stacked sections resulting from all profiles are analysed in a 3D environment to visualize the overall structure and to compare the six identified horizons (R1-R6) with a borehole (Stenlille-6) present in the area (Figure 4.8). The 3D analysis helped to identify the expected domal structure and the main reflectors of interests, with R1 and R2 as respectively top and base of the Chalk Group, R3 and R4 as respectively top and base of the Gassum formation, R5 as the top of the Zechstein group and R6 as the Zechstein salt. The high resolution obtained in the sections resulted in images of not only the main reflectors but often also the internal layering of the formations. This information is important especially at the reservoir depth to better estimate the reservoir capacity. A fault structure intersecting the Chalk Group (F1 in Figure 4.8) is imaged in profile 3 with structural characteristics typical of faults expected in the area (Hjelm et al., 2020). This identification is of particular relevance for CCS reservoir investigations, where the mapping of faults, even at depths different to the reservoir level, is crucial for the safety evaluation of the reservoir.

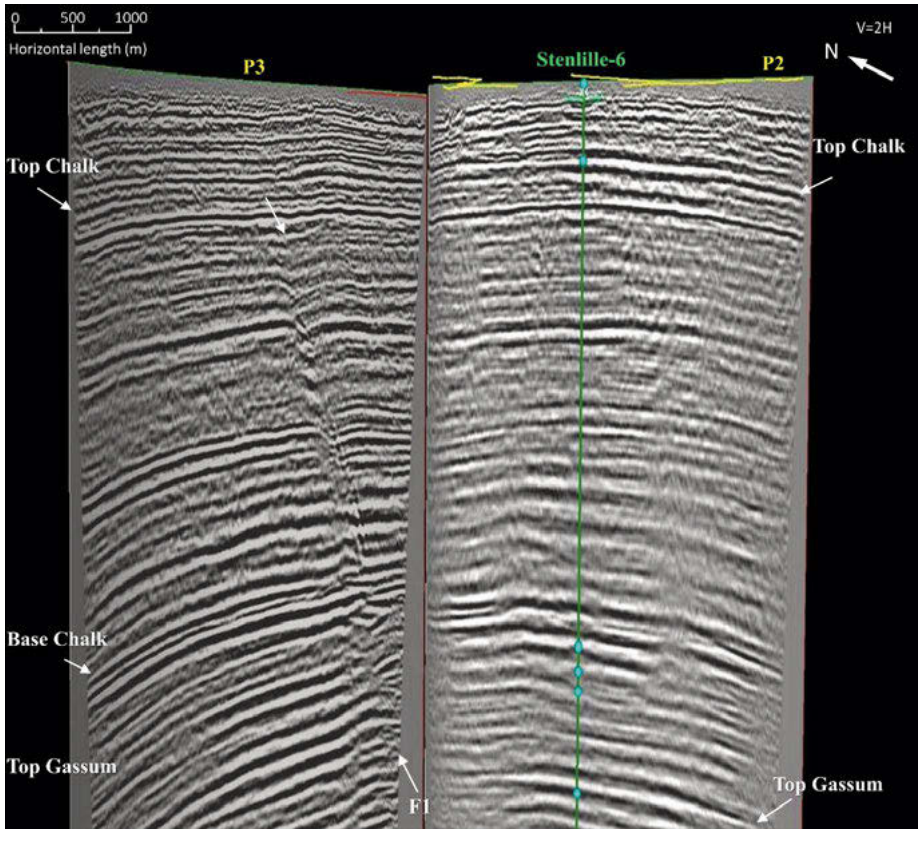

Figure 4.8. A vertically exaggerated 3D view of the migrated stacked sections of profile 2 (P2) and profile 3 (P3) and Stenlille-6 borehole. Along P3, a fault is indicated as F1, whereas P2 shows a general anticline stratigraphy. Note that P2 and P3 are approximately 1000 m away from each other (see Figure 4.5), not visible here due to the view orientation.

4.2.2 Conclusions

The dual-element data acquisition system demonstrated again to be feasible for an urban environment as earlier supported in **Papers I** and **II**. Due to the less densely populated area compared to Seoul city in **Paper II**, it was often possible to use a higher number of landstreamer segments allowing a longer offset and a higher fold in the data. The proposed processing approach explores a new way of handling the two separate datasets, aimed to retrieve a unique seismic section that combines the high-resolution of the landstreamer system and the greater depth range of the nodal array. **Paper III** is successful in demonstrating (1) the applicability of the dual-element acquisition system for onshore CCS reservoir investigations, and (2) the capability of the proposed processing to enhance structures of interest for CCS reservoir investigations, such as trap and fault structures.

4.3 Paper IV: Combined onshore and offshore wide scale seismic data acquisition and imaging for carbon capture and storage exploration in Havnsø, Denmark

After the successful pilot survey described in **Paper III**, the designed system was upscaled and applied on larger subsurface structures. **Paper IV** focuses on the longest profile of the first of these upscaled surveys, located in the Havnsø area. This work presented new challenges, some derived from its larger scale. The processing method initiated in **Paper III** is here refined for higher quality results and expanded on a transition zone environment for the merging of land and marine sensors. The resulting migrated stacked section is a culmination of combining four different datasets and is therefore interpreted for a first geological reconstruction in accordance with borehole data in the area.

4.3.1 Synopsis

The study area of **Paper IV** is close to the town of Havnsø in the northwestern part of Zealand island, in Denmark. This first upscaled onshore CCS reservoir investigation project consisted of eight 2D seismic profiles covering the expected extension of the Havnsø domal structure, for a total length of approximately 130 km (Figure 4.9). Profile 1, the longest profile of this acquisition with a length of around 40 km, connects the Havnsø structure with the Stenlille area of the pilot survey (**Paper III**) to the south. Towards the north this profile crosses a marine channel ending on the small Nekselø island in front of the town of Havnsø (Figure 4.9). The reason for this profile, and the focus of **Paper IV**, is to allow an interpretation with the deep borehole present in Stenlille area (Stenlille-19 from Schokker, 2001) and to cover the expected east domal structure closure from south to north, where the marine channel covers a part of the closure never previously imaged. The imaging of the marine channel will also connect the onshore results with previous offshore results (Gregersen et al., 2020; Larsen et al., 2006).

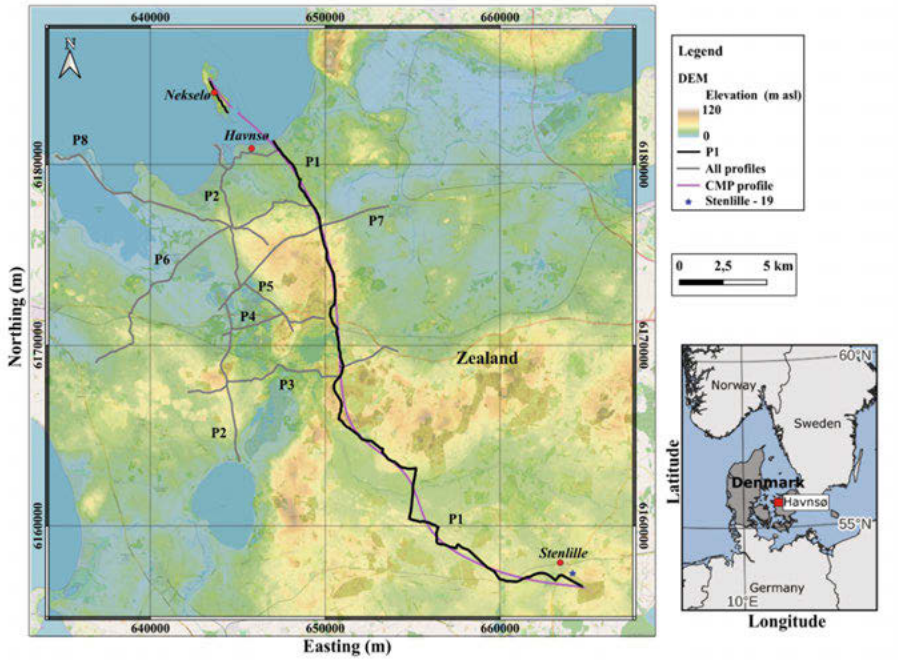

Figure 4.9. Location of profile 1 (black line) and the additional seismic profiles acquired (grey lines, not discussed in **Paper IV**) in the Havnsø area. The light purple line shows the CMP locations used to process the merged datasets. The blue star indicates the location of the well Stenlille-19. The map is modified after Papadopoulou et al. (2023). Coordinates are in the UTM zone 32N. Elevation above sea level is color-coded in the background.

The onshore acquisition was set similar to the pilot survey, with two vibrator trucks as source and the dual-element acquisition system as receivers, with 10 m spacing for the nodal array and 2 m spacing for the landstreamer. At the northernmost part of the profile, the nodal array was recording on both sides of the marine channel while the source was closer than 3 km from the coast, allowing a far offset coverage of the marine channel. In addition to this, a special set up was designed for the marine channel where 18 OBSs and a 600-m-long marine streamer equipped with 96 hydrophones were deployed (Figure 3.2). The marine streamer was deployed from Havnsø coast towards Nekselø island, covering near the shoreline, while the OBSs were deployed along the whole channel but with a large average spacing of 170 m (Figure 3.2). This setup simultaneously recorded the same shots both on the marine and land sensors with a total of four simultaneous datasets that would be merged in a similar fashion to **Paper III** for the dual-element recording system. Environmental and marine life restrictions (Natura2000 zone from Council Directive 92/43/CEE) did not allow to operate a marine source and thus only the land source was operated and recorded from the different sensors.

The four datasets were initially processed separately, with unique challenges for each of them. The same CMP geometries are applied to all datasets to allow their later merging using a 5 m CMP spacing. The three recording domains of this acquisition, velocity for the geophones, acceleration for the MEMs and pressure for the hydrophones, are compared to evaluate their differences and how to compensate for them. The application of deconvolution during the FDSD with the theoretical sweep (Brittle et al., 2001) to retrieve an impulse signal from the seismic vibrator data, compensates for most of the velocity and acceleration domain differences (Malehmir et al., 2017). In fact, the different responses measured in the amplitude spectra of the acceleration and velocity sensors are corrected by applying deconvolution (Malehmir et al., 2017). The remaining 90° phase shift resulting from the difference of the two sensors (Tellier & Lainé, 2017) is compensated during surface-consistent residual static corrections. Geophone and hydrophone data merging is commonly used in marine datasets (Barr et al., 1993; Dragoset & Barr, 1994; Hoffe et al., 1999; Soubaras, 1996). They differ only on the amplitude value and on the absence of directionality in the pressure domain (hydrophones). After ensuring that the datasets have same polarity, the amplitude difference can be compensated for by applying a scaling function. The absence of directionality is relevant in the case of reflections with change of polarity (horizons with negative impedance contrasts) that are not recorded in our datasets. After matching geometries and headers of all datasets, an AGC function was applied to the merged shot gathers to compensate for amplitude differences, followed by a spectral balancing (20-30-100-120 Hz) to balance the frequency ranges. These two steps particularly boosted the remaining airwave recorded in the landstreamer traces, probably stronger because of the short offset, and thus a second run of an airwave attenuation filter was applied. Three iterations of velocity analysis and surface-consistent residual static corrections were applied to compensate for minor phase differences and to improve the velocity model by exploiting the full information of the data. The resulting shot gathers (Figure 4.10) show good reflection continuity and similar amplitude across datasets, proving their achieved coherency after the processing and implying a likelihood of better quality in the stack of the merged dataset.

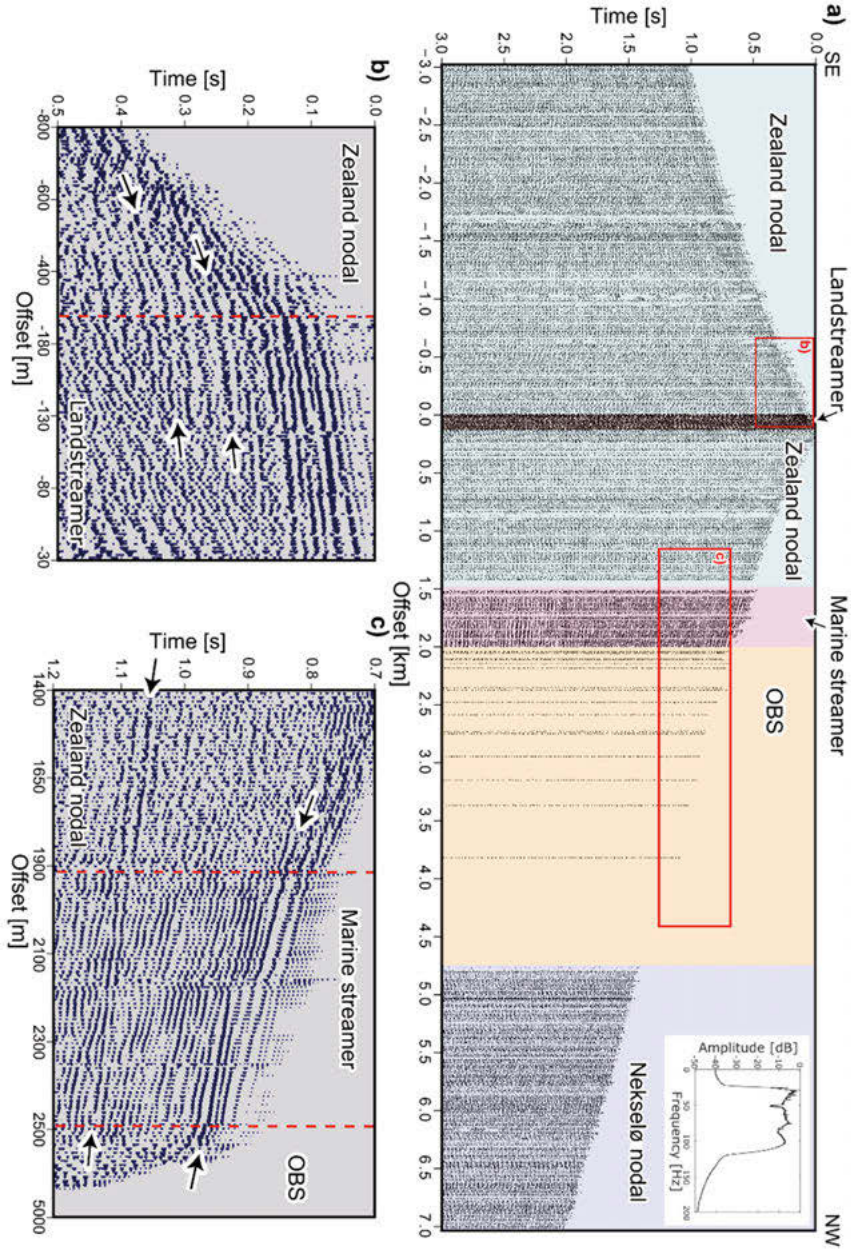

Figure 4.10. An example processed shot gather after merging all the different datasets. (a) Full shot gather where the different shaded colours correspond to the different datasets and sensor types. The traces are plotted with real offset. (b) Magnified window of the landstreamer and nodal datasets. (c) Magnified window of the nodal, marine streamer, and OBS datasets. (b and c) The traces are equally spaced but note the variable scale along the offset axis. Arrows mark some of the continuous reflections. The dashed red lines define the different sensor types.

Comparing the stacked sections of landstreamer, nodal array and merged datasets, it is notable that differences are similar to those previously observed in **Paper III**, with the merged section inheriting the qualities of the single datasets but with the landstreamer datasets this time contributing down to 1.5 s reflections in certain areas. Focusing on the marine channel zone, the comparison of the stacked sections resulting from the marine streamer (Figure 4.11a), the OBSs (Figure 4.11b) and the onshore sensors (Figure 4.11c) highlights the contribution of each of them to the final merged section (Figure 4.11d). In detail, the marine streamer unmigrated stacked section shows high resolution and continuity of most of the horizons (R2 to R5) in the southern part of the channel close to the coast, the north side of the channel is also imaged due to the source positions placed at Nekselø island but the far offset (> 4 km) results in a low S/N. The OBSs unmigrated stacked section shows a good continuity for the deeper reflections (T and R5) extending them towards the centre of the channel, but, because of technical issues on different sensors, the already low CMP fold coverage of these data is worsened on the second day of acquisition (while the source was placed on Nekselø island) resulting in a lower S/N ratio in the northern part of the channel. The landstreamer contribution to the onshore stacked section increases the CMP fold coverage on the coastal sides, while the cross-shooting from Zealand island to Nekselø island and vice versa recorded on the nodal array imaged the deep reflections in the central part of the channel (T and R5). The merged stacked section shows continuous deep reflections (T and R5) for almost the whole channel length, while shallower reflections are imaged in the southern part of the channel. The absence of a marine source hindered the recovery of shallow reflectivity in the central part of the channel.

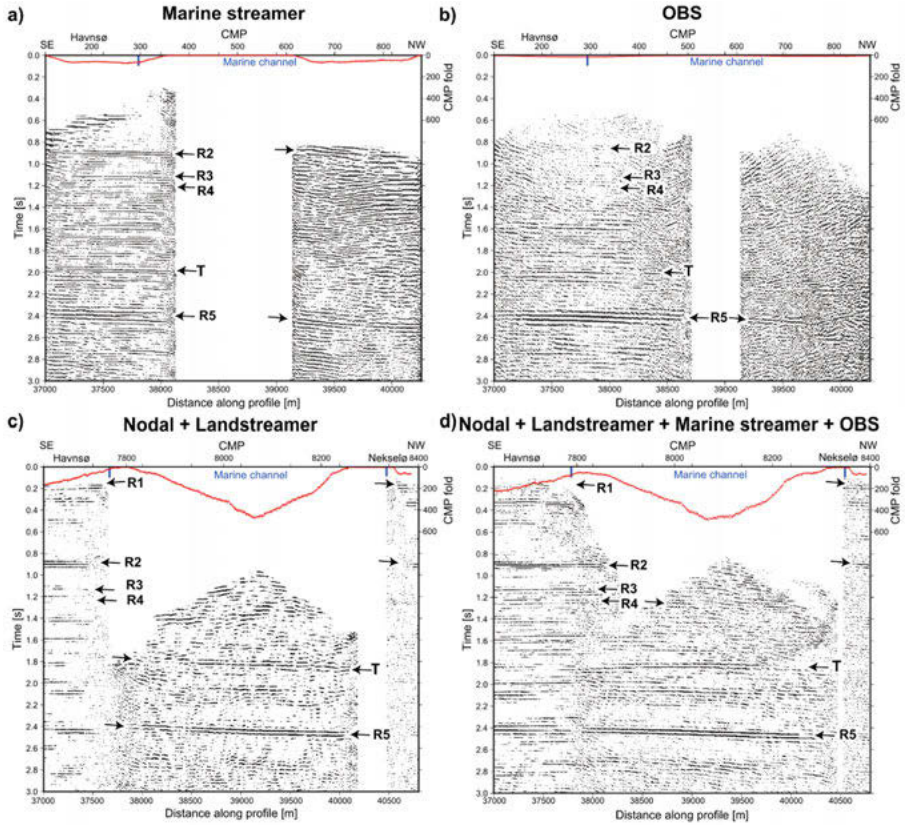

Figure 4.11. Comparison of the unmigrated stacked sections of (a) the marine streamer dataset, (b) the OBS dataset, (c) the onshore sensors merged datasets, and (d) all the merged datasets. AGC (300 ms) is applied to the stacked sections for display purposes. The main reflections are labelled. The red dots show the CMP fold coverage. The blue bars mark the locations of the coastline and, thereby, the extent of the marine channel.

The migrated stacked section is compared with the Stenlille-19 borehole stratigraphy (Figure 2.10) and with the local known geology (Larsen et al., 2003; Nielsen, 2003; Nielsen & Japsen, 1991) for its geological interpretation (Figure 4.12). The identified horizons in the migrated section are interpreted as: top and bottom of the Chalk Group (R1 and R2), top and bottom of the Gassum Formation (R3 and R4), internal layering of the Triassic formations (T), top of the Zechstein Group (R5), Zechstein salt (R6) and top of the Pre-Zechstein (PZ). In addition, the Stenlille and Havnsø domal structures are identified together with a possible smaller intermediate domal structure (Figure 4.12).

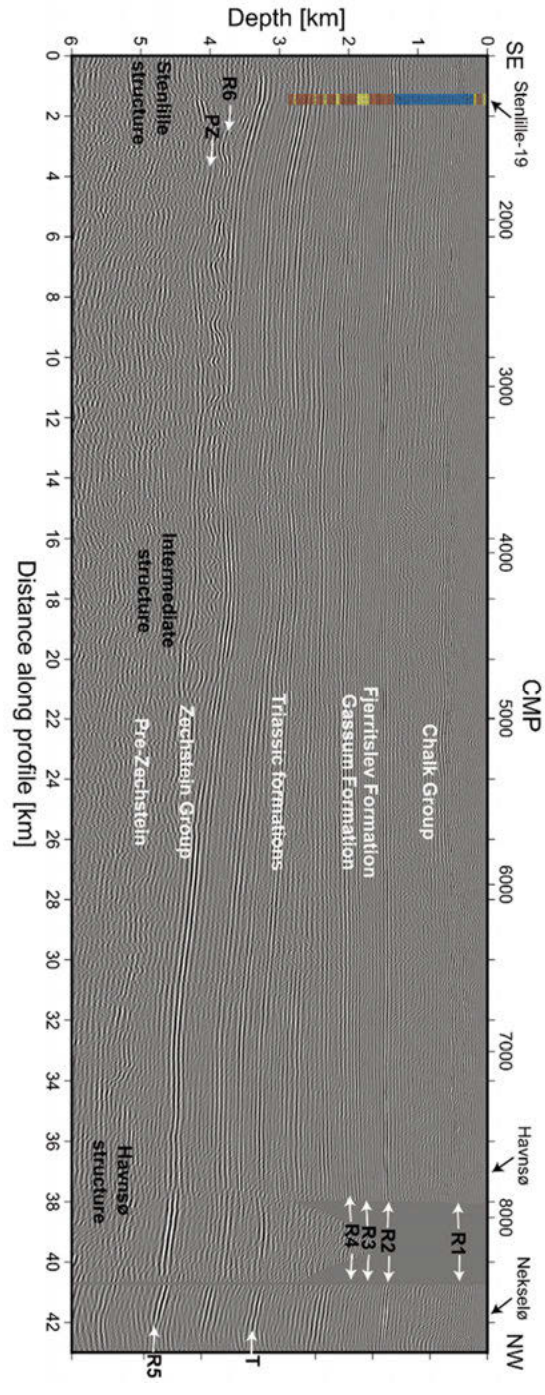

Figure 4.12. The merged and migrated, time-to-depth converted section of profile 1. In white are the interpreted formations, in black, the horizons and interpreted domal structures. The stratigraphic reconstruction of the projected Stenlille-19 well (see Figure 2.10 for details) is superimposed for reference.

4.3.2 Conclusions

After a detailed study of the different domains of the recording sensors, the seismic processing elaborated in **Paper III** is refined in **Paper IV**. Results show improved details and continuity in the merged migrated section with both datasets affecting also deeper portions of the final section with respect to the previous work. Extending this multi-element recording approach to a more complex case, the imaging of the subsurface beneath a marine channel zone was possible. In this area four different categories of sensors, two in offshore and two in onshore, were deployed, and the adapted processing allowed their synergistic merging in a single migrated section. The migrated section shows continuous reflectivity down to the Pre-Zechstein formations at 5-6 km of depth. After the merging, a higher resolution down to 1 km of depth is achieved and a particular improvement on the reflections' continuity between 1 and 2 km (the depth of the target reservoir) is noticeable compared to the individual sections. The structure closure underlying the marine channel was imaged for the first time, but restricted to depths beyond 3 km, highlighting the expected limitation from the absence of a marine source. The intersection with the borehole in the south and the high continuity of reflection signals permitted the geological interpretation of the main horizons and structures relevant for CCS reservoir investigations along the whole profile. No major faults or fractured areas have been detected along the profile.

4.4 Paper VI: Shear-wave tailored moveout corrections to improve multicomponent reflection seismic imaging

Paper VI explores the 3C potential of the MEMs sensors in the dual-element acquisition system as a by-product of large-scale site investigations. The data show PP-, PS- and SS-wavefield reflections from a shallow horizon. The seismic processing of the SS-wavefield section was challenging and required an alternative definition and application of the moveout correction specifically designed on the desired reflection. The applied moveout correction is described in the paper and referred to as reflection-picked moveout correction. Multicomponent and velocity analyses are performed for near-surface geological interpretation, allowing the identification of the water table and the top of the Chalk Group.

4.4.1 Synopsis

This study is performed in the Gassum area of Northern Jutland (Denmark), close to the city of Randers. It focuses on a portion of the larger Gassum survey, 1 km long, to analyse the recorded 3C data. The acquisition setup was the same as the one applied in **Paper IV**, with two vibrator trucks as source and the dual-element acquisition system as receivers, using 10 m spacing for the nodal array and 2 m spacing for the landstreamer. For the data analysed in this study, 60-3C units were used on the landstreamer (120 m long) while 100 units in a fixed geometry were considered for the nodal array. The 3C resulting data show reflections with different NMO velocities and with different continuity among the components (Figure 4.13a-c). Analysing the relative hodograms (Figure 4.13d-f) and measured velocities, three main reflections are identified corresponding to different wave modes of a single horizon, specifically, from the fastest to the slowest, PP-, PS- and SS-wave modes.

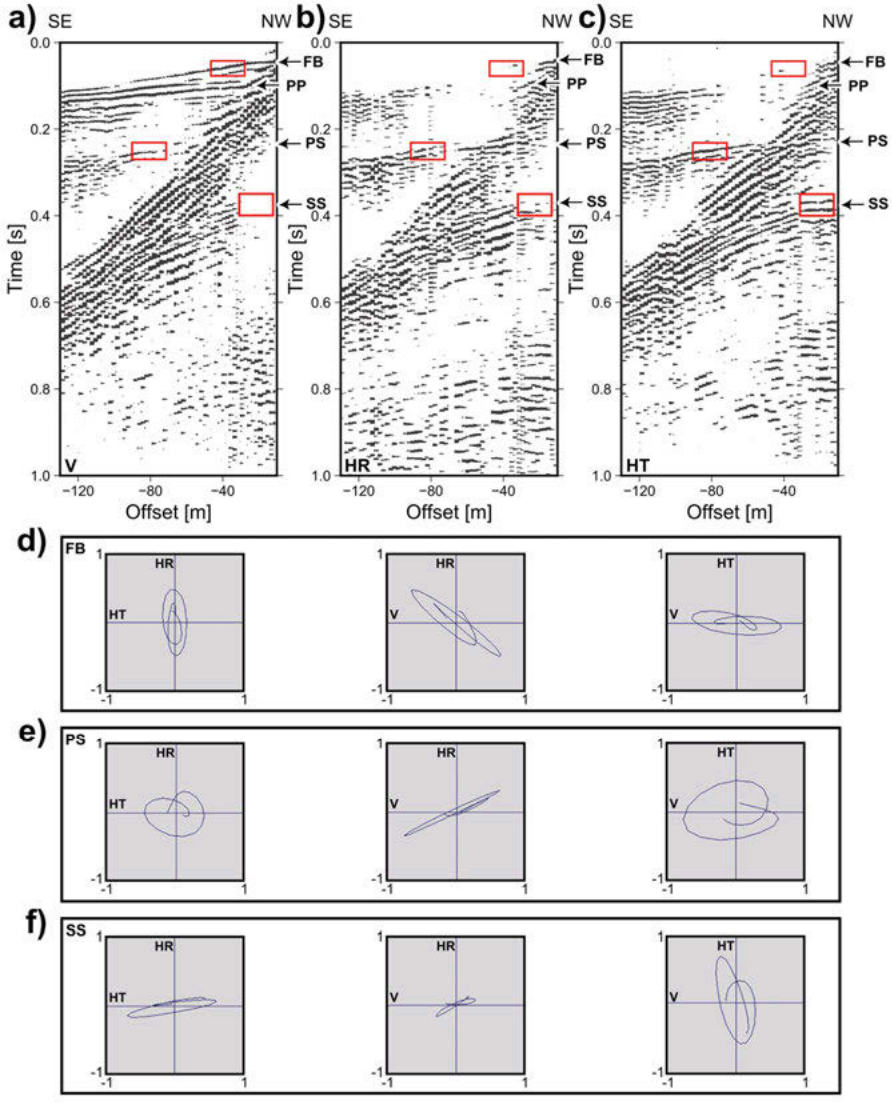

Figure 4.13. An example of a shot gather from the landstreamer data shown for (a) vertical (V) component, (b) horizontal radial (HR) component and (c) horizontal transverse (HT) component. Hodograms are calculated from the red boxes shown in a-c for (d) the first-break arrivals (FB), (e) the interpreted PS-wavefield reflection, and (f) the SS-wavefield reflection.

Data from the V and HT components exhibited the best quality, respectively for the PP- and SS-wavefield reflections and therefore they were processed to retrieve PP- and SS-wave mode stacked sections. For the PP-wave data, a standard processing flow was applied, resulting in a sub-horizontal horizon at around 100 ms presenting good continuity along the whole profile. For the SS-wavefield data, the processing flow applied to the PP-wave data was adjusted

to particularly address one main challenge, the similar arrival time and velocity between the detected SS-wavefield reflection and the recorded surface-waves, a challenge already described in the literature (Burschil & Buness, 2020; Van Zanen, 2004; Wadas et al., 2016). Considering also the SS-wavefield static issues and the similar frequency range of the two wave modes, their automatic separation by coherency processing steps is ineffective. This problem strongly affects the velocity analysis and subsequent NMO corrections, decreasing the continuity of the reflection horizon in the final stacked section. This study proposes an alternative method to the velocity analysis and NMO corrections that at the same time compensates for the SS-wave static corrections. Note that the static corrections resulting from this method are not surface consistent. The proposed method is based on the visual detection and manual picking of the desired reflection, thus ensuring to properly distinguish the desired reflection from the surrounding noise, as surface-waves for this case, and a correct flattening of the reflection prior to the stacking process (Figure 4.14). The process consists of 6 steps: in step 1, the reflection is manually picked in the shot gather domain; in steps 2 and 3, the noisy traces are removed and a theoretical hyperbola of V_{rms} velocity is fitted with the picked reflection in the CMP gathers assuming a horizontal nature of the reflectors; step 4 involves estimating the hyperbola apex (x_0, t_0) based on an extrapolation from the fitted hyperbola to the picked traveltimes; step 5 computes the difference from the picked time of the reflection (x, t) to the estimated apex time for the traces at non-zero offset, which in turn is an improved moveout correction; in step 6 the reflection is flattened at the hyperbola apex time (t_0) after the reflection-picked moveout correction for each CMP gather prior to stack (Figure 4.14).

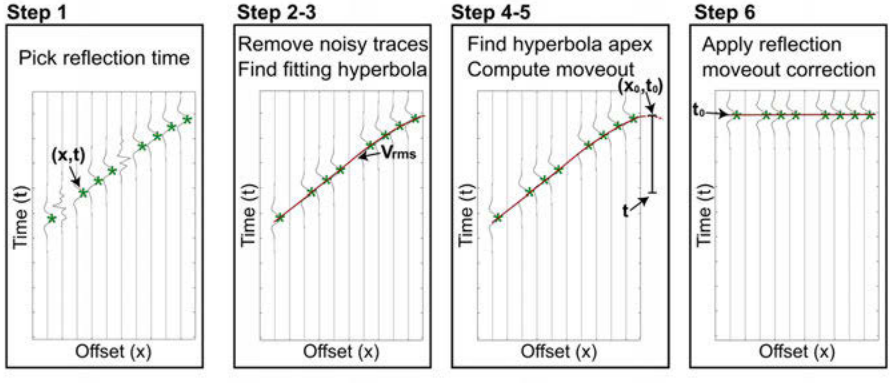

Figure 4.14. Example of the proposed reflection-picked moveout correction process on synthetic data. This method tackles the issues of SS-wavefield static and NMO corrections.

Applied to the data this method appears effective in increasing the flattening of the reflections in CMP gathers and the reflection horizon continuity in the final SS-wavefield stacked section with respect to the traditional NMO method (Figure 4.15). The SS-wavefield unmigrated stacked section shows a continuous horizon at 300 to 400 ms, with improved details compared to the PP-wavefield stacked section due to the characteristic lower velocities of S-waves with respect to P-waves (Carr et al., 1998; Krawczyk et al., 2013a).

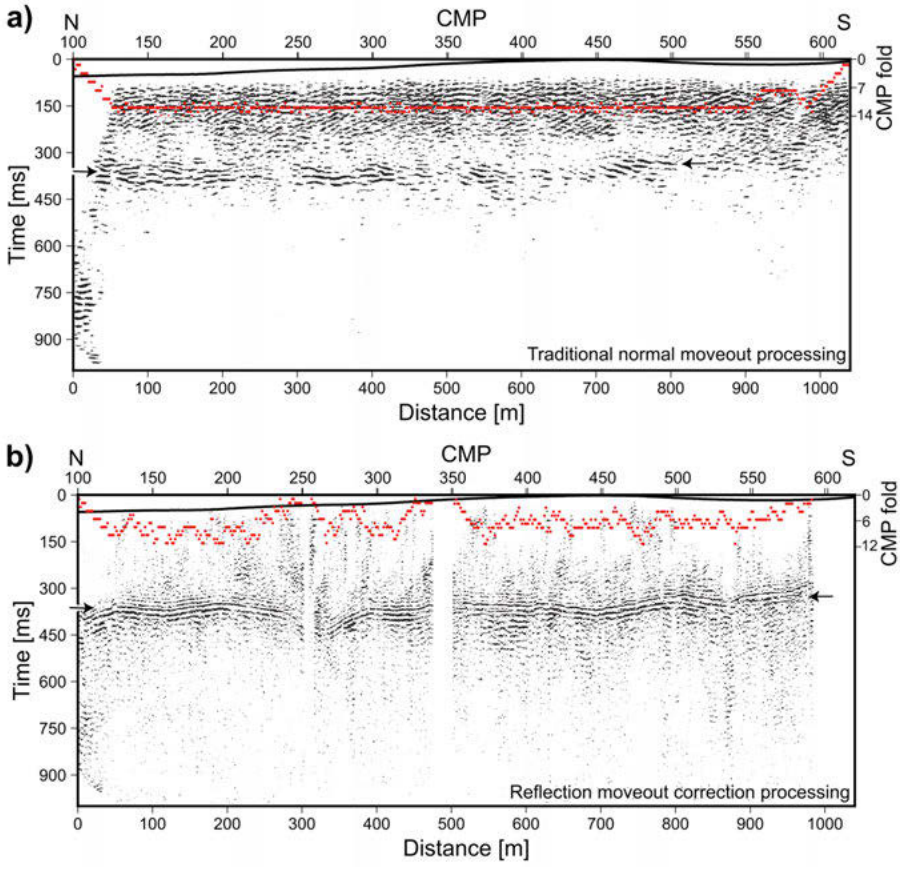

Figure 4.15. Unmigrated stacked section of SS-wavefield from the HT component data after (a) NMO correction and (b) the reflection-picked moveout correction developed in this study. Red dots correspond to the CMP fold for each section, it is lower in (b) due to the discarded traces with no-picks.

To validate the results and to assist the near-surface interpretation, a detailed velocity analysis was performed. P-wave first-break traveltime tomography (Tryggvason et al., 2002) was applied to the nodal array data. The choice of a different dataset ensures a higher independency of the results while the higher offset and fold coverage of the nodal array data with respect to the

landstreamer data permits inversion stability and deeper ray penetration. The resulting velocities range from 800 m/s at the surface to 2700 m/s at around 100 m below sea level. High velocity contrasts are visible at approximately 15 and -15 m elevations. To compute the S-wave velocity model, a laterally constrained inversion from the recorded surface-waves (Socco et al., 2009) in the vertical component data of the landstreamer was performed. The resulting velocities are from 150 m/s at the surface to 600 m/s at the sea level, with a general trend of southwards increasing velocity. The resulting V_P/V_S between the two computed models shows peak values from 3 to 4 forming a horizon at around 5-10 m elevation on background values from 1.5 to 2.

Implementing the unmigrated SS-wavefield stacked section converted to depth and the velocity analysis results, a near-surface interpretation is suggested according to the local geology (Figure 4.16). The depth of the V_P/V_S anomaly (5-10 m elevation) is located just below the first P-wave high velocity contrast (15 m elevation); this correlation has been interpreted as the result of the water table, where the substitution of air in the pores by water increases the P-wave velocity but does not affect the S-wave velocity (Pasquet et al., 2015). This interpretation is also supported by the boreholes in the area that report a water table depth between 15 and 20 m elevation. The second P-wave high velocity contrast (-15 m elevation) matches the horizon imaged on the SS-wavefield stacked section. This boundary is interpreted as the top of the Chalk Group (first pre-Quaternary layer) and specifically the top of the Danian limestones (Figure 4.16).

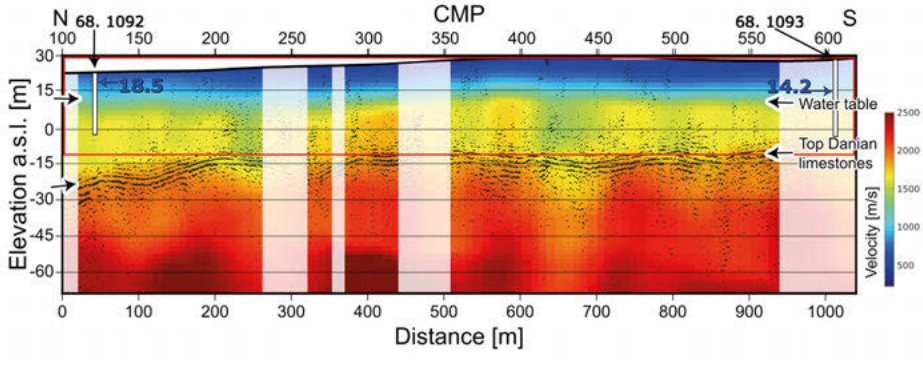

Figure 4.16. P-wave traveltime tomography superimposed to the SS-wavefield unmigrated stacked section converted to depth. Available boreholes with water table information are plotted onto the section. The interpreted water table and top of the Danian limestones are indicated by the arrows. The white areas correspond to low CMP fold (<5) hence excluded from the interpretation.

4.4.2 Conclusions

Exploring the 3C data recorded from the landstreamer during the main CCS survey in the Gassum area highlighted the potential and versatility of this

acquisition setup for different investigation scales. The presented data show another case study where a SS-wavefield can be generated and recorded from P-wave sources. The acquired SS-wavefield data present higher resolution with respect to the PP-wavefield data, but specific processing steps are required to separate SS-waves and surface-waves. In this study, a processing method is developed to substitute the standard velocity analysis, NMO and static corrections to tackle this challenge. Results from the proposed reflection-picked moveout correction method appear robust and efficient with increased continuity on the flattened CMP gathers and on the imaged horizon in the final SS-wavefield stacked section. However, the method can be time consuming for large datasets since a manual pick of the desired reflection is required. Additionally, the actual method focuses the stacked section on a single reflection, disturbing eventual extra reflections at different depths. The final interpretation successfully detects the water table depth and the base of the quaternary sequence at approximately 15 and -15 m of elevation, respectively. The quality of the results obtained from the HT component underscores the applicability of the proposed method in multicomponent acquisitions for providing additional subsurface geological information as a by-product of large-scale site investigations.

5 Conclusions

In this thesis work, an onshore dual-element recording system is applied to broaden reflection seismology applications in the domains of acquisition, processing and interpretation. The acquisition system is used in different environments and processing techniques are developed to enhance the imaging quality resulting from this acquisition setup. The adaptability of the dual-element acquisition system enables its application in complex urban environments and, together with the developed processing, ensures high quality subsurface images with high-resolution in a wide depth range.

This thesis demonstrates the feasibility of the proposed acquisition system for hard-rock environments (**Paper II**) and CCS reservoir investigations (**Papers III** and **IV**), highlighting its advantages and disadvantages. This unique setup required to develop a processing flow to optimize strengths of both recording systems, resulting in a single wide-scale high-resolution seismic image from the two acquisition elements (**Paper III**). This paradigm was further developed in **Paper IV**, where the acquisition system and processing flow applied to the onshore data were extended and adapted to an onshore transition to offshore zone using a total of four receiver systems. This updated approach proved effective, as evidenced by improved S/N and complimentary illumination of seismic reflectors at different depths, showing subsurface information of the area for the first time. An SS-wavefield processing flow was developed in **Paper VI** to exploit the previously unused horizontal components of the landstreamer. In this study, the traditional NMO correction was replaced with a reflection-picked moveout correction that was more successful in discriminating shallow SS-wave reflections from surface-waves noise. The extracted SS-wave reflection was then used to provide a more detailed model of the near-surface geology. The application of complementary analyses along the whole thesis highlights the importance of exploiting the strengths of different data characteristics to gain information for helping the subsurface reconstruction.

The solutions developed in this thesis are applied to real-world scenarios to showcase their relevance in diverse environments and fields of research. Three major crustal-scale fault systems are partially imaged, and their relative structures reconstructed in the densely populated hard-rock environment of

metropolitan Seoul for the first time in the region (**Paper II**). The deep structures were retrieved from the nodal array while the bedrock geometries were reconstructed from a single segment of the landstreamer. The implementation of the two datasets constrained the location of faults along the profile. This required the design of an acquisition and processing flow that compensated for the low S/N typical of this environment. **Papers III** and **IV** successfully investigated structures of interest for CCS characterization, particularly the target reservoir and its internal structure, the primary seal and the presence of faults. The applied acquisition setup and developed merging technique were crucial to reach the desired resolution at all pertinent depths. Multicomponent analyses and S-wave imaging performed on the 3C landstreamer data proposed a method to obtain a highly detailed near-surface image as a by-product of larger scale acquisitions (**Paper VI**). Results with the complementary analyses lead to the identification of the water table depth and of the top Chalk Group (first pre-Quaternary layer), proving the multicomponent analyses potential of this acquisition setup and its suitability for engineering and hydrological investigations.

The work performed in **Papers I** and **II** is an important step for the seismic risk mitigation in metropolitan Seoul. The relation between seismicity and faults helps in understanding the characteristics of the possible earthquakes (e.g., spatial distribution, depth, magnitude, frequency occurrence, focal mechanism) and therefore to properly prepare the city for their occurrence, with building and construction regulations and with the preparation of safe plans for the citizens. Furthermore, this case study presents the effectiveness of reflection seismology and of the applied system for cases in similar environments, often challenging for subsurface studies.

Reduction of greenhouse gases from the atmosphere is one of the globally proposed solutions to mitigate climate change. **Papers III-V** are part of this solution and propose a method to map the subsurface structures identified as possible storage for sequestrated CO_2 and to identify areas with risk of CO_2 leakage towards the surface. The applied methods are developed as a time-cost effective solution for a first stage structural exploration.

The development in this thesis of novel acquisition and processing methods addressing seismic risk and climate change underscores the role of reflection seismology in tackling major contemporary challenges.

5.1 Future developments

While working on this thesis, ideas for future research and development were also considered.

In settings as the one presented in **Paper II**, a denser nodal array may help to increase the CMP fold coverage and further improve the S/N, thus a spacing of 10 m for the nodal array is suggested for future similar studies when possible. This choice is justified by the results in **Papers III** and **IV**.

Migration of all seismic data of this work have been applied in the post-stack domain. Different migration methods for more complex geometries should be considered for further developments. The application of pre-stack migrations, RTM or FWI to the pre-stack merged data may require additional studies and development, likely necessitating different or additional steps during the processing flow. The resulting effects to the data should also be evaluated to avoid the occurrence of artefacts.

The onshore transition to offshore zone acquisition implemented in **Paper IV** will benefit from an additional marine streamer deployed on the other side of the marine channel for a symmetric and higher CMP fold coverage. A higher number of OBSs with a smaller spacing will also improve the quality of the data in the central part of the marine channel with a higher CMP fold coverage. The development and implementation of a nature-friendly marine source will allow the detection of shallow subsurface horizons that were not sampled along the marine channel, increasing the continuity with the onshore data for shallow horizons.

The landstreamer positioning with the DGPS system tested in **Paper VI** should be further developed on the hardware side to enable its implementation in a time-cost efficient way and to ensure a more accurate analysis of the acquired landstreamer data.

The reflection-picked moveout correction method proposed in **Paper VI** can be further developed to consider more complex geometries. Integration with other processing steps, such as dip moveout (DMO) correction, is needed to consider dipping reflections. The application of a layer stripping approach is suggested to enable the detection of multiple reflections.

6 Additional studies

6.1 Paper I: Fault intersections control short period intraplate start-stop seismicity in the Korean Peninsula

After the occurrence in 2011 of the Tohoku-Oki mega-thrust Mw 9.0 earthquake in Japan, the Korean peninsula faced an increase in recorded seismicity (Hong et al., 2017). **Paper I** presents the first in-depth study on the relation between this seismicity and crustal-scale fault structures in the region. Two profiles of 6 and 12 km, profiles 1 and 2 respectively, were recorded using the dual-element acquisition system above previously recorded seismicity clusters (Figure 2.7). Profile 1 is placed north of Seoul city while profile 2 is placed on the outskirt of Seoul city, facing a complex environment with high background noise. The challenging seismic processing complemented with velocity analysis allowed different interpretations. Profile 1 imaged two fault zones intersecting the seismicity clusters in depth (approximately 4 and 8 km) at the intersection with a main sub-vertical mapped fault. This suggests that fault systems control the seismicity in the area at their intersecting points (Figure 6.1). Profile 2 migrated section shows shallow reflections down to 1 km of depth, most likely corresponding to the fault systems imaged in profile 1 and highlighting the potential seismic risk of the city (Figure 6.1).

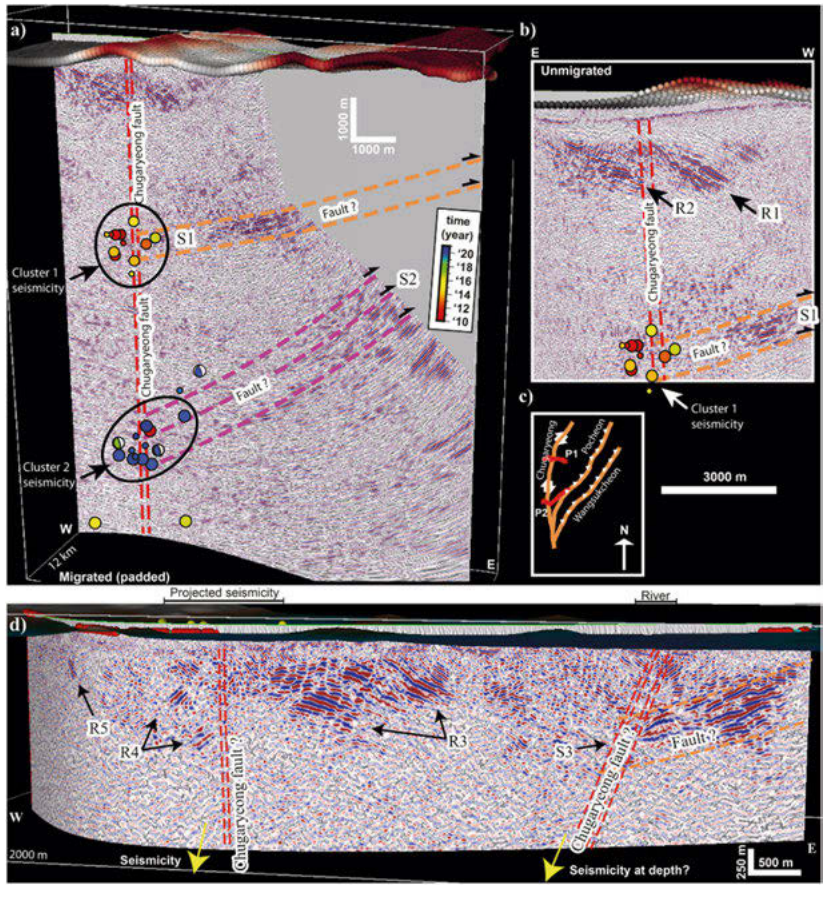

Figure 6.1. (a) Seismic section of profile 1 showing strong temporal and spatial correlation between zones of reflectivity and the two clusters of seismicity. (b) The sudden increase in bedrock depth along with the interruption in the reflectivity at shallow depth (R1 and R2) is interpreted as due to the presence of the Chugaryeong sub-vertical fault. (c) Aerial view of the three main fault systems. (d) Seismic section of profile 2 with seismicity (at depth of 7–9 km) projected onto the surface (yellow spheres).

6.2 Paper V: Advancements in seismic imaging for geological carbon storage: Study of the Havnsø structure, Denmark.

After processing all the acquired profiles in the Havnsø site, **Paper V** proceeds with the geological interpretation of the structures in the area from the resulting migrated sections. The applied acquisition system and processing are the same as described in **Paper IV**, with minor changes depending on local differences. Migrated sections are plotted in 3D and the horizons of interest for the CCS investigation are picked as follows: top of the Chalk Group, base of

the Chalk Group, top of the Fjerritslev Formation, top of the Gassum Formation, base of the Gassum Formation and top of the Zechstein Group. Horizons are extrapolated from a 2D interpolation of the picks and compared with the previous onshore and offshore seismic sections. A mismatch between the interpolated horizons and the nearby offshore seismic sections indicated the need for a higher point coverage on the Nekselø island area and thus the nearby offshore seismic sections were picked and included to update the interpolated horizons (Figure 6.2). These horizons were used for computing the thickness of the Chalk Group, the Fjerritslev Formation (primary seal) and the Gassum Formation (reservoir rock). The interpretation identified a clear four-way-closure domal structure defined at the reservoir depth (red contour in Figure 6.2c) used for an estimation of the CO_2 static storage capacity (27 Mt). Primary seal and reservoir rock exhibit mostly a uniform thickness with no significant faults detected in the area, supporting future explorations for the reservoir exploitation.

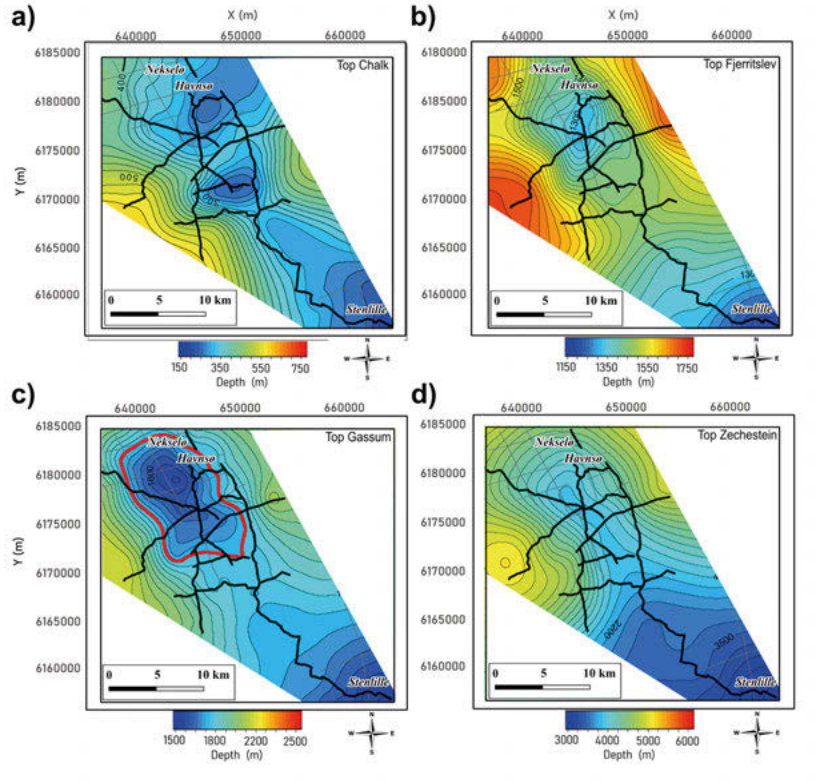

Figure 6.2. Estimated depth of (a) the Top Chalk, (b) the Top Fjerritslev Formation, (c) the Top Gassum Formation and (d) the Top Zechstein. The Top Fjerritslev and Top Gassum display a similar oval shape and northwest-southeast orientation, indicating the four-way domal structure of the Havnsø reservoir caused by the movements of the underlying Zechstein salt.

6.3 Paper VII: Reflection seismic imaging across the Thinia valley (Greece)

The Greek Kefalonia island is the background of **Paper VII**. Over the last years, the closure of a marine channel along the actual isthmus connecting the main part of the island to the Paliki peninsula has been disputed, suggesting a relation between Paliki and Homer's Ithaca. To improve the subsurface knowledge of this area, three 2D onshore seismic profiles (3.5 km long in total) were acquired using a nodal array with a 5 m receiver and shot spacing and an accelerated weight drop as a source in the Thinia valley. The sharp topographic changes and morphological features of the valley were the main challenge for this survey, however, the acquired data show visible reflections with variable quality for the different profiles. First-break traveltime tomography, 3D reflection traveltime modelling and borehole lithological columns complemented the seismic reflection processing work. Profile 1 have the highest S/N ratio among the profiles, its results (Figure 6.3) suggest the presence of a low-velocity zone with no reflectivity from the surface to approximately 100 m depth, probably related to the presence of loose material. Below it, an interpreted east-dipping reflector is displaced by three highly east-dipping structures interpreted as reverse faults and expression of the Hellenide thrusts that govern the regional tectonics. These findings further constrain the recent tectonic history of the area and prove the efficiency of the applied method in similar environments. The retrieved in-depth information will be the base for future acquisitions and will contribute to the water channel debate.

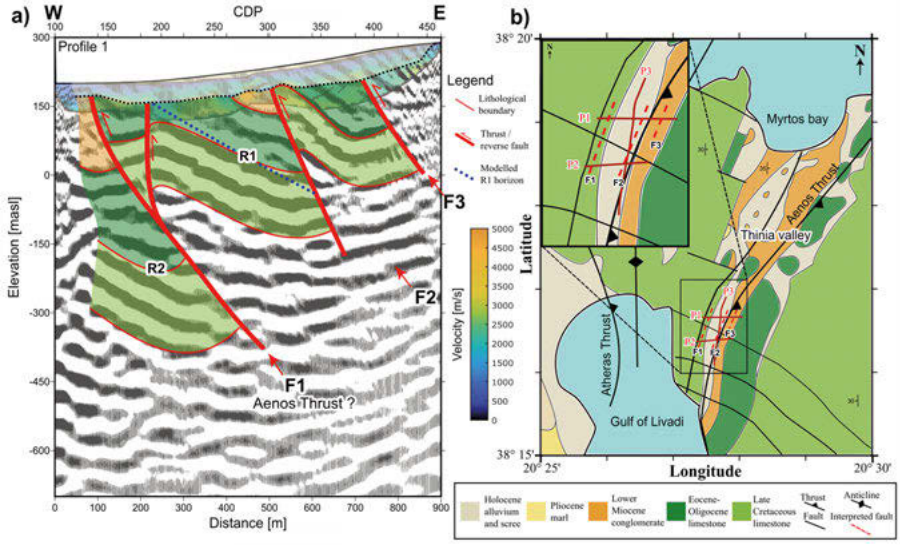

Figure 6.3. Interpreted results from profile 1 in Kefalonia island. (a) Migrated stacked section with interpreted reverse faults system and velocity model resulting from the first-break traveltime tomography. Blue dots show the modelled horizon resulting from the 3D reflection traveltime modelling. (b) Geological map of the Thinia valley. In red are the locations of the seismic profiles and as dashed lines the projection of F1, F2 and F3 to the surface.

7 Swedish summary

År 2015 antog världsledare de 17 globala målen för hållbar utveckling (SDG) för att hantera globala miljö- och samhällsutmaningar fram till 2030. Av dessa är mål 9 (Hållbar industri, innovation och infrastruktur) och mål 13 (Bekämpa klimatförändringarna) särskilt relevanta för denna forskning. I denna avhandling skalas ett innovativt 2D-reflektionsseismiskt insamlingssystem upp för seismisk riskbedömning och undersökning av berggrunden och ytnära sediment, med fokus på koldioxidlagring (CCS) och minskning av utsläpp av växthusgaser till atmosfären.

Seismiska insamlingssystemet består av seismiska vibratorer som signalkällor och två olika registreringssystem: ett nodbaserat array-system med vertikala geofoner (1C) för långa avstånd mellan källpunkt och mottagare, med geofon intervaller mellan 10 och 20 meter, samt ett MEMS-baserat landstreamer-system (3C) för korta avstånd, med geofon intervaller på 2 meter. Detta dubbelelementssystem möjliggör samtidig registrering av högkvalitativa seismiska data för både yt- och djupundersökningar. De metoder som utvecklats i denna avhandling har tillämpats i fält, vilket bekräftar deras relevans inom olika forskningsfält och miljöer.

Bedömning av seismiska risker i städer är avgörande för att säkerställa hållbar infrastruktur, särskilt i områden såsom Koreahalvön, som fungerar som en viktig tektonisk länk mellan östra Kina och Japan. Tohoku-Oki-megajordbävningen (Mw 9,0) 2011 ledde till ökad seismisk aktivitet i regionen, vilket innebär betydande risker för Seoul, en storstadsregion med cirka 20 miljoner invånare. Med tanke på den höga seismiska risken undersöker denna forskning sambandet mellan förkastningssystem i jordskorpan och registrerad seismisk aktivitet. **Artikel I** fokuserar på att identifiera relationer mellan tektoniska strukturer och nyligen observerade seismiska kluster, **Artikel II** presenterar avbildningsresultat av större sprickzoner. Tre större sprick-system i jordskorpan avbildades delvis, och deras strukturer rekonstruerades. De djupa strukturerna erhölls med hjälp av det nodala array-systemet, medan berggrundsgeometrier rekonstruerades med data från landstreamern. Kombinationen av dessa data möjliggjorde en mer exakt bedömning av sprick-system lokalisering, vilket förbättrade förståelsen av seismiska faror i Koreahalvön och bidrog till bättre jordbävningsberedskap.

Danmark, en global ledare inom CCS, har prioriterat geologisk lagring av CO_2 som en del av sin klimatstrategi, med målet att uppnå koldioxidneutralitet

till 2050. Dock kvarstår betydande kunskapsluckor angående lämpliga geologiska formationer för CO_2-lagring. För att adressera detta initierades en serie seismiska undersökningar i 2022 för att kartlägga fem potentiella geologiska lagringsplatser på land och uppskatta deras lagringskapacitet, samtidigt som säkerhet och hållbarhet i CCS-verksamheten säkerställdes. **Artiklar III-V** beskriver insamlingen och bearbetningen av seismiska data vid två av dessa platser, inklusive ett område där insamlingen övergår från land- till havsbaserad seismik. Upp till fyra simultana registreringssystem användes, vilket krävde en anpassad bearbetningsstrategi för att hantera individuella dataset och deras efterföljande sammanfogning. Detta förbättrade signal-brusförhållandet (S/N) och förbättrade avbildningen av seismiska reflektorer på olika djup. De resulterande högupplösta bilderna gav, för första gången, en detaljerad berggrundskarta över dessa områden, inklusive reservoar-sandstenen och dess interna struktur, det primära tätskiktet och närvaron av sprickor. Den anpassade insamlingsmetoden och den utvecklade sammanfogningstekniken var avgörande för att uppnå den önskade upplösningen på alla relevanta djup.

Det dubbelelementssystem som föreslås i denna avhandling har också en betydande fördel för skjuvvågsavbildning (S-vågor), vilken vanligtvis ger högre upplösning än traditionell tryckvågsavbildning (P-vågor), förutsatt att liknande frekvenser uppnås. **Artikel VI** utnyttjar denna potential genom att tillämpa S-vågsavbildning på delar av CCS-reservoarundersökningarna. Bearbetningen av S-vågsdata krävde en specialdesignad reflektionsbaserad korrigering av gångtider, för att förstärka reflektioner som tidigare var maskerade av ytvågor. Denna nya bearbetningsmetod förbättrade avsevärt reflektionskontinuiteten, och kompletterande analyser möjliggjorde identifiering av grundvattenytans djup samt överdelen av kalkstensformationen (Chalk Group), den första pre-kvartära enheten. Dessa resultat visar potentialen hos multikomponentanalys, vilket möjliggör högupplösta bilder av ytnära strukturer till låga insamlingskostnader, som en biprodukt av storskaliga undersökningar.

Detta flexibla seismiska insamlingssystem är särskilt användbart i komplexa urbana miljöer. Tillsammans med de utvecklade bearbetningsteknikerna säkerställs högkvalitativa avbildningar av berggrunden och ytnära sediment över ett brett djupintervall. Denna avhandling visar genomförbarheten av det föreslagna insamlingssystemet för både hårda bergarter (**Artikel II**) och CCS-reservoarundersökningar (**Artiklar III** och **IV**). Vidare presenteras en ny bearbetningsstrategi som effektivt sammanfogar data från flera registreringssystem till en enhetlig högupplöst seismisk bild, där både land- och havsbaserade insamlingselement integreras (**Artiklar III** och **IV**). Dessutom utnyttjar den utvecklade S-vågsbearbetningen i **Artikel VI** tidigare oanvända horisontella komponenter från landstreamern, genom att ersätta den traditionella NMO-korrektionen (normal moveout) med en reflektionsbaserad korrigering av gångtider, vilket visade sig vara mer framgångsrikt i att särskilja grunda S-vågsreflektioner från ytvågsbrus. De kompletterande analyserna genom hela

avhandlingen betonar vikten av att utnyttja olika seismiska datakarakteristiker för att förbättra avbildning och rekonstruktion av sediment och berg under markytan.

Genom att utveckla innovativa insamlings- och bearbetningsmetoder för att hantera seismiska risker och klimatförändringar, framhäver denna forskning den avgörande rollen som reflektionsseismologi spelar i att lösa globala utmaningar.

Acknowledgments

These years in Uppsala have been filled with both joy and challenges (such a cold winter!), but most importantly, they have been filled with friends. Friends from Sweden, Italy, and all over the world and I want to thank each and every one of you.

To **Alireza**, my main supervisor, I am deeply grateful for the countless lessons and valuable advice that have shaped both my career and personal growth. Your dedication to revising my research over and over again until we achieved the best possible results has been invaluable. But above all, I am thankful for the many field campaigns we conducted around the world, where I learned so much in every possible way.

I extend my sincere thanks to all the professors who guided me at Uppsala University, especially my co-supervisors **Ayse** and **Chris**, for always being ready to answer my questions and support my research.

I am also grateful to all my co-authors, who contributed to making my research more thorough and complete, and to the reviewers who dedicated their time to providing insightful feedback, helping to refine my work and make it accessible to a broader audience.

To my colleagues and friends **Arianna, Bojan, Emmanuel, Ewelina, Felix, Gabriele, George, Greg, Isabelle, Jolanta, Kristina, Lea, Liuqing, Magdalena, Manos, Mike, Myrto, Ruth, Tatiana, Viktor, Yinshuai,** and **Zibi**, thank you for sharing this journey with me and for patiently listening to my complaints! **Tatiana**, thank you for your guidance; you did an incredible job as a mentor, introducing me to Sweden (I am sure my PhD twin **Zibi** will agree). You not only taught me about academic life but also how to enjoy this cold country, always smiling no matter the circumstances! **Myrto**, I truly appreciate your experience and willingness to share knowledge. After many papers together, we still have so much to learn from each other, and every discussion sparks new ideas to explore. **Lea**, thank you for sharing the office with me. Long hours of work always seemed to pass faster after a quick chat together, even when it was -10° outside and you were opening the window! **Mike** (and **Ruth**), I am grateful for the fun times we had both at work and

outside. Even if our home countries are far from each other, we discovered how much we have in common, from our passion for research to board games and movie nights. You remind me that no matter how far apart we are, we are all part of the same world! Thanks to everyone that was in the field with me, facing all the challenges in every condition, but always ready to enjoy the deserved free time after them!

To my **family**, my grandparents, cousins, aunts, and uncles, who have followed my journey from afar and always welcomed me back with open arms. To my **mum** and **dad**, who have supported me unconditionally and given me advice on every decision, I hope I have made you proud. **Miriam**, thank you for taking care of everyone while I have been away, it looks like you are finally growing up! And **Cristian**, you still have some time before growing up, but you are on the right track. Keep giving your best.

Clelia, more than anyone else, you know how difficult some moments were during these years. But likely I was not alone, you were there, ready to give me the strength to stand up and move further. I hope that all our adventures and sacrifices will, at some point, bring us where we want.

Finally, I want to extend my gratitude to everyone who has contributed, directly or indirectly, to this journey, making this PhD more fruitful and enjoyable.

To all of you, thanks!

Samuel,

Uppsala, April 2025

References

Abramovitz, T., Vosgerau, H., Gregersen, U., Smit, F. W. H., Bjerager, M., Jusri, T. A., Mathiesen, A., Mørk, F., Schovsbo, N. H., Petersen, H. I., Nielsen, L. H., Laghari, S., Rasmussen, L. M., & Keiding, M. (2024). CCS2022-2024 WP1: The Rødby structure Seismic data and interpretation to mature potential geological storage of CO_2. *Geological Survey of Denmark and Greenland Danish Ministry of Climate, Energy and Utilities*, Report 2024/18. https://doi.org/10.22008/gpub/34739

Adly, A., Poggi, V., Fäh, D., Hassoup, A., & Omran, A. (2017). Combining active and passive seismic methods for the characterization of urban sites in Cairo, Egypt. *Geophysical Journal International*, 210(1), 428–442. https://doi.org/10.1093/gji/ggx176

Aki, K., & Richards, P. G. (2002). Quantitative seismology (2nd ed.). *University Science Books*, Mill Valley, USA. ISBN: 1891389637

ANCORP Working group. (1999). Seismic reflection image revealing offset of Andean subduction-zone earthquake locations into oceanic mantle. *Nature*, 397(6717), 341–344. https://doi.org/10.1038/16909

Ayarza, P., Juhlin, C., Brown, D., Beckholmen, M., Kimbell, G., Pechnig, R., Pevzner, L., Pevzner, R., Ayala, C., Bliznetsov, M., Glushkov, A., & Rybalka, A. (2000). Integrated geological and geophysical studies in the SG4 borehole area, Tagil Volcanic Arc, Middle Urals: Location of seismic reflectors and source of the reflectivity. *Journal of Geophysical Research: Solid Earth*, 105(B9), 21333–21352. https://doi.org/10.1029/2000jb900137

Bae, H.-K., & Lee, H.-K. (2016). Quaternary activity patterns of the Wangsukcheon Fault in the Pocheon-Namyangju area, Korea. *Journal of the Geological Society of Korea*, 52(2), 129–147. https://doi.org/10.14770/jgsk.2016.52.2.129

Barr, F. J., Nyland, D. L., & Sitton, G. A. (1993). Attenuation of flexural ice waves and random noise using both geophones and hydrophones. *1993 SEG Annual Meeting*, 555–557. https://doi.org/10.1190/1.1822549

Beckel, R. A., & Juhlin, C. (2019). The cross-dip correction as a tool to improve imaging of crooked-line seismic data: a case study from the post-glacial Burträsk fault, Sweden. *Solid Earth*, 10(2), 581–598. https://doi.org/10.5194/se-10-581-2019

Bellefleur, G., Barnes, A., Calvert, A., Hubert, C., & Mareschal, M. (1995). Seismic reflection constraints from Lithoprobe line 29 on the upper crustal structure of the northern Abitibi greenstone belt. *Canadian Journal of Earth Sciences*, 32(2), 128–134. https://doi.org/10.1139/e95-011

Bharadwaj, P., Drijkoningen, G., Mulder, W., Thorbecke, J., Neducza, B., & Jenneskens, R. (2017). A shear-wave seismic system using full-waveform inversion to look ahead of a tunnel-boring machine. *Near Surface Geophysics*, 15(3), 210–225. https://doi.org/10.3997/1873-0604.2017014

Bredesen, K., Lorentzen, M., Smit, F., & Gregersen, U. (2022). Quantitative seismic interpretation of the Gassum Formation at the Stenlille aquifer gas storage. *Proceedings of the 16th Greenhouse Gas Control Technologies Conference.* http://dx.doi.org/10.2139/ssrn.4276697

Brittle, K. F., Lines, L. R., & Dey, A. K. (2001). Vibroseis deconvolution: A comparison of cross-correlation and frequency-domain sweep deconvolution. *Geophysical Prospecting*, 49, 675–686. https://doi.org/10.1046/j.1365-2478.2001.00291.x.

Brodic, B., Malehmir, A., Juhlin, C., Dynesius, L., Bastani, M., & Palm, H. (2015). Multicomponent broadband digital-based seismic landstreamer for near-surface applications. *Journal of Applied Geophysics*, 123, 227–241. https://doi.org/10.1016/j.jappgeo.2015.10.009

Brodic, B., Malehmir, A., Pugin, A., & Maries, G. (2018). Three-component seismic land streamer study of an esker architecture through S- and surface-wave imaging. *Geophysics*, 83(6), B339–B353. https://doi.org/10.1190/geo2017-0747.1

Brown, L., Barazangi, M., Kaufman, S., & Oliver, J. (1986). The first decade of COCORP: 1974–1984. In *Reflection Seismology: A Global Perspective* (Vol. 13, pp. 107–120). American Geophysical Union. https://doi.org/10.1029/GD013p0107

Burschil, T., & Buness, H. (2020). S-wave seismic imaging of near-surface sediments using tailored processing strategies. *Journal of Applied Geophysics*, 173. https://doi.org/10.1016/j.jappgeo.2019.103927

Carr, B. J., Hajnal, Z., & Prugger, A. (1998). Shear-wave studies in glacial till. *Geophysics*, 63(4), 1273–1284. https://doi.org/10.1190/1.1444429

Chen, Y., Hu, J., & Peng, F. (2018). Seismological challenges in earthquake hazard reductions: reflections on the 2008 Wenchuan earthquake. *Science Bulletin*, 63(17), 1159–1166. https://doi.org/10.1016/j.scib.2018.06.015

Cheraghi, S., White, D. J., Draganov, D., Bellefleur, G., Craven, J. A., & Roberts, B. (2017). Passive seismic reflection interferometry: A case study from the Aquistore CO_2 storage site, Saskatchewan, Canada. *Geophysics,* 82(3), B79–B93. https://doi.org/10.1190/geo2016-0370.1

Choi, S.-J., Chwae, U.-C., Lee, H.-K., Song, Y.-G., & Kang, I.-M. (2012). Review on the Chugaryeong Fault. *Economic and Environmental Geology*, 45(4), 441–446. https://doi.org/10.9719/EEG.2012.45.4.441

Chough, S., Kwon, S. T., Ree, J. H., & Choi, D. K. (2000). Tectonic and sedimentary evolution of the Korean peninsula: a review and new view. *Earth-Science Reviews*, 52(1–3), 175–235. https://doi.org/10.1016/S0012-8252(00)00029-5

Colombero, C., Comina, C., & Valentina Socco, L. (2019). Imaging near-surface sharp lateral variations with surface-wave methods – Part 1: Detection and location. *Geophysics*, 84(6), EN93–EN111. https://doi.org/10.1190/geo2019-0149.1

Colombero, C., Papadopoulou, M., Kauti, T., Skyttä, P., Koivisto, E., Savolainen, M., & Socco, L. V. (2022). Surface-wave tomography for mineral exploration: a successful combination of passive and active data (Siilinjärvi phosphorus mine, Finland). *Solid Earth*, 13(2), 417–429. https://doi.org/10.5194/se-13-417-2022

Cox, D. R., Newton, A. M. W., & Huuse, M. (2020). An introduction to seismic reflection data: acquisition, processing and interpretation. In *Regional Geology and Tectonics: Principles of Geologic Analysis* (pp. 571–603). Elsevier. https://doi.org/10.1016/B978-0-444-64134-2.00020-1

Danish Ministry of Climate - Energy and Utilities. (2021). A Road Map for the Capture, Transport and Storage of CO_2. The second part of a complete CCS strategy. https://en.kefm.dk/climate/carbon-capture-and-storage

Draganov, D., Campman, X., Thorbecke, J., Verdel, A., & Wapenaar, K. (2009). Reflection images from ambient seismic noise. *Geophysics*, 74(5), A63–A67. https://doi.org/10.1190/1.3193529

Draganov, D., & Ruigrok, E. (2015). Passive Seismic Interferometry for Subsurface Imaging. In: Beer, M., Kougioumtzoglou, I., Patelli, E., Au, IK. (eds) *Encyclopedia of Earthquake Engineering.* Springer, Berlin, Heidelberg. https://doi.org/10.1007/978-3-642-36197-5_378-1

Dragoset, B., & Barr, F. J. (1994). Ocean-bottom cable dual-sensor scaling. *SEG Technical Program Expanded Abstracts*, 857–860. https://doi.org/10.1190/1.1932022

Dziejarski, B., Krzyżyńska, R., & Andersson, K. (2023). Current status of carbon capture, utilization, and storage technologies in the global economy: A survey of technical assessment. *Fuel*, 342, 127776. https://doi.org/10.1016/j.fuel.2023.127776

Eaton, D. W., Milkereit, B., & Salisbury, M. H. (Eds.). (2003). Hardrock Seismic Exploration. *Society of Exploration Geophysicists*. https://doi.org/10.1190/1.9781560802396

Feng, R., & McEvilly, T. V. (1983). Interpretation of seismic reflection profiling data for the structure of the San Andreas fault zone. *Bulletin of the Seismological Society of America*, 73(6A), 1701–1720. https://doi.org/10.1785/BSSA07306A1701

Forbes, S. M., Verma, P., Curry, T. E., Friedmann, S. J., & Wade, S. M. (2008). Guidelines for carbon dioxide capture, transport and storage. *World Resources Institute*. http://pdf.wri.org/ccs_guidelines.pdf

Frery, E., Gratier, J. P., Ellouz-Zimmerman, N., Loiselet, C., Braun, J., Deschamps, P., Blamart, D., Hamelin, B., & Swennen, R. (2015). Evolution of fault permeability during episodic fluid circulation: Evidence for the effects of fluid-rock interactions from travertine studies (Utah-USA). *Tectonophysics*, 651, 121–137. https://doi.org/10.1016/j.tecto.2015.03.018

Green, A. G., & Mair, J. A. (1983). Subhorizontal fractures in a granitic pluton: Their detection and implications for radioactive waste disposal. *Geophysics*, 48(11), 1428–1449. https://doi.org/10.1190/1.1441428

Gregersen, U., Hjelm, L., Vosgerau, H., Smit, F. W. H., Nielsen, C. M., Rasmussen, R., Bredesen, K., Lorentzen, M., Mørk, F., Lauridsen, B. W., Pedersen, G. K., Nielsen, L. H., Mathiesen, A., Laghari, S., Kristensen, L., Sheldon, E., Dahl-Jensen, T., Dybkjaer, K., Hidalgo, C. A., & Rasmussen, L. M. (2023a). CCS2022-2024 WP1: The Stenlille structure Seismic data and interpretation to mature potential geological storage. *Geological Survey of Denmark and Greenland Danish Ministry of Climate, Energy and Utilities*, Report 2022/26. https://doi.org/https://doi.org/10.22008/gpub/34661

Gregersen, U., Vosgerau, H., Laghari, S., Bredesen, K., Rasmussen, R., & Mathiesen, A. (2020). Capture, Storage and Use of CO_2 (CCUS) Seismic interpretation of existing 2D and 3D seismic data around the Havnsø structure. *Geological Survey of Denmark and Greenland Danish Ministry of Climate, Energy and Utilities*, Report 2020/33.

Gregersen, U., Vosgerau, H., Smit, F. W. H., Lauridsen, B. W., Mathiesen, A., Mørk, F., Nielsen, L. H., Rasmussen, R., Funck, T., Dybkjaer, K., Sheldon, E., Pedersen, G. K., Nielsen, C. M., Bredesen, K., Laghari, S., Olsen, M. L., & Rasmussen, L. M. (2023b). CCS2022-2024 WP1: The Havnsø structure Seismic data and interpretation to mature potential geological storage of CO_2. *Geological Survey of Denmark and Greenland Danish Ministry of Climate, Energy and Utilities*, Report 2023/38. https://doi.org/10.22008/gpub/34705

Han, J.-W., & Lee, H.-K. (2019). Structural behavior and ESR age of the Wangsukcheon Fault developed in Naechon-myeon and Hwahyeon-myeon area, Pocheon, Gyeonggi, Korea. *Journal of the Geological Society of Korea*, 55(4), 377–401. https://doi.org/10.14770/jgsk.2019.55.4.377

Hardage, B. A., & Wagner, D. (2014a). S-S imaging with vertical-force sources. *Interpretation*, 2(2), SE29–SE38. https://doi.org/10.1190/INT-2013-0097.1

Hardage, & Wagner. (2014b). Generating direct-S modes with simple, low-cost, widely available seismic sources. *Interpretation*, 2(2), SE1–SE15. https://doi.org/10.1190/INT-2013-0095.1

Hartog, A.H. (2017). An Introduction to Distributed Optical Fibre Sensors (1st ed.). *CRC Press*. https://doi.org/10.1201/9781315119014

Heinonen, S., Heikkinen, P. J., Kousa, J., Kukkonen, I. T., & Snyder, D. B. (2013). Enhancing hardrock seismic images: Reprocessing of high resolution seismic reflection data from Vihanti, Finland. *Journal of Applied Geophysics*, 93, 1–11. https://doi.org/10.1016/j.jappgeo.2013.03.004

Hjelm, L., Anthonsen, K. L., & Dideriksen, K. (2020). Evaluation of the CO_2 storage potential in Denmark. *Geological Survey of Denmark and Greenland Danish Ministry of Climate, Energy and Utilities*, Report 2020/46.

Hoffe, B. H., Cary, P. W., & Lines, L. R. (1999). A simple and robust method for combining dual-sensor OBC data? *CREWES, Research Report* (Vol. 11).

Hong, T., Chung, D., Lee, J., Park, S., Kim, B., & Kim, W. (2021). Earthquake-Spawning Faults in the Seoul Metropolitan Area and Their Seismic Implications. *Earth and Space Science*, 8(7). https://doi.org/10.1029/2021EA001662

Hong, T., Lee, J., Chi, D., & Park, S. (2017). Seismic Velocity Changes in the Back-arc Continental Crust After the 2011 Mw 9.0 Tohoku-Oki Megathrust Earthquake. *Geophysical Research Letters*, 44(21). https://doi.org/10.1002/2017GL075447

Iding, M., & Ringrose, P. (2009). Evaluating the impact of fractures on the long-term performance of the In Salah CO_2 storage site. *Energy Procedia*, 1(1), 2021–2028. https://doi.org/10.1016/j.egypro.2009.01.263

Ishiyama, T., Sato, H., Abe, S., Kawasaki, S., & Kato, N. (2016). High-resolution 3D seismic reflection imaging across active faults and its impact on seismic hazard estimation in the Tokyo metropolitan area. *Tectonophysics*, 689, 79–88. https://doi.org/10.1016/j.tecto.2016.01.042

Ito, K. (1999). Seismogenic layer, reflective lower crust, surface heat flow and large inland earthquakes. *Tectonophysics*, 306(3–4), 423–433. https://doi.org/10.1016/S0040-1951(99)00069-4

Juhlin, C., Hedin, P., Gee, D. G., Lorenz, H., Kalscheuer, T., & Yan, P. (2016). Seismic imaging in the eastern Scandinavian Caledonides: siting the 2.5 km deep COSC-2 borehole, central Sweden. *Solid Earth*, 7(3), 769–787. https://doi.org/10.5194/se-7-769-2016

Juhlin, C., & Lund, B. (2011). Reflection seismic studies over the end-glacial Burträsk fault, Skellefteå, Sweden. *Solid Earth*, 2(1), 9–16. https://doi.org/10.5194/se-2-9-2011

Juhlin, C., & Stephens, M. B. (2006). Gently dipping fracture zones in Paleoproterozoic metagranite, Sweden: Evidence from reflection seismic and cored borehole data and implications for the disposal of nuclear waste. *Journal of Geophysical Research: Solid Earth*, 111(B9). https://doi.org/10.1029/2005JB003887

Kearey, P., Brooks, M., & Hill, I. (2002). An introduction to geophysical exploration – Third edition. *Blackwell Science*. ISBN: 0-632-04929-4

KIGAM, (Korea Institute of Geology, Mining & Materials). (2008). *Geological report of the Yeoncheon sheet*.

Koivisto, E., Malehmir, A., Heikkinen, P., Heinonen, S., & Kukkonen, I. (2012). 2D reflection seismic investigations at the Kevitsa Ni-Cu-PGE deposit, northern Finland. *Geophysics*, 77(5), WC149–WC162. https://doi.org/10.1190/geo2011-0496.1

Krawczyk, C. M., Polom, U., & Beilecke, T. (2013). Shear-wave reflection seismics as a valuable tool for near-surface urban applications. *The Leading Edge*, 32(3), 256–263. https://doi.org/10.1190/tle32030256.1

Krawczyk, C. M., Polom, U., Malehmir, A., & Bastani, M. (2013). Quick-clay Landslides in Sweden - Insights from Shear-wave Reflection Seismics and Geotechnical Integration. *Near Surface Geoscience 2013-19th EAGE European Meeting of Environmental and Engineering Geophysics*, cp-354. https://doi.org/10.3997/2214-4609.20131348

Larsen, M., Bech, N., Bidstrup, T., & Christensen, N. P. (2006). Kalundborg Case Study, a Feasibility Study of CO_2 Storage in Onshore Saline Aquifers, A CO2STORE Contribution. *Geological Survey of Denmark and Greenland Danish Ministry of Climate, Energy and Utilities*, Report 2007/3.

Larsen, M., Christensen, N. P., & Bidstrup, T. (2003). Saline Aquifer Storage of CO_2 from Major Point Sources — A Danish Case Study. In *Greenhouse Gas Control Technologies - 6th International Conference* (pp. 657–661). Elsevier. https://doi.org/10.1016/B978-008044276-1/50105-7

Lee, K., & Yang, W. S. (2006). Historical Seismicity of Korea. *Bulletin of the Seismological Society of America*, 96(3), 846–855. https://doi.org/10.1785/0120050050

Lee, Y., Park, S., Kim, J., Kim, H. C., & Koo, M.-H. (2010). Geothermal resource assessment in Korea. *Renewable and Sustainable Energy Reviews*, 14(8), 2392–2400. https://doi.org/10.1016/j.rser.2010.05.003

Leonard, M. (2010). Earthquake Fault Scaling: Self-Consistent Relating of Rupture Length, Width, Average Displacement, and Moment Release. *Bulletin of the Seismological Society of America*, 100(5A), 1971–1988. https://doi.org/10.1785/0120090189

Lucas, S. B., White, D., Hajnal, Z., Lewry, J., Green, A., Clowes, R., Zwanzig, H., Ashton, K., Schledewitz, D., Stauffer, M., Norman, A., Williams, P. F., & Spence, G. (1994). Three-dimensional collisional structure of the Trans-Hudson Orogen, Canada. *Tectonophysics*, 232(1–4), 161–178. https://doi.org/10.1016/0040-1951(94)90082-5

Mabon, L., Shackley, S., & Bower-Bir, N. (2014). Perceptions of sub-seabed carbon dioxide storage in Scotland and implications for policy: A qualitative study. *Marine Policy*, 45, 9–15. https://doi.org/10.1016/j.marpol.2013.11.011

Maggio, G., Subašić, S., & Bean, C. J. (2022). Subsurface characterization using passive seismic in the urban area of Dublin City, Ireland. *Geophysical Prospecting*, 70(8), 1432–1454. https://doi.org/10.1111/1365-2478.13255

Malehmir, A., & Bellefleur, G. (2009). 3D seismic reflection imaging of volcanic-hosted massive sulfide deposits: Insights from reprocessing Halfmile Lake data, New Brunswick, Canada. *Geophysics*, 74(6), B209–B219. https://doi.org/10.1190/1.3230495

Malehmir, A., Dahlin, P., Lundberg, E., Juhlin, C., Sjöström, H., & Högdahl, K. (2011). Reflection seismic investigations in the Dannemora area, central Sweden: Insights into the geometry of polyphase deformation zones and magnetite-skarn deposits. *Journal of Geophysical Research: Solid Earth*, 116(B11). https://doi.org/10.1029/2011JB008643

Malehmir, A., Heinonen, S., Dehghannejad, M., Heino, P., Maries, G., Karell, F., Suikkanen, M., & Salo, A. (2017). Landstreamer seismics and physical property measurements in the siilinjärvi open-pit apatite (phosphate) mine, central Finland. *Geophysics*, 82(2), B29–B48. https://doi.org/10.1190/GEO2016-0443.1

Malehmir, A., Hong, T. K., Lee, J., Zappalá, S., Brodic, B., Chung, D., Kim, B., Park, S., Lee, J., & Kil, D. (2022). Fault intersections control short period intraplate start-stop seismicity in the Korean Peninsula. *Tectonophysics*, 834. https://doi.org/10.1016/j.tecto.2022.229387

Malehmir, A., Markovic, M., & Abramovitz, T. (2024). Unravelling Detailed Geological Structures for CCS Applications in Rødby-Denmark. *85th EAGE Annual Conference & Exhibition*, 1–5. https://doi.org/10.3997/2214-4609.202410758

Malehmir, A., Schmelzbach, C., Bongajum, E., Bellefleur, G., Juhlin, C., & Tryggvason, A. (2009). 3D constraints on a possible deep > 2.5 km massive sulphide mineralization from 2D crooked-line seismic reflection data in the Kristineberg mining area, northern Sweden. *Tectonophysics*, 479(3–4), 223–240. https://doi.org/10.1016/j.tecto.2009.08.013

Malehmir, A., Socco, L. V., Bastani, M., Krawczyk, C. M., Pfaffhuber, A. A., Miller, R. D., Maurer, H., Frauenfelder, R., Suto, K., Bazin, S., Merz, K., & Dahlin, T. (2016). Near-Surface Geophysical Characterization of Areas Prone to Natural Hazards. In *Advances in Geophysics* (Vol. 57, pp. 51–146). Elsevier. https://doi.org/10.1016/bs.agph.2016.08.001

Markovic, M., Maries, G., Malehmir, A., von Ketelhodt, J., Bäckström, E., Schön, M., & Marsden, P. (2020). Deep reflection seismic imaging of iron-oxide deposits in the Ludvika mining area of central Sweden. *Geophysical Prospecting*, 68(1), 7–23. https://doi.org/10.1111/1365-2478.12855

Ma, Z., & Qian, R. (2020). Overview of seismic methods for urban underground space. *Interpretation*, 8(4), SU19–SU30. https://doi.org/10.1190/INT-2020-0044.1

McBride, J. H., Hildenbrand, T. G., Stephenson, W. J., & Potter, C. J. (2002). Interpreting the Earthquake Source of the Wabash Valley Seismic Zone (Illinois, Indiana, and Kentucky) from Seismic-reflection, Gravity, and Magnetic-intensity Data. *Seismological Research Letters*, 73(5), 660–686. https://doi.org/10.1785/gssrl.73.5.660

Metz, B., Davidson, O., De Coninck, H., Loos, M., & Meyer, L. (2005). IPCC special report on carbon dioxide capture and storage. *Intergovernmental Panel on Climate Change*. Cambridge University Press, Cambridge, United Kingdom and New York, NY, USA, 442 pp. ISBN-10 0-521-68551-6

Milkereit, B., Berrer, E. K., King, A. R., Watts, A. H., Roberts, B., Adam, E., Eaton, D. W., Wu, J., & Salisbury, M. H. (2000). Development of 3-D seismic exploration technology for deep nickel-copper deposits – A case history from the Sudbury basin, Canada. *Geophysics*, 65(6), 1890–1899. https://doi.org/10.1190/1.1444873

Miller, G., & Pursey, H. (1954). The field and radiation impedance of mechanical radiators on the free surface of a semi-infinite isotropic solid. *Proceedings of the Royal Society of London.* Series A. Mathematical and Physical Sciences, 223(1155), 521–541. https://doi.org/10.1098/rspa.1954.0134

Miocic, J. M., Gilfillan, S. M. V., Roberts, J. J., Edlmann, K., McDermott, C. I., & Haszeldine, R. S. (2016). Controls on CO2 storage security in natural reservoirs and implications for CO_2 storage site selection. *International Journal of Greenhouse Gas Control*, 51, 118–125. https://doi.org/10.1016/j.ijggc.2016.05.019

Moon, S., Kim, H.-J., Kim, C., Jun, H., Lee, S.-H., Joo, H.-T., & Kim, K.-H. (2021). The Quaternary slip rate of the Yangsan Fault offshore the SE Korean Peninsula and implications for seismic hazard assessment. *Geomatics, Natural Hazards and Risk*, 12(1), 310–327. https://doi.org/10.1080/19475705.2021.1872718

Musarra, R. M. L. M., Tassinari, C. C. G., & Cañas, S. S. M. (2022). Perspectives to CO_2 Geological Storage and Greenhouse Gas Negative Emissions in South-Southeastern Brazil: Paraná and Santos Sedimentary Basins. In *Perspectives to CO_2 Geological Storage and Greenhouse Gas Negative Emissions in South-Southeastern Brazil: Paraná and Santos Sedimentary Basins*. Editora Blucher. https://doi.org/10.5151/9786555501346

Nedimović, M. R., & West, G. F. (2003). Crooked-line 2D seismic reflection imaging in crystalline terrains: Part 1, data processing. *Geophysics*, 68(1), 274–285. https://doi.org/10.1190/1.1543213

Nielsen, L. H. (2003). Late Triassic – Jurassic development of the Danish Basin and the Fennoscandian Border Zone, southern Scandinavia. *Geological Survey of Denmark and Greenland Bulletin*, 1, 459–526. https://doi.org/10.34194/geusb.v1.4681

Nielsen, L. Henrik., & Japsen, Peter. (1991). Deep wells in Denmark, 1935-1990 : lithostratigraphic subdivision. *Danmarks geologiske undersøgelse* Serie A, 31, 1-179. https://doi.org/10.34194/seriea.v31.7051

Nielsen, L. H., Mathiesen, A., & Bidstrup, T. (2004). Geothermal energy in Denmark. *Geological Survey of Denmark and Greenland Bulletin*, 4, 17–20. https://doi.org/10.34194/geusb.v4.4771

OECD. (2019). Environmental Performance Reviews: Denmark 2019. *OECD Publishing*, Paris. https://doi.org/10.1787/1eeec492-en

Papadopoulou, M., Zappalà, S., Malehmir, A., Kucinskaite, K., Westgate, M., Gregersen, U., Hjelm, L., Funck, T., & Nielsen, L. (2023). Upscaling Innovative Land Seismic Acquisitions for Geological Storage of CO_2 in Denmark. *84th EAGE Annual Conference & Exhibition*, 1–5. https://doi.org/10.3997/2214-4609.202310385

Park, S., Baek, I., & Hong, T.-K. (2020). Six Major Historical Earthquakes in the Seoul Metropolitan Area during the Joseon Dynasty (1392–1910). *Bulletin of the Seismological Society of America*, 110(6), 3037–3049. https://doi.org/10.1785/0120200004

Pasquet, S., Bodet, L., Dhemaied, A., Mouhri, A., Vitale, Q., Rejiba, F., Flipo, N., & Guérin, R. (2015). Detecting different water table levels in a shallow aquifer with combined P-, surface and SH-wave surveys: Insights from VP/VS or Poisson's ratios. *Journal of Applied Geophysics*, 113, 38–50. https://doi.org/10.1016/j.jappgeo.2014.12.005

Pawar, R. J., Bromhal, G. S., Carey, J. W., Foxall, W., Korre, A., Ringrose, P. S., Tucker, O., Watson, M. N., & White, J. A. (2015). Recent advances in risk assessment and risk management of geologic CO_2 storage. *International Journal of Greenhouse Gas Control*, 40, 292–311. https://doi.org/10.1016/j.ijggc.2015.06.014

Pertuz, T., & Malehmir, A. (2023a). Ultrahigh-resolution shear-wave reflection imaging of vertical-component data in a quick-clay prone to landslide area in southwest Sweden. *Geophysics*, 88(3), B121–B133. https://doi.org/10.1190/geo2021-0832.1

Pertuz, T., & Malehmir, A. (2023b). Ultrahigh-resolution 9C seismic survey in a landslide prone area in southwest of Sweden. *Geophysical Journal International*, 235(3), 2094–2106. https://doi.org/10.1093/gji/ggad346

Pretorius, C. C., Jamison, A., & Irons, C. (1987). Seismic Exploration in the Witwatersrand Basin., Republic of South Africa. *Proceedings of Exploration 87, Ontario Geological Survey*, 3, 241–253.

Pugin, A. J. M., & Yilmaz, O. (2017). There is no pure P- or S-wave land seismic source. *SEG Technical Program Expanded Abstracts*, 5162–5166. https://doi.org/10.1190/segam2017-17650931.1

Punzo, M., Cianflone, G., Cavuoto, G., De Rosa, R., Dominici, R., Gallo, P., Lirer, F., Pelosi, N., & Di Fiore, V. (2021). Active and passive seismic methods to explore areas of active faulting. The case of Lamezia Terme (Calabria, southern Italy). *Journal of Applied Geophysics*, 188, 104316. https://doi.org/10.1016/j.jappgeo.2021.104316

Reynolds, J. (2011). An Introduction to Applied and Environmental Geophysics (2nd ed.). *Wiley*. ISBN: 9780471485360

Ringrose, P. S., Furre, A.-K., Gilfillan, S. M. V., Krevor, S., Landrø, M., Leslie, R., Meckel, T., Nazarian, B., & Zahid, A. (2021). Storage of Carbon Dioxide in Saline Aquifers: Physicochemical Processes, Key Constraints, and Scale-Up Potential. *Annual Review of Chemical and Biomolecular Engineering*, 12(1), 471–494. https://doi.org/10.1146/annurev-chembioeng-093020-091447

Rodriguez-Tablante, J., Tryggvason, A., Malehmir, A., Juhlin, C., & Palm, H. (2007). Cross-profile acquisition and cross-dip analysis for extracting 3D information from 2D surveys, a case study from the Western Skellefte District, northern Sweden. *Journal of Applied Geophysics*, 63(1), 1–12. ISSN 0926-9851. https://doi.org/10.1016/j.jappgeo.2007.03.001

Rogers, A. (1999). Distributed optical-fibre sensing. *Measurement Science and Technology*, 10 R75. https://doi.org/10.1088/0957-0233/10/8/201

Rosenblueth, E., & Ordaz, M. (1990). Maximum Earthquake Magnitude at Fault. *Journal of Engineering Mechanics*, 116(1), 204–216. https://doi.org/10.1061/(ASCE)0733-9399(1990)116:1(204)

Sato, H., Ito, K., Abe, S., Kato, N., Iwasaki, T., Hirata, N., Ikawa, T., & Kawanaka, T. (2009). Deep seismic reflection profiling across active reverse faults in the Kinki Triangle, central Japan. *Tectonophysics*, 472(1–4), 86–94. https://doi.org/10.1016/j.tecto.2008.06.014

Schokker, H. (2001). Final well report - Stenlille Gas Storage Well Stenllille-19. *Geological Survey of Denmark and Greenland Danish Ministry of Climate, Energy and Utilities*, Report file no. 28567.

Sheriff, R. E. (1980). Seismic stratigraphy. *Springer Dordrecht*. https://doi.org/10.1007/978-94-011-6395-8

Singh, S. K., Bazan, E., & Esteva, L. (1980). Expected earthquake magnitude from a fault. *Bulletin of the Seismological Society of America*, 70(3), 903–914. https://doi.org/10.1785/BSSA0700030903

Smith, M., Campbell, D., Mackay, E. B., & Polson, D. (2012). CO_2 aquifer storage site evaluation and monitoring, understanding the challenges of CO_2 storage: results of the CASSEM Project. *Scottish Carbon Capture and Storage*. http://hdl.handle.net/1842/15704

Socco, L. V., Boiero, D., Foti, S., & Wisén, R. (2009). Laterally constrained inversion of ground roll from seismic reflection records. *Geophysics*, 74(6), G35–G45. https://doi.org/10.1190/1.3223636

Song, A., Ren, J., Liu, A., Zhang, G., & Lei, X. (2023). Active seismic surveys based on distributed acoustic sensing in near-surface active fault exploration: A test in Datong Basin, North China. *Journal of Applied Geophysics*, 213, 105041. https://doi.org/10.1016/j.jappgeo.2023.105041

Soubaras, R. (1996). Ocean bottom hydrophone and geophone processing. *1996 SEG Annual Meeting*, 24–27. https://doi.org/10.1190/1.1826611

Stefatos, A., Papatheodorou, G., Ferentinos, G., Leeder, M., & Collier, R. (2002). Seismic reflection imaging of active offshore faults in the Gulf of Corinth: their seismotectonic significance. *Basin Research*, 14(4), 487–502. https://doi.org/10.1046/j.1365-2117.2002.00176.x

Sun, R., Kaslilar, A., & Juhlin, C. (2022). High resolution seismic reflection PP and PS imaging of the bedrock surface below glacial deposits in Marsta, Sweden. *Journal of Applied Geophysics*, 198, 104572. https://doi.org/10.1016/j.jappgeo.2022.104572

Tellier, N., & Lainé, J. (2017). Understanding MEMS-based digital seismic sensors. *First Break*, *35*(1). https://doi.org/10.3997/1365-2397.35.1.87386

Tryggvason, A., Rögnvaldsson, S. T., & Flóvenz, G. (2002). Three-dimensional imaging of the P- and S-wave velocity structure and earthquake locations beneath Southwest Iceland. *Geophysics Journal International* (Vol. 151). https://doi.org/https://doi.org/10.1046/j.1365-246X.2002.01812.x

United Nations - General assembly. (2015). Transforming our world: the 2030 Agenda for Sustainable Development. chrome-extension://oemmndcbldboiebfnladdacbdfmadadm/https://documents-dds-ny.un.org/doc/UNDOC/GEN/N15/291/89/PDF/N1529189.pdf?OpenElement

Van Zanen, L. S. (2004). Removing Love waves from shallow seismic SH-wave data. *PhD Thesis*, *TU Delft*, 1-149 pp. https://resolver.tudelft.nl/uuid:d467c131-3e61-47b1-809a-3b15f69b7765

Vosgerau, H., Gregersen, U., & Laghari, S. (2020). Capture, Storage and Use of CO_2 (CCUS). Seismic interpretation of existing 3D seismic data around the Stenlille structure within the framework of sequence stratigraphy and with focus on the Gassum Formation (Part of Work package 6 in the CCUS project). *Geological Survey of Denmark and Greenland Danish Ministry of Climate, Energy and Utilities*, Report 2020/34.

Wadas, S. H., Polom, U., & Krawczyk, C. M. (2016). High-resolution shear-wave seismic reflection as a tool to image near-surface subrosion structures – a case study in Bad Frankenhausen, Germany. *Solid Earth*, 7(5), 1491–1508. https://doi.org/10.5194/se-7-1491-2016

Wang, Z. (2009). Seismic Hazard vs. Seismic Risk. *Seismological Research Letters*, 80(5), 673–674. https://doi.org/10.1785/gssrl.80.5.673

Wells, D. L., & Coppersmith, K. J. (1994). New empirical relationships among magnitude, rupture length, rupture width, rupture area, and surface displacement. *Bulletin of the Seismological Society of America*, 84(4), 974–1002. https://doi.org/10.1785/BSSA0840040974

Westgate, M., Kucinskaite, K., Konstantinidis, E., Malehmir, A., Papadopoulou, M., Gregersen, U., Keiding, M., & Bjerager, M. (2025). Seismic imaging of halokinetic sequences and structures with high-resolution, dual-element acquisition, and processing: Applications to the Gassum structure in eastern Jutland, Denmark. *Earth and Space Science*, 12(1). https://doi.org/10.1029/2024EA004014

White, D. (2013). Seismic characterization and time-lapse imaging during seven years of CO_2 flood in the Weyburn field, Saskatchewan, Canada. *International Journal of Greenhouse Gas Control*, 16, S78–S94. https://doi.org/10.1016/j.ijggc.2013.02.006

White, D. J., Burrowes, G., Davis, T., Hajnal, Z., Hirsche, K., Hutcheon, I., Majer, E., Rostron, B., & Whittaker, S. (2004). Greenhouse gas sequestration in abandoned oil reservoirs: The International Energy Agency Weyburn pilot project. *GSA Today*, 14(7), 4. https://doi.org/10.1130/1052-5173(2004)014<004:GGSIAO>2.0.CO;2

White, D. J., Easton, R. M., Culshaw, N. G., Milkereit, B., Forsyth, D. A., Carr, S., Green, A. G., & Davidson, A. (1994). Seismic images of the Grenville Orogen in Ontario. *Canadian Journal of Earth Sciences*, 31(2), 293–307. https://doi.org/10.1139/e94-028

Wilczynski, Z., Kaslilar, A., Malehmir, A., Manzi, M., Vivin, L., Lepine, J., Valishin, O., & Högdahl, K. (2024). Ambient noise surface-wave imaging in a hardrock environment: implications for mineral exploration. *Geophysical Journal International*, 240(1), 571–590. https://doi.org/10.1093/gji/ggae392

Wu, J. (1996). Potential pitfalls of crooked-line seismic reflection surveys. *Geophysics*, 61(1), 277–281. https://doi.org/10.1190/1.1443949

Yilmaz, Ö. (2001). Seismic Data Analysis. *Society of Exploration Geophysicists*. https://doi.org/10.1190/1.9781560801580

Yilmaz, Ö. (2021). Land Seismic Case Studies for Near-Surface Modeling and Subsurface Imaging. *Society of Exploration Geophysicists*. https://doi.org/10.1190/1.9781560803812

Zappalà, S., Malehmir, A., Papadopoulou, M., Westgate, M., Putnaite, J., Markovic, M., Gregersen, U., Abramovitz, T., Keiding, M., & Bjerager, M. (2024). Reflection Seismic Acquisition for Onshore CCS Applications in Denmark – an Overview. *Fifth EAGE Global Energy Transition Conference & Exhibition (GET 2024)*, 1–5. https://doi.org/10.3997/2214-4609.202421062

Zerwer, A., Polak, M. A., & Santamarina, J. C. (2005). Detection of Surface Breaking Cracks in Concrete Members Using Rayleigh Waves. *Journal of Environmental and Engineering Geophysics*, 10(3), 295–306. https://doi.org/10.2113/JEEG10.3.295

Zoback, mark, Hickman, S., & Ellsworth, W. (2010). Scientific Drilling into the San Andreas Fault Zone. *Eos, Transactions American Geophysical Union*, 91(22), 197–199. https://doi.org/10.1029/2010EO220001

Acta Universitatis Upsaliensis

Digital Comprehensive Summaries of Uppsala Dissertations from the Faculty of Science and Technology 2509

Editor: The Dean of the Faculty of Science and Technology

A doctoral dissertation from the Faculty of Science and Technology, Uppsala University, is usually a summary of a number of papers. A few copies of the complete dissertation are kept at major Swedish research libraries, while the summary alone is distributed internationally through the series Digital Comprehensive Summaries of Uppsala Dissertations from the Faculty of Science and Technology. (Prior to January, 2005, the series was published under the title "Comprehensive Summaries of Uppsala Dissertations from the Faculty of Science and Technology".)

Distribution: publications.uu.se
urn:nbn:se:uu:diva-550140

ACTA UNIVERSITATIS
UPSALIENSIS
2025